DSPACE

https://dspace.org/

# Morphological evaluation of the heart, kidney and liver following simvastatin treatment of a mouse model of adolescent alcoholism

**Nchodu, Makgotso**

**2024**

https://hdl.handle.net/10539/37659

Downloaded from a DSpace repository. https://dspace.org/

# MORPHOLOGICAL EVALUATION OF THE HEART, KIDNEY AND LIVER FOLLOWING SIMVASTATIN TREATMENT OF A MOUSE MODEL OF ADOLESCENT ALCOHOLISM

**Makgotso Nchodu**

**1325876**

A dissertation submitted to the Faculty of Health Sciences, University of the Witwatersrand, School of Anatomical Sciences, Johannesburg, in fulfilment of the requirements for the degree of Master of Science in Medicine.

Johannesburg, 2023.

**DECLARATION**

I, Makgotso Nchodu hereby declare that this dissertation is my own work, unaided work. It is being submitted for the degree of Master of Science in Medicine in the Faculty of Health Sciences at the University of the Witwatersrand, Johannesburg. It has not been submitted before for any degree or examination at any other University.

Makgotso Nchodu

Signed on the 5th day of May 20 23 at Johannesburg

**DEDICATION**

In memory of my grandmother

**Elizabeth Zwane**

**1945 - 2016**

For instilling the love and value of education, thank you.

**ACKNOWLEDGEMENTS**

I would like to thank God for his grace and mercy throughout this journey.

1. **My supervisor: Dr Oladiran Olateju.** Thank you for your excellence supervision. The knowledge and skills you have shared with me are invaluable and very much appreciated.
2. **My parents: Tseko Nchodu and Phindile Nchodu.** Thank you for your patience and overwhelming support. Thank you for reminding me to pray and to have faith, you believed in me even when I did not believe in myself. Your unconditional love is a gift from God.
3. **My brother: Katlego Nchodu.** Thank you for always checking up on me and reminding me to be fearless.
4. **My friends: Nosipho Zwane, Nicole Mlauzi and Nolwazi Hlabangane.**
5. **Ms Hasiena Ali.** Thank you for your guidance and assistance with optimization.
6. **My co-workers: Robin du Preez, Sabiha Latiff and Alice Efuntayo.**
7. **National Research Foundation:** For funding my research.

**ABSTRACT**

Individuals that begin drinking during adolescence are more likely to become alcohol addicts, resulting in the development of alcohol-related diseases such as alcoholic cardiomyopathy, renal tubulointerstitial fibrosis and steatohepatitis. This study investigated the protective capabilities of simvastatin against alcohol-induced damage on the heart, kidney, and liver of adolescent mice administered chronic alcohol. Fifty four–week old C57BL/6J mice (F = 5; M = 5) were assigned to each experimental group: (i) NT; no treatment; (ii) ALC; 2.5 g/Kg/day of 20% alcohol (iii) SIM; 5 mg/Kg/day (iv) ALC+SIM5; 5 mg/Kg/day of simvastatin followed by 2.5 g/Kg/day of 20% alcohol (v) ALC+SIM15; 15 mg/Kg/day of simvastatin followed by 2.5 g/Kg/day of 20% alcohol. Lower dosage of simvastatin was more effective against alcohol-induced myocardial hypertrophy in females while a higher dosage of simvastatin was more effective in males. Both simvastatin concentrations significantly reduced alcohol-induced myocardial fibrosis in the females but only the low simvastatin dosage was effective in the males. ALC+SIM5 improved inflammation only in the females. Alcohol increased the area of the renal corpuscles and glomeruli, the collagen and TNF-α distributions. 5 mg simvastatin was more effective against renal hypertrophy in both males and females. Both doses of SIM were effective against renal inflammation. Both concentrations of simvastatin were not beneficial in stimulating hepatocyte regeneration except for 15 mg simvastatin in males. Only a higher dose of simvastatin prevented alcohol effect on hepatic collagen distribution. Both concentrations of simvastatin following a chronic alcohol were not beneficial against alcohol-induced inflammation in the liver.

**TABLE OF CONTENTS**


| | |
|---|---|
| DECLARATION | i |
| DEDICATION | ii |
| ACKNOWLEDGEMENTS | iii |
| ABSTRACT | iv |
| TABLE OF CONTENTS | v-vii |
| LIST OF FIGURES | viii-ix |
| LIST OF TABLES | x |
| NOMENCLATURE | xi-xiii |
| CHAPTER 1: INTRODUCTION | 1 |
| 1.1 Intro: Adolescent alcoholism | 2-3 |
| 1.2 The heart | 4-5 |
| 1.3 The kidney | 6-7 |
| 1.4 The liver | 8-9 |
| 1.5 Rationale | 10 |
| 1.6 Aims and specific objectives | 11 |
| CHAPTER 2: MATERIALS AND METHODS | 12 |
| 2.1 Animal study | 13-14 |
| 2.2 Experimental study | 14 |

2.2.1 Preparation and administration of simvastatin and alcohol 14-16

2.2.2 Animal perfusion and organ harvesting 18

2.3 Tissue processing and morphometry of the heart 19-22

2.4 Tissue processing and morphometry of the kidney 22-24

2.5 Tissue processing and morphometry of the liver 24-26

2.6 Statistical analysis 26

CHAPTER 3: RESULTS 27

3.1.1 Animal and organ masses 28

3.1.2 Blood alcohol concentration 29

3.2 The heart 30

3.2.1 General morphology of the cardiomyocytes 30

3.2.2 Measurements of the cardiomyocyte area and diameter 35

3.2.3 Measurement of collagen distribution 39-40

3.2.4 Measurement of TNF-α distribution 41

3.3 The kidney 43

3.3.1 General morphology of the renal corpuscles and tubules 43

3.3.2 Morphometry of renal corpuscle area 49

3.3.3 Morphometry of the glomerular area 49-50

3.3.4 Morphometry of the area of the urinary space 50-51

3.3.5 Measurement of collagen distribution 56

3.3.6 Measurement of TNF-α distribution 56-57

3.4 The liver 62

3.4.1 General morphology of the liver 62

3.4.2 Density of the hepatocytes 66

3.4.3 Measurement of collagen distribution 67

3.4.4 Measurement of TNF-α distribution 67-68

CHAPTER 4: DISCUSSION 73

4.1 The heart 74-77

4.2 The kidney 77-80

4.3 The liver 81-84

CHAPTER 5: CONCLUSION AND RECOMMENDATIONS 85

5.1 Conclusion and recommendations 86

CHAPTER 6: REFERENCES 87-94

APPENDICES 95

Ethical clearance certificate 95

Turnitin report 96

Buffer and fixative recipes 97

**LIST OF FIGURES**

Figure 3.1: Histological section of the ventricles of the heart and the layers of the heart wall. 31

Figure 3.2: Histological section of area and length measurements and morphology of the cardiomyocytes from the left ventricle. 32

Figure 3.3: Histological section of collagen distribution in the left ventricle. 33

Figure 3.4: Histological section of TNF-α distribution in the left ventricle. 34

Figure 3.5: Cardiomyocyte area boxplots. 37

Figure 3.6: Cardiomyocyte diameter boxplots. 38

Figure 3.7: Left ventricle collagen distribution boxplots. 40

Figure 3.8: Left ventricle TNF-α distribution boxplots. 42

Figure 3.9: Histological section of horizontal section of the kidney. 44

Figure 3.10: Histological section of kidney ultrastructure morphology. 45

Figure 3.11: Histological section of renal corpuscle and renal tubule measurements. 46

Figure 3.12: Histological section of collagen distribution in the kidney. 47

Figure 3.13: Histological section of TNF-α distribution in the kidney. 48

Figure 3.14: Renal corpuscle area boxplots. 53

Figure 3.15: Glomerular area boxplots. 54

Figure 3.16: Urinary space area boxplots. 55

Figure 3.17: Renal collagen distribution boxplots. 59

Figure 3.18: Renal tubule TNF-α distribution boxplots. 60

Figure 3.19: Renal corpuscle TNF-α distribution boxplots. 61

Figure 3.20: Histological section of liver parenchyma morphology. 63

Figure 3.21: Histological section of hepatic collagen distribution. 64

Figure 3.22: Histological section of hepatic TNF-α distribution. 65

Figure 3.23: Hepatocyte cell density boxplots. 70

Figure 3.24: Hepatic collagen distribution boxplots. 71

Figure 3.25: Hepatic TNF-α distribution boxplots. 72

**LIST OF TABLES**

Table 2.1: Summary of the different experimental groups 17

Table 3.1: Summary of animal and organ masses 28

Table 3.2: Summary of the morphometries of the cardiomyocyte area and the diameter 35

Table 3.3: Summary of the morphometries of the renal ultrastructure 52

Table 3.4: Summary of the collagen and TNF-α distributions in the kidney 58

Table 3.5: Summary of hepatocyte morphometries, collagen and TNF-α distributions 69

**NOMENCLATURE**

α: Alpha

α-SMA: Alpha-Smooth Muscle Actin

β: Beta

%: Percentage

ADH: Antidiuretic hormone

ALC: Alcohol only

ALC+SIM5: Alcohol and simvastatin 5 mg

ALC+SIM15: Alcohol and simvastatin 15 mg

AREC: Animal Research Ethics Committee

BAC: Blood alcohol concentration

BB: Brush border

BD: Ballooning degeneration

$CCl_4$: Carbon tetrachloride

DNA: Deoxyribonucleic acid

eNOS: Endothelial nitric oxide synthase

Endo: Endocardium

Epi: Epicardium

F: Fibrosis

FDA: Food and drug administration

GL: Glomerulus

H & E: Haematoxylin and eosin

HCl: Hydrochloric acid

KC: Kupffer cells

Klf2: Krüppel-like Factor 2

LPS: lipopolysaccharide

LV: Left ventricle

LVW: Left ventricular wall

MT: Masson's Trichrome

Myo: Myocardium

NaOH: Sodium hydroxide

NHLS: National Health Laboratory Service

NS: Not signficant

NT: Non-treatment

PB: Phosphate buffer

PFA: paraformaldehyde

RAS: Renin-angiotensin system

RC: Renal corpuscle

RT: Renal tubule

RV: Right ventricle

RVW: Right ventricular wall

SD: Standard deviation

SIM: Simvastatin 5 mg

TNF-α: Tumour necrosis factor alpha

TGF-β: Transforming growth factor beta

TGF-β1: Transforming growth factor beta 1

WRAF: Witwatersrand Research Animal Facility

# CHAPTER 1: INTRODUCTION

# Chapter One

## 1.0 Introduction

### 1.1 Adolescent alcoholism

Adolescence is the period of growth and development that occurs during puberty, and it is characterized by physical, psychosocial, and psychological changes (Ramsoomar, *et al*., 2013; Marshall, 2014). During this growth phase, young people tend to experiment with alcohol resulting in heavy episodic drinking, especially where there are lapses in policies to regulate access to alcohol (Ramsoomar, *et al*., 2013; Marshall, 2014). In addition, factors such as low socio-economic status, peer pressure, and psychological trauma are among the many reasons why adolescents may experiment with alcohol (Ramsoomar, *et al*., 2013; Marshall, 2014). Alcohol is the most socially acceptable drug globally (Dawodu *et al*., 2019). Unfortunately, South Africa is one of the countries with the most harmful drinking patterns (Ramsoomar *et al*., 2013) therefore, the increasing rate of alcohol misuse among adolescents in South Africa is a major health concern which is at a high cost to the government (Letsela *et al*., 2019).

Binge drinking, also referred to as heavy episodic drinking is classified as the consumption of 5 or more drinks on one occasion for males and 4 or more drinks on one occasion for females (Morojele & Ramsoomar, 2016). Chronic alcohol consumption is described as a pattern of abstaining from alcohol use followed by heavy episodic drinking (Morojele & Ramsoomar, 2016). Binge drinking among youth (15-24 years) was reported to have increased from 29% to 31%, from 1998 to 2005 (Chauke et al., 2015). Approximately 33.5% of male and 23.7% of female South African high school learners were reported to binge drink by the South African Youth Risk Behaviour Survey 2008 (Swart et al., 2015). The South African Department of Education

estimated alcohol consumption among high school learners to be 28% and approximately 12% of the youth in South begin drinking at the age of 13 years (Maserumule et al., 2019).

Alcohol misuse is greater for male than female adolescents (Olsson *et al*., 2016). Adolescents who misuse alcohol are more likely to engage in sexual activities at an early age (Letsela *et al*., 2019) which often promotes having multiple sexual partners (Letsela *et al*., 2019). The effects of these are multi-faceted which include sexually transmitted diseases, relationship-related violence, teenage pregnancy, rape, mental illness, and post-traumatic stress disorders (Letsela *et al*., 2019). In addition, prolonged or chronic alcohol consumption followed by abstinence may sensitize receptors that regulate excitability and memory which may result in aggravated withdrawal symptoms such as headaches, sweating, anxiety, insomnia, and nausea (Olsson *et al*., 2016). Individuals that begin drinking during adolescence are also more likely to become alcohol addicts (Olsson *et al*., 2016).

Chronic alcohol consumption could make an individual become violent, a sex 'predator' (i.e., rapist), a criminal, be involved in a road accident-causing harm, disability, or death to both the perpetrator and the citizens (Ramsoomar *et al*., 2013; Matzopoulos *et al*., 2014; Swart *et al*., 2015). According to Swart *et al.* (2015), alcohol-related violence is prevalent among South African adolescents during an altercation between/amongst intoxicated individuals. Apart from the social economic impact of alcohol abuse, alcohol misuse is among many factors contributing to the burden of disease in several countries (Ramsoomar *et al*., 2013; Olsson *et al*., 2016; Bertscher *et al*., 2020).

Chronic alcohol increases the incidence of infectious and cardiovascular diseases (Matzopoulos *et al*., 2014; Obad *et al*., 2018)which are also a burden on the health systems as huge funds are allocated to caring for alcohol-related diseases (Matzopoulos *et al*., 2014; Obad *et al*.,

2018). Even though the South African alcohol industry is beneficial to the economy (e.g., job creation and profits) (Matzopoulos, *et al*., 2014), the uncontrolled and unregulated access to alcohol (especially in the townships where adolescents can easily buy alcohol) are detrimental and costly to the government (Matzopoulos, *et al*., 2014). The lapse in policies guiding access to alcohol promotes abnormal drinking patterns and behaviours, especially in adolescents (Olsson, *et al*., 2016). This has thus provoked an interest in public health to find solutions to tackle alcohol use disorders in adolescents (Ramsoomar *et al*., 2013; Marshall, 2014; Olsson *et al*., 2016). It is also crucial to address alcohol use during the early stage of development to prevent the development of alcohol-related diseases (e.g., cardiovascular diseases, diabetes, liver cirrhosis, and renal failure, etc.) later in life (Ramsoomar *et al*., 2016; Marshall, 2014).

### 1.2 The heart

Chronic alcohol increases the incidence of cardiovascular diseases (Matzopoulos, *et al*., 2014; Obad, *et al*., 2018) which is a huge financial burden on the health systems (Matzopoulos, *et al*., 2014; Obad, *et al*., 2018). Chronic alcohol consumption changes the cardiac function and structure which may result in the weakening and loss of cardiomyocytes (Piano, 2016). In addition, the mitochondria, plasma membrane, ribosomes, and receptors of the cardiomyocytes are also damaged due to the high reactivity, low molecular mass, high diffusion rate, and the ability of alcohol to easily cross membranes (Fernández-Solà, 2020). Alcohol also disrupts signalling processes, activates apoptosis, and decreases heart contractility (Obad, *et al*., 2018; Fernandez-Sola, 2020). Likewise, the repair mechanism of cardiomyocytes is hindered by alcohol (by reducing regeneration and proliferation of cardiomyocytes) while promoting cardiac lesions (by increasing apoptosis and necrosis of cardiomyocytes), the outcome of which leads to myocardial fibrosis (Fernandez-Sola, 2020) and ventricular dysfunction (Wang *et al*., 2005). Alcohol is also

known to induce inflammation and promote the secretion of cytokines such as tumour necrosis factor-α (TNF-α) (Obad, *et al*., 2018) which is a pro-inflammatory cytokine that regulates myocardial homeostasis by signalling inflammation and cell abnormality (e.g., apoptosis) (Obad, *et al*., 2018). An increased level of TNF-α in chronic alcoholism is an indication of cardiac pathologies, fibrosis, and necrosis (Obad *et al*., 2018; Schumacher & Naga Prasad, 2018).

With the prevalence of chronic alcoholism (especially in adolescents) and its associated cardiovascular diseases, it is important to investigate interventions that may mask or reduce the damaging effects of alcohol on the heart tissues. One of such interventions that is gaining popularity, due to its anti-inflammatory and immune-regulatory properties, is simvastatin (Cahyawati, 2019; Gao *et al*., 2015; Xiao *et al*., 2016). It is an FDA–approved drug, primarily, used for lowering blood cholesterol (hypercholesterolaemia) (Thabit *et al*., 2014; Liu *et al*., 2016; Morse *et al*., 2018; Murphy *et al*., 2020). It also prevents coronary heart disease (Atef et al., 2019; Murphy et al., 2020), prevents cardiomyocyte death (MacDougall *et al*., 2017), myocardial inflammation and fibrosis (Sun *et al*., 2015; Xiao *et al*., 2016; Lee, *et al*., 2019). Simvastatin stimulates autophagy by inhibiting the mTOR signalling pathway, reducing damage to the cardiomyocytes, and stimulating their regeneration (Gao, et al., 2015), and may prevent cardiac hypertrophy through an antioxidant mechanism which inhibits Rac1 geranylgeranylation (Zhou & Liao, 2009). Simvastatin also prevents myocarditis (Skrzypiec-Spring *et al*., 2021) and improves endothelial functions (Cahyawati, 2019; Xiao et al., 2016) as well as inhibiting TGF-β1 pathway which triggers the development of interstitial fibrosis and cardiomyocyte hypertrophy (Xiao *et al*., 2016).

Simvastatin may be beneficial against alcohol-induced myocardial damage by preventing or potentially reversing the structural alterations caused by chronic alcohol use. Thus, this study

investigated the protective capabilities of simvastatin against alcohol-induced damage on the heart of adolescent mice administered chronic alcohol. Preventing and/or reversing alcohol-induced damage could alleviate the financial burden caused by alcohol-related diseases (Matzopoulos, *et al*., 2014).

### 1.3 The kidney

The kidneys play an important role in the regulation of blood pressure (Leal *et al*., 2017). They are also responsible for metabolizing, detoxifying, and excreting alcohol, or its metabolites from the body (Wu *et al*., 2021) and which makes the kidneys highly vulnerable to damage by alcohol (Brzóska *et al*., 2003). Due to the functions of the kidneys, damage or a loss of function could negatively affect the functions of other organs, especially the heart (Rikalo & Romanenko, 2018)and it is a fact that chronic alcohol consumption increases the incidence of cardiovascular diseases (Matzopoulos, *et al*., 2014; Obad, *et al*., 2018). Chronic alcohol increases blood pressure through various mechanisms, one of which is the activation of the renin-angiotensin system (RAS) in the kidney which raises the systemic blood pressure, causes glomerular hypertension and vasoconstriction (Leal *et al*., 2017). The activated intrarenal RAS induced by chronic alcohol also promotes renal damage by altering the morphologies of the glomeruli, the tubules, and the renal blood vessels (Das & Vasudevan, 2008; Hu *et al*., 2018; Leal *et al*., 2017). At the same time, it prolongs hypertension which is detrimental to the heart and other organs (Fard *et al*., 2022; Leal *et al*., 2017). This inter-relationship shows that the severity of a cardiovascular disease increases the probability of renal failure and vice versa (Hu *et al*., 2018). Unfortunately, chronic alcohol consumption is a social problem amongst adolescents. They tend to experiment with alcohol resulting in heavy episodic drinking patterns, especially in places where there are lapses in the regulation of access to alcohol (Ramsoomar *et al*., 2013; Marshall, 2014; Dawodu *et al*., 2019).

These adolescents often become alcohol addicts later in life thus creating social, economic, and health problems (Ramsoomar *et al*., 2013; Matzopoulos, *et al*., 2014; Swart *et al*, 2015; Olsson, *et al*., 2016; Bertscher *et al*., 2020).

Alcohol-induced renal damage changes the morphologies of the renal structures e.g., the glomeruli and the renal tubules causing renal functions such as glomerular filtration and tubular reabsorption to fail (Edelstein *et al*., 1997; Epstein, 1997; Das and Vasudevan, 2008; Rikalo and Romanenko, 2018; Wu *et al*., 2021). At the same time, chronic alcohol inhibits the function of antidiuretic hormone (ADH) in the kidneys thus resulting in the loss of water from the body (Epstein, 1997). Likewise, extracellular matrix deposition (i.e., renal fibrosis) between the renal tubules and the surrounding capillaries may increase in response to chronic alcohol thus delaying the oxygen supply and nutrients to the renal tubular cells (Wu *et al*., 2021).

Like the heart, tumour necrosis factor-alpha (TNF-α) is also produced in the kidney by vascular endothelial, mesangial, and renal tubular epithelial cells (Mehaffey and Majid, 2017; Fard *et al*., 2022). The basal concentration of TNF-α is considerably low or undetectable under normal conditions but it sporadically increases at the onset of inflammation which makes the TNF-α an indicator of renal failure or disease as well as helping to trigger pathways for rescue or repair (Mehaffey & Majid, 2017). In addition, the ability of TNF-α to induce apoptosis may be beneficial or detrimental to the renal tissues as apoptosis may contribute to the pathogenesis of renal diseases or it may trigger cell proliferation to compensate for cell death (Ortiz, 2000). Simvastatin targets Bcl-XL, which inhibits apoptosis by preventing the release of cytochrome C from the mitochondria and targets the cell-survival signalling pathway survivin/NF-κB/p65, therefore, protecting renal tissue from lipoprotein-induced apoptosis (Nezic, et al., 2020). Simvastatin has been reported to

significantly reduce the fraction area of myofibroblasts and reduced myofibroblast expansion by decreasing the expression of α-SMA, which is a marker for the expansion of myofibroblasts (Cahyawati, et al., 2017).

## 1.4 The liver

The liver metabolizes about 90% of alcohol and ensures that it is removed from the body (Hassan *et al*., 2015; Obad *et al*., 2018; Hu *et al*., 2020). Alcohol metabolism affects the regulation of lipids in the body (Jeon and Carr, 2020) by reducing the oxidation of fatty acids, increasing the production of fatty acids, and inhibiting the transportation of triglycerides from the liver (Cohen & Nagy, 2011; Sengupta *et al*., 2021). These often cause triglycerides and fatty acids to accumulate in the hepatocytes, a condition called steatosis (fat deposit). Steatosis may progress into alcoholic steatohepatitis in chronic alcoholism which is characterized by inflammation, cell death, and increased levels of liver enzymes (e.g., alanine aminotransferase and aspartate aminotransferase (Cohen and Nagy, 2011; Celli and Zhang, 2014; Duly *et al*., 2015; de Lucca *et al*., 2018; Jeon and Carr, 2020; Sengupta *et al*., 2021).

Chronic alcohol also induces hepatic stress which then impairs liver functions as well as promotes the death of hepatocytes (Cohen and Nagy, 2011). Enlargement of hepatocytes (i.e., hydropic swelling or ballooning degeneration) is also common in steatohepatitis where the cells appear pale with a distended cytoplasm (Celli & Zhang, 2014; Hassan *et al*., 2015). As the alcohol damage continues, the hepatic stellate cells are activated resulting in an increase in collagen deposition and the loss of hepatic sinusoids – a condition called liver fibrosis (Cohen and Nagy, 2011). In a situation where alcohol continues to be consumed in excess, liver fibrosis may

eventually progress to a life-threatening condition called cirrhosis (Cohen & Nagy, 2011; de Almeida *et al*., 2020).

Most cells including the Kupffer cells and the hepatic stellate cells produce reactive oxygen species for normal cell function or in response to pathogens (Gandhi, 2012). Following an excessive consumption of alcohol, the Kupffer cells usually become sensitized to endotoxins which cause more Kupffer cells to be activated (Cohen and Nagy, 2011). This invariably leads to the upregulation of reactive oxygen species causing the death of hepatocytes and hepatic failure (Cohen and Nagy, 2011). The activated Kupffer cells also produce TNF-α which at a non-pathological level is essential for suppressing apoptosis but promotes the proliferation and regeneration of hepatocytes (Cohen and Nagy, 2011). Based on these, it is true that chronic alcohol sensitizes the liver thus increasing its susceptibility to damage by a secondary risk factor (Cohen and Nagy, 2011).

The diverse effects that statins have on the diseases of the cardiovascular system (Matzopoulos *et al*., 2014; Obad *et al*., 2018) are being proposed to be effective in modifying the progression of hepatic diseases. Several observational studies have reported on the effectiveness of statins in reducing portal hypertension, preventing hepatic dysfunction, preventing the development of hepatic carcinoma, and improving the survival of hepatocytes (la Mura *et al*., 2013). It has also been shown that the ability of statins to improve vascular remodelling and reactivity makes it effective in preventing the development of cirrhosis (Kaplan, 2018). Likewise, simvastatin improves hepatic steatosis by inducing autophagy and maintaining lipid homeostasis in the liver (Atef *et al*., 2019). Simvastatin also improved the function of endothelial tissue in hypercholesterolemic patients using the nitric oxide synthase dependent pathway (Gu *et al*., 2019; MacDougall *et al*., 2017; Zhou & Liao, 2009) as well as preventing inflammatory responses by

inhibiting the production of harmful by-products and excess free radicals in liver cirrhosis (Gu *et al*., 2019). Oxidation of alcohol by the aldehyde dehydrogenase in the liver may induce an overproduction of TNF-α, causing inflammation but simvastatin reduces the severity of hepatic inflammation through its ability to inhibit the upregulation of TNF-α expression as well as nitric oxide (Atef *et al*., 2019; Kolovou *et al*., 2006).

## 1.5 Rationale

In reviews by Kolovou *et al*. (2006) and Fang *et al*., (2019), Simvastatin was reported to increase the production of nitric oxide to stabilize inflammation in the liver, heart, and kidney in response to acute alcohol consumption (Kolovou *et al*., 2006; Fang *et al*., 2019). Simvastatin was reported to prevent the production and secretion of TNF-α (Kolovou *et al*., 2006; Fang *et al*., 2019). This responsive mechanism provides these organs with protection against oxidative injury and ischaemia (Kolovou *et al*., 2006). Therefore, Simvastatin may be helpful in preventing and potentially reversing the functional and structural alterations in these organs induced by early alcohol consumption as often seen in adolescent alcoholics (Kolovou *et al*., 2006; Fang *et al*., 2019). Alcoholism and alcohol-related diseases increase the financial burden on the government (Matzopoulos *et al*., 2014). Preventing and/or reversing alcohol-induced damage could alleviate the burden on the health system (Matzopoulos, *et al*., 2014) improve the socio-economic status of the country and ultimately improve the quality of life of sufferers (Matzopoulos, *et al*., 2014). It is thus important to further explore the beneficial effects of Simvastatin in preventing alcohol-related damages in the heart, kidney and liver using a mouse model of adolescent alcoholism.

## 1.6 Aim and specific objectives

The aim of the study is to explore the protective effects of Simvastatin against alcohol-induced damages in the heart, kidney, and liver in a mouse model of adolescent alcoholism by assessing the morphological and morphometrical changes in the different organs.

The specific objectives are:

A. To evaluate the protective effects of Simvastatin (reduced hypertrophy, fibrosis and inflammation) against alcohol-induced damage on the heart of adolescent chronic alcoholic mice using histology (H+E and MT) and immunohistochemistry (TNF-α) techniques.

B. To evaluate the protective effects of Simvastatin (reduced glomerular swelling, fibrosis and inflammation) against alcohol-induced damage on the kidney of adolescent chronic alcoholic mice using histology (H+E and MT) and immunohistochemistry (TNF-α) techniques.

C. To evaluate the protective effects of Simvastatin (improved hepatocyte density, reduced fibrosis and inflammation) against alcohol-induced damage on the liver of adolescent chronic alcoholic mice using histology (H+E and MT) and immunohistochemistry (TNF-α) techniques.

# CHAPTER 2: MATERIALS AND METHODS

# Chapter 2

## 2.0 Materials and methods

### 2.1 Animal study

This study forms part of a broad study on the beneficial properties of the Simvastatin against alcohol-induced damage in some selected organs e.g., brain, sciatic nerve, long bones, heart, kidneys, and livers, harvested from adolescent mouse that were administered a prolonged alcohol consumption. This study was approved (Ethical Clearance No: 2019/11/63/C) by the Animal Research Ethics Committee (AREC) of the University of the Witwatersrand Johannesburg, South Africa. The mice were supplied by the National Health Laboratory Service (NHLS), Johannesburg and they were housed in the animal facility of the Witwatersrand Research Animal Facility (WRAF) of the Faculty of Health Sciences, University of the Witwatersrand. Ten (10) (50% sex ratio) C57BL/6J mice were assigned to each experimental group: (i) Non-treatment group (no administration of alcohol or simvastatin); (ii) Alcohol only group (intraperitoneal injection of 20% alcohol (2.5 g/Kg) in saline water); (iii) Simvastatin only group (5 mg/Kg oral dose in sterile water); (iv) Alcohol + Simvastatin 5 (5 mg/Kg oral dose in sterile water followed by intraperitoneal injection of 20% alcohol (2.5 g/Kg) in sterile saline water) (v) Alcohol + Simvastatin 15 (15 mg/Kg oral dose in sterile water followed by intraperitoneal injection of 20% alcohol (2.5 g/Kg) in sterile saline water). All treatments were performed for 28 consecutive days. Throughout the experimentation, the animals were handled and treated humanely. At the end of the treatment period, the mice were sacrificed using Euthanaze (sodium pentobarbital, 80 mg/Kg, i.p.) before trans-cardially perfusing with 0.9% cold saline followed by 4% paraformaldehyde in

0.1 M phosphate buffer (PM). The heart, kidneys and liver were immediately removed, weighed, immersed in 10% buffered formalin, and then stored at 4 °C before further processing.

## 2.2 Experimental study

The animals were randomly allocated into five experimental groups and then allowed to acclimatize for one week, following which alcohol, simvastatin or appropriate controls were administered to the mice starting from postnatal day 28 (at 4 weeks old) to postnatal day 56 days (at 8 weeks old) according to Table 2.1. Alcohol was administered intraperitoneally while Simvastatin was administered via oral gavage. Both procedures were performed with utmost care by the trained staff of WRAF to reduce introducing stress into the animal. Mice of the same sex and belonging to the same experimental group were housed together in a group of five mice per cage (cage dimensions: 200 × 200 × 300 mm) and kept under a reversed 12–hour day/ 12–hour dark cycle (with the light switched off from 06:00 – 18:00). For this study, the period of adolescent in the mice was taken as (period between 3 – 8 weeks old) (Lespine and Tirelli, 2017).

### 2.2.1 Preparation and administration of simvastatin and alcohol

Simvastatin (Cat no: 1612700 Merck, South Africa) was prepared according to McKay et al. (2004). 80 mg simvastatin was weighed and dissolved in a solution containing 1 ml 0.1 M sodium hydroxide (NaOH) and 1 ml absolute alcohol under a gently stirring for 1 hr at room temperature until the simvastatin had completely dissolved. The stock solution was prepared every fifth day and they were aliquoted and stored in – 4 °C until use. A serial dilution of the stock solution was then used to prepare the high concentration (i.e., 4 mg/ml in distilled water) and the low concentration (i.e., 1 mg/ml in distilled water) of simvastatin from which the final dosages (i.e., 15 mg/Kg/per day and 5 mg/Kg/per day respectively) were determined (Christensen *et al*.,

2006; Mohammadi *et al*., 2015). These solutions were prepared daily and filtered sterilized using a 0.20–µm sterile filter under a sterile condition. Any unused solution per day was discarded.

Using a serial dilution, a pharmacological grade absolute alcohol (96%) (Sigma–Aldrich, South Africa; Cat no: SAAR2233510LP) was diluted in saline (0.9% NaCl) into 20% alcohol solution which was then administered intraperitoneally to the mice at a dose of 2.5 g/kg (Maldonado-Devincci *et al*., 2010). The alcohol solution was also prepared daily, and the solution was filtered sterilized using a 0.20–µm sterile filter under a sterile condition. Alcohol was administered to the alcohol group (ALC) intraperitoneally and within 30 min after administering simvastatin to the alcohol + simvastatin 5 mg or 15 mg (ALC+SIM5 or ALC+SIM15) experimental groups. The injection site was alternated daily to reduce introducing stress or discomfort in the animal. To control for stress that may arise from handling or the administration of drugs in the mice, the mice in the non-treatment group (NT) were not administered alcohol or simvastatin and they were not handled throughout the experimental period (28 days) except for daily weighing or periodical cleaning of the cages which were performed by WRAF trained personnel. Alcohol was also not administered to the simvastatin 5 mg group (SIM) as it served as a control for the effect of simvastatin. Food and water were provided *ad libitum* to the mice, except in the NT and SIM groups, where it was withheld for 2 hrs post-intraperitoneal injection to partially control for the reduction in feeding during the period of peak alcohol intoxication in the alcohol-treated mice (Haycock and Ramsay 2009).

On the last day of administration of alcohol or simvastatin, 50 µl of saphenous blood was collected through saphenous vein bleeding on the left hind legs of all the mice in all the experimental groups except in the NT group to determine the level of blood alcohol concentration (BAC) in each mouse (Bielawski and Abel, 1997). Blood was collected from the SIM group to

equilibrate the experimental groups, but BAC analysis was not performed on the blood from this group because they were not administered alcohol. Blood was collected, within 30 mins after the administration of alcohol, in heparinized capillary tubes and then stored at – 80 ºC before further processing. Prior to the determination of BAC, the blood in the capillary tubes were stored at 4 ºC overnight before being centrifuged with Vivaspin500© 100 µm membrane tubes (Biotech, South Africa) at 5000 rpm for 15 minutes to separate the serum. The serum was extracted and then the BAC was determined using an EnzyChrom™ Ethanol Assay Kit (BioVision, South Africa) according to the manufacturer's recommendations.

Table 2.1: Summary of the different experimental groups

| Groups | Experimental groups | Abbreviations of groups | No. of mice per experimental group | | Dose of administered substances | Duration of administration (days) |
|---|---|---|---|---|---|---|
| | | | Female | Male | | |
| 1 | No treatment | NT | 5 | 5 | No alcohol, no Simvastatin<br>To control for the procedures and treatments. | |
| 2 | Simvastatin (5 mg/Kg) | SIM | 5 | 5 | 5 mg/Kg per day (in distilled water) administered by oral gavage. To obtain a baseline effect of simvastatin | 28 |
| 3 | Alcohol | ALC | 5 | 5 | 2.5 g/Kg alcohol (in saline) administered intraperitoneally | 28 |
| 4 | Alcohol + 5 mg/Kg SIM | ALC+SIM5 | 5 | 5 | Daily oral dose of 5 mg/Kg SIM (in distilled water) followed by 2.5 g/Kg alcohol (in saline) administered intraperitoneally | 28 |
| 5 | Alcohol + 15 mg/Kg SIM | ALC+SIM15 | 5 | 5 | Daily oral dose of 15 mg/Kg SIM (in distilled water) followed by 2.5 g/Kg alcohol (in saline) administered intraperitoneally | 28 |
| | **TOTAL** | | **25** | **25** | | |

2.2.2 Animal perfusion and organ harvesting

At the end of the experimental period, the mice were euthanized using Euthanaze (sodium pentobarbital, 80 mg/Kg, i.p.). Thereafter, the mice were transcardially perfused with 4% paraformaldehyde (in 0.1 M phosphate buffer, PB) (PFA). The thoracic and abdominal regions were cut open, then the heart, kidneys and liver were carefully harvested. They were dipped twice (in quick succession) in PB to wash-off any blood on the organs and thereafter a dry filter paper was used to mop-off any fluid on the organs. They were weighed and then post-fixed for 24 hr in 4% PFA in 0.1 M PB before further processing.

For the removal of the sciatic nerve, the carcasses were placed in a supine position on a dissecting board. The skin on the left hind limb was reflected to expose the muscles of the hind limb. The thigh muscles were then split longitudinally to expose the whole length of the sciatic nerve. The nerve was gently lifted using a forceps and the section of the nerve overlying the hip joint and at its bifurcation at the popliteal fossa was carefully cut and immediately fixed in 10% buffered formalin (in 0.1M PB) and stored at 4 ºC overnight before further processing.

2.3 Tissue processing and morphometry of the heart

The PFA–fixed heart was cut midway across the ventricles. The lower portion of the ventricles was processed for histology using an automated processing machine (Microme STP 120, Thermo Fisher Scientific, Walldorf, Germany) before embedding in paraffin wax. It was sectioned horizontally across the ventricles at 2 µm thickness using a microtome (Leica Biosystems RM2125 RTS, China). Serial sections were performed for haematoxylin and eosin (H&E) or Masson's trichrome (MT) staining as well as TNF-α immunolabelling.

For haematoxylin and Eosin or Masson's Trichrome staining, sections were cleared in xylene to remove the paraffin wax and then hydrated in a graded series of alcohol (70%, 95% and 100%). The sections were washed in a running tap water for 5 minutes and stained with H&E (for general morphology and morphometry of the cardiomyocytes) for 5 mins or with MT (for determination of collagen deposition) for 5 mins. Thereafter, sections were dehydrated in a graded series of alcohol and then cover-slipped with entellen.

For the TNF-α immunolabelling, sections were also cleared in xylene to remove the paraffin wax and hydrated in a graded series of alcohol (70%, 95% and 100%). An antigen retrieval was performed by immersing the sections in citrate buffer at 60 °C overnight. The sections were washed three times, thereafter, endogenous peroxidase activity was blocked by immersing the sections in 1% hydrogen peroxide, 49.5% methanol and 49.5% PB for 30 minutes. It was subsequently washed twice in PB before incubating in a blocking buffer solution (5% normal goat serum in PB at room temperature) for 30 minutes to block unspecified binding sites. Thereafter, the sections were incubated overnight at 4 °C in the primary antibody (1:250, mouse anti-TNF-α ab220210, Abcam, in PB). After the incubation period, the sections were washed twice in PB before incubating in the secondary antibody (1:1000 dilution of biotinylated goat anti-mouse IgG,

BA-9200-1.5, Vector labs, in PB). Following this, the sections were again washed twice in PB and then incubated for 1 hr in an avidin-biotin solution (25 µl advin + 25 µl biotin + 1.25 ml PBS, 1:125; Vector Labs). The sections were further washed twice in PB and then immersed in a DAB working solution containing 0.05% DAB (3,3'-Diaminobenzidine), 2 ml Tris HCl, 29 µl cold distilled water and 1 µl hydrogen peroxide for 10 mins and the reaction was terminated by adding an equal volume of PB. The slides were rinsed in running tap water before counterstaining with haematoxylin. Thereafter, the sections were dehydrated in a graded series of alcohol, cleared in xylene and cover-slipped with entellen. To rule out non-specific staining of the immunohistochemical protocol, tests were conducted on the sections where the primary or the secondary antibody was omitted. In both cases no staining was observed (results not shown).

For the morphometries of the cardiomyocytes, images of the myocardium along the length of the left ventricular wall of the H&E–stained sections were taken using an Olympus EP50 camera (Serial No. 3H23424, Japan) attached to an Olympus BX41 microscope (Model BX41TF, Olympus Corporation, Tokyo, Japan) at times 100 objective lens (under oil immersion). The left ventricular wall was identifiable as the larger of the two ventricular walls. The inter-ventricular wall was not considered in this study. With the scale set on the software, the area, and the diameter of cardiomyocytes (Harash *et al*., 2019) were measured from the digitized images using an EPview software (EPview 1.3, Build 19857). The diameter of the long axis of a cardiomyocyte was measured across the level of the nucleus with the line passing through the nucleolus using the straight-line tool of the software (Baudouy *et al*., 2017; Harash *et al*., 2019). In addition, the border of cardiomyocyte was carefully traced using the polygonal tool of the software and then the area of each cardiomyocyte was analysed by the same software (Baudouy *et al*., 2017; Harash *et al*.,

2019). The field of view was changed by moving the microscope stage to prevent duplicating measurements. In total, a minimum of 100 cardiomyocytes were measured per mouse.

To determine the distribution of collagen deposition in the heart tissue, digitized images of the left ventricular wall of the MT–stained sections were taken using a Carl Zeiss Axiocam 208 color camera (Serial No. 5318003446, China) attached to a Carl Zeiss Axioskop 2 microscope (Serial No. 804161, Germany) at times 40 objective lens. The images were subsequently saved in a JPEG file format. Similar to the cardiomyocyte morphometry, the field of view was changed by moving the microscope stage along the length of the left ventricular wall. The distribution of collagen within the myocardium was determined using the deconvolution plugin settings on an ImageJ software (ImageJ 1.53q/Java 1.8.0_322, Oracle America Inc.) (Chen *et al*., 2017; Latiff and Olateju, 2022). The 24-bit RGB format was selected as a requirement for the deconvolution plugin setting in the ImageJ software where the green component on the processed image indicated collagen stain (Chen *et al*., 2017; Latiff and Olateju, 2022). Collagen distribution on each image was quantified using the threshold tool on the ImageJ software which was adjusted until all the collagen (i.e., green) stain had been highlighted (Chen *et al*., 2017; Latiff and Olateju, 2022). The percentage collagen distribution per image was calculated as the threshold area divided by the area of the image.

Similar to the analyses used for the MT-stain sections, the percentage distribution of the TNF-α positive immunolabelling of the myocardium was performed using digitized images at 40 times objective lens. The field of view was changed, and the digitized images were also saved in the JPEG file format before processing with ImageJ software. Using the 24-bit RGB format, the DAB staining was selected for the deconvolution plugin setting on ImageJ software (Balzano *et al*., 2020) where the brown component was identified as the DAB staining (Balzano *et al*., 2020).

The distribution of TNF-α immunolabelling in each image was quantified by adjusting the threshold tool of ImageJ until all the DAB stain had been highlighted (Balzano *et al*., 2020). Thereafter, the percentage distribution of the TNF-α immunolabelling was determined by dividing the threshold area by the area of the image.

2.4 Tissue processing and morphometry of the kidneys

The PFA–fixed right kidney was cut horizontally at its equator and then the inferior half of the tissue processed for H&E and MT staining as well as TNF-α immunolabelling using the same antibody and dilutions as described in 2.3. For the kidney, the sections were made at 5 µm thickness. Serial sections were prepared for haematoxylin and eosin (H&E) (for general morphology and morphometries of renal corpuscles and the glomeruli), Masson's trichrome (MT) (for evaluating collagen deposition i.e., fibrosis around the renal tubules and the renal corpuscles) or TNF-α immunolabelling with incubation in primary antibody (1:250, mouse anti-TNF-α, ab220210, Abcam, in PB) (for quantifying the expression of TNF-α in the renal tissue).

For the morphometries of the renal corpuscles and the glomeruli, images along the length of the renal cortex of the H&E–stained sections were taken using a Carl Zeiss Axiocam 208 colour camera (Serial No. 5318003446, China) attached to a Carl Zeiss Axioskop 2 microscope (Serial No. 804161, Germany) at times 63 objective lens. The field of view was randomized by moving the microscope stage to prevent duplicating measurements. With the scale set on the ImageJ software (ImageJ 1.53q/Java 1.8.0_322, Oracle America Inc.), the areas of the renal corpuscle and the glomerulus were measured from the digitized images by tracing the boundary of the parietal layer of the Bowman's capsule and the boundary of the glomerulus using the freehand tool of the

software before the areas were then analysed. The area of the Bowman's space was then calculated by subtracting the area of the glomerulus from the area of the renal corpuscle (Fernandes *et al*., 2019).

To determine the collagen distribution in the kidney tissue, digitized images of the MT–stained sections were taken using a Carl Zeiss Axiocam 208 color camera attached to a Carl Zeiss Axioskop 2 microscope at times 40 objective lens. The images were subsequently saved in a JPEG file format. Similar to the renal corpuscle morphometry, the field of view was also randomised by moving the microscope stage along the length of the renal cortex. The distribution of collagen within the kidney tissue was determined using the deconvolution plugin settings on the ImageJ software (Chen *et al*., 2017; Latiff and Olateju, 2022). The 24-bit RGB format was selected as a requirement for the deconvolution plugin setting in the software where the green component on the processed image indicates collagen stain (Chen *et al*., 2017; Latiff and Olateju, 2022). Collagen distribution on each image was quantified using the threshold tool on the software which was adjusted until all the collagen (i.e., green) stain had been highlighted (Chen *et al*., 2017; Latiff and Olateju, 2022). The percentage collagen distribution per image was calculated as the threshold area divided by the area of the image.

Like the analyses used for the MT-stain sections, the percentage distribution of the TNF-α positive immunolabelling of the renal tubules or the renal corpuscles were performed using digitized images at 63 times objective lens. The field of view was also randomised, and the digitized images saved in the JPEG file format. Using the 24-bit RGB format, the region of interest (ROI) manager was used to select the area of the renal corpuscle or the tubules and the size of the ROI (620368 $\mu m^2$) was kept constant throughout the analyses (Balzano *et al*., 2020). The ROI was then duplicated so that only the areas of the renal corpuscle and the tubules were used for

deconvolution. The DAB staining was selected for the deconvolution plugin setting on the ImageJ software where the brown component was identified as the DAB staining. The distribution of TNF-α immunolabelling in each ROI was quantified by adjusting the threshold tool of ImageJ until all the DAB stain had been highlighted (Balzano *et al*., 2020). Thereafter, the percentage distribution of the TNF-α immunolabelling was determined by dividing the threshold area by the area of the region of interest.

2.5 Tissue processing and morphometry of the liver

The PFA–fixed left lateral lobe (the largest lobe) of the liver was cut and processed for H&E and MT staining as well as TNF-α immunolabelling using the same antibody and dilutions as described in 2.3. For the liver, the sections were made at 10 µm thickness across the flatter surface of the liver. Serial sections were performed for haematoxylin and eosin (H&E) or Masson's trichrome (MT) staining as well as TNF-α immunolabelling.

For the morphometries of the hepatocytes, images along the length of the liver of the H&E–stained sections were taken using a Carl Zeiss Axiocam 208 color camera (Serial No. 5318003446, China) attached to a Carl Zeiss Axioskop 2 microscope (Serial No. 804161, Germany) at times 10 objective lens. With the scale set on the software, the number of hepatocytes per grid were counted (Matsuo *et al*., 2016) from the digitized images using the ImageJ software (ImageJ 1.53q/Java 1.8.0_322, Oracle America Inc.). A grid (31560 $\mu m^2$) was placed on the image, and then the hepatocytes were counted (Matsuo *et al*., 2016). Cells that were touching the boundaries of the grids were not counted. The field of view was changed by moving the microscope stage at every 1–mm interval to prevent duplicating measurements.

To determine the distribution of collagen deposition in the liver tissue, digitized images of the length of the liver of the MT–stained sections were taken using a Carl Zeiss Axiocam 208 color camera (Serial No. 5318003446, China) attached to a Carl Zeiss Axioskop 2 microscope (Serial No. 804161, Germany) at times 40 objective lens. The images were subsequently saved in a JPEG file format. Similar to the liver morphometry, the field of view where images were taken was also randomised by moving the microscope stage at every 1–mm interval along the length of the liver. The distribution of collagen within the liver tissue was determined using the deconvolution plugin settings on an ImageJ software (ImageJ 1.53q/Java 1.8.0_322, Oracle America Inc.) (Chen *et al*., 2017; Latiff and Olateju, 2022). The 24-bit RGB format was selected as a requirement for the deconvolution plugin setting in the ImageJ software where the green component on the processed image indicates collagen stain (Chen *et al*., 2017; Latiff and Olateju, 2022). Collagen distribution on each image was quantified using the threshold tool on the ImageJ software which was adjusted until all the collagen (i.e., green) stain had been highlighted (Chen *et al*., 2017; Latiff and Olateju, 2022). The percentage collagen distribution per image was calculated as the threshold area divided by the area of the image multiplied by 100.

Similar to the analyses used for the MT-stain sections, the percentage distribution of the TNF-α positive immunolabelling of the length of the liver was performed using digitized images at 40 times objective lens. The field of view was randomised similar to the H&E–stained sections and the digitized images were also saved in the JPEG file format. Using the 24-bit RGB format, the H-DAB staining was selected for the deconvolution plugin setting on ImageJ software (Balzano *et al*., 2020) where the brown component was identified as the DAB staining (Balzano *et al*., 2020). The distribution of TNF-α immunolabelling in each image was quantified by adjusting the threshold tool of ImageJ until all the DAB stain had been highlighted (Balzano *et al*.,

2020). Thereafter, the percentage distribution of the TNF-α immunolabelling was determined dividing the threshold area by the area of the image and then multiplying by 100.

## 2.6 Statistical analysis

A descriptive statistic using mean (± SD) and median were performed. The data was not normally distributed, thus the median of all measurements in the different experimental groups were compared using a Kruskal–Wallis test followed by a Dunn's post hoc test. All statistical tests were performed using a PAST freeware data analyser (version 4.03; Germany) and graphs were plotted using the Excel software (Word Office Pro, USA). Statistical difference of 5% was regarded as significant for all the statistical analyses.

# CHAPTER 3: RESULTS

# Chapter 3

## 3.0. Results

### 3.1.1 Animal and organ weights

Table 3.1: Summary of animal and organ weights

| Experimental Group | Animal mass (mg) Mean±SD | Heart mass (mg) Mean±SD | Combined kidney mass (mg) Mean±SD | Liver mass (mg) Mean±SD |
|---|---|---|---|---|
| NT | 16.7 ± 2.78 | 0.25 ± 0.078 | 0.882 ± 0.470 | 0.347 ± 0.476 |
| SIM | 16.6 ± 2.139 | 0.214 ± 0.088 | 0.704 ± 0.493 | 0.614 ± 0.546 |
| ALC | 16.3 ± 2.263 | 0.296 ± 0.040 | 1.179 ± 0.333 | 0.136 ± 0.040 |
| ALC+SIM5 | 16 ± 2.345 | 0.245 ± 0.103 | 1.026 ± 0.616 | 0.343 ± 0.346 |
| ALC+SIM15 | 15.6 ± 1.595 | 0.261 ± 0.100 | 1.01 ± 0.494 | 0.327 ± 0.041 |

### 3.1.2 Blood alcohol concentration

The average blood alcohol concentration across the ALC, ALC+SIM5 and ALC+SIM15 ranged from 27.02 to 509.76 mg/dL. The average blood alcohol concentration at the time of termination in the ALC was 244.14 mg/dL, 253.36 mg/dL in the ALC+SIM5, and 182.51 mg/dL in the ALC+SIM15. The BAC values confirm the presence of alcohol in the blood of the animals in the ALC, ALC+SIM5 and ALC+SIM15 experimental groups.

## 3.2 The heart

### 3.2.1 General morphology of the cardiomyocytes

There were no changes observed in the morphology of the cardiomyocytes across all treatment groups. The layers of the ventricular wall were present in all treatment groups. The cardiomyocytes were elongated, with a nucleus and a nucleolus. There were changes in the size of the cardiomyocytes that were observed across the treatment groups. The cardiomyocytes in the ALC appeared enlarged compared to the other treatment groups. The myocardium in the ALC has a significantly increased collagen deposition compared to the other treatment group. The myocardium in the NT showed little to no TNF-α expression while the myocardium in the ALC showed intense TNF-α expression.

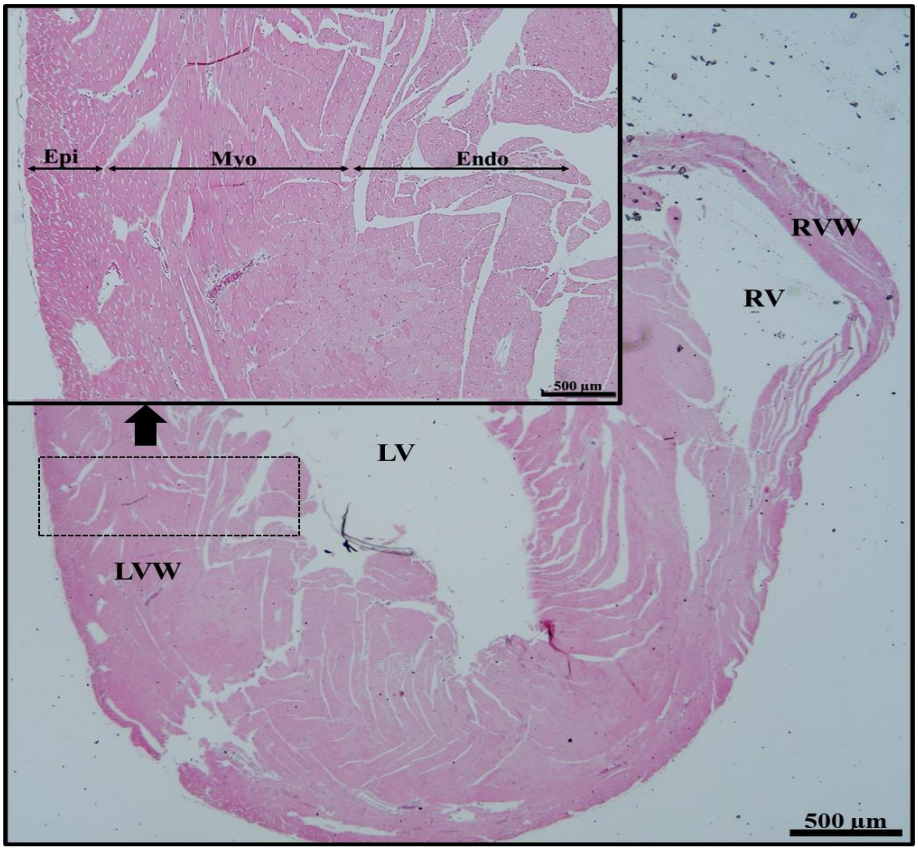



Figure 3.1: Representative micrographs of the ventricles of the heart demosntrating the layers of the heart wall of a heart from the NT treatment group. LV= left ventricle, RV= right ventricle, LVW= left ventricular wall, RVW= right ventricular wall, Epi= epicardium, Myo= myocardium, Endo= endocardium.

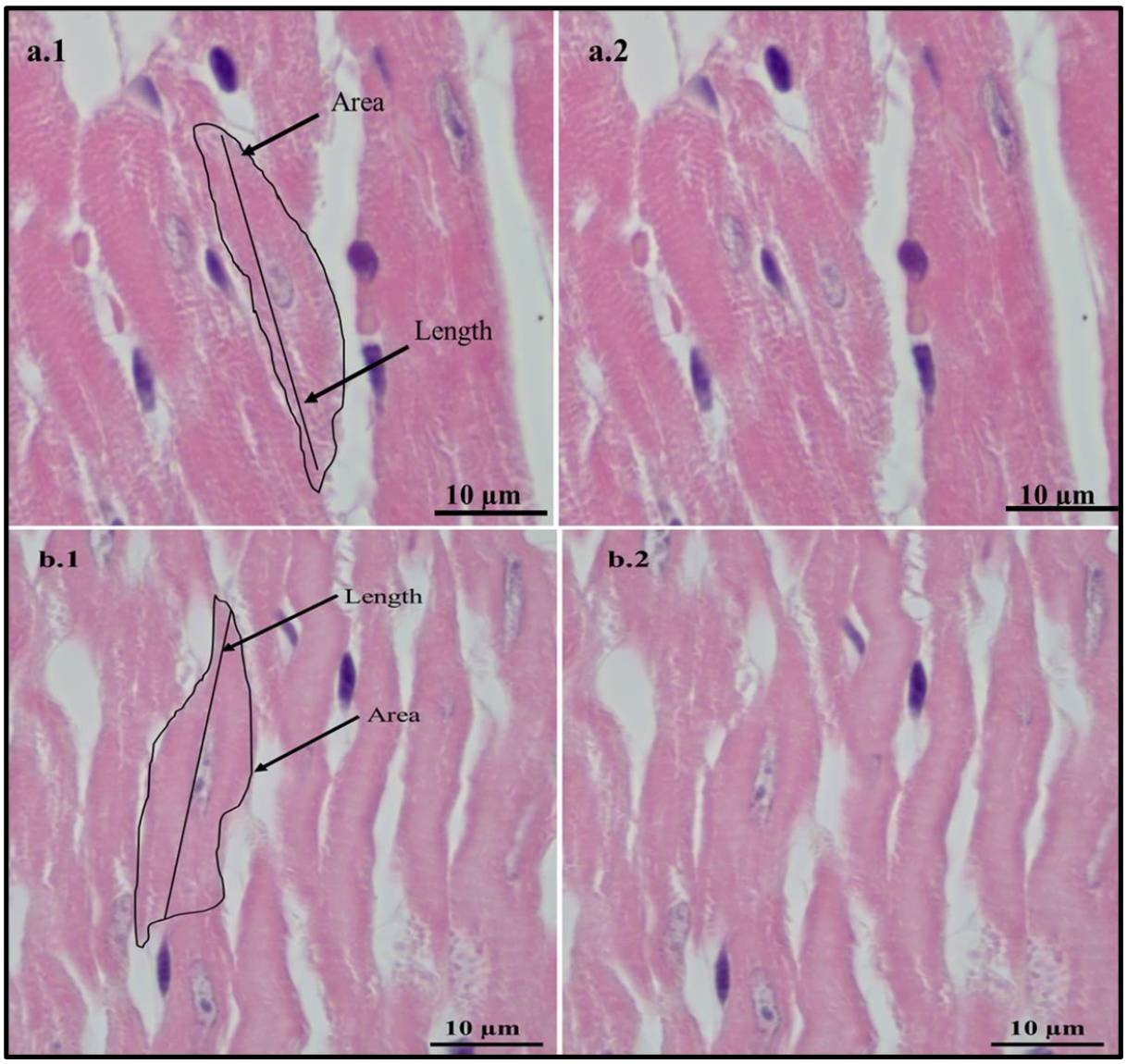



Figure 3.2: Representative micrographs of cardiomyocytes in the left ventricle. A.1 and B.1 demonstrate how the area and lengths of the cardiomyocytes were measured; A.2 and B.2 show the same cells in the left ventricular wall. A.1 and B.1. Area and length measurements of the cardiomyocytes from the left ventricle, A.2. cardiomyocyte from left ventricular wall of NT heart, B.2. cardiomyocyte from left ventricular wall of ALC heart. NT= non-treatment group, ALC= alcohol only group.

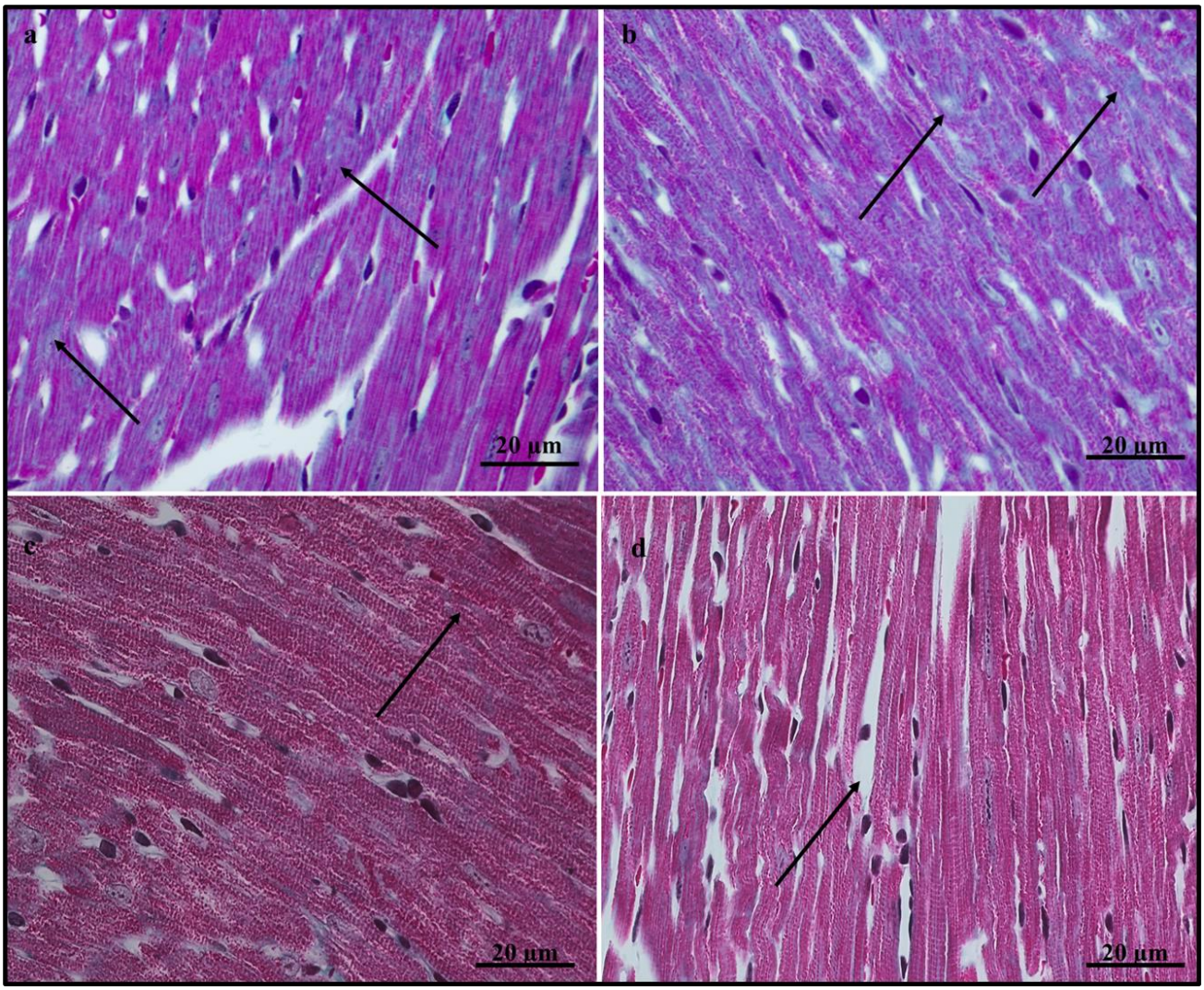



Figure 3.3: Representative micrographs of the heart demonstrating the levels of collagen in the left ventricular walls of (a) a control heart and (b, c, d) treated hearts. a. Myocardium from the NT left ventricle showing little collagen distribution, b. Myocardium from the ALC left ventricle showing increased collagen deposition, c. Myocardium from the ALC+SIM5 left ventricle showing little collagen distribution, d. Myocardium from the SMI left ventricle showing no collagen distribution. Collagen stain [arrow]. NT= non-treatment group, ALC= alcohol only group.

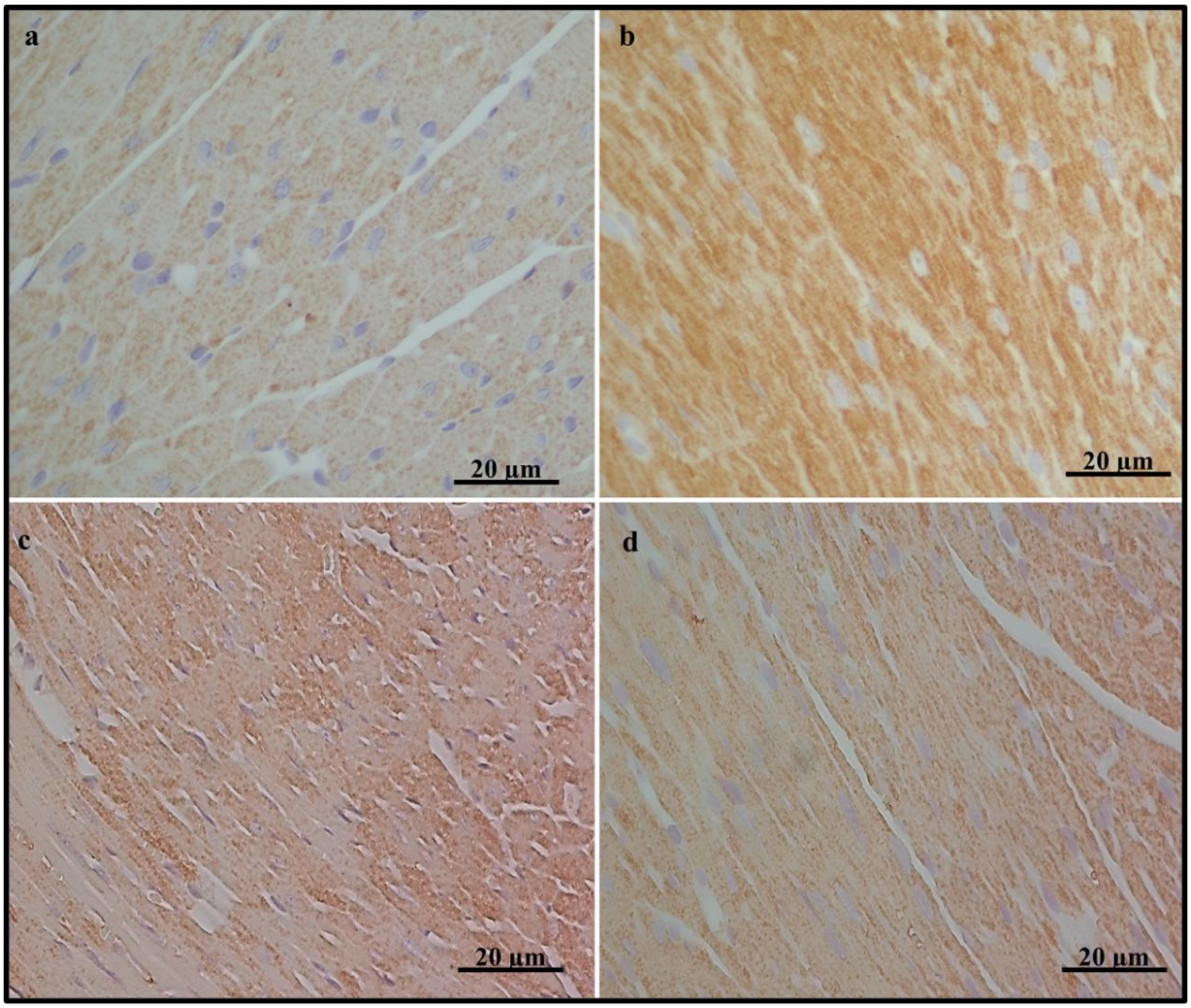



Figure 3.4: Representative micrographs of the heart demonstrating the levels of inflammation in the left ventricular walls of (a) a control heart and (b, c, d) treated hearts. a. Myocardium from the NT showing minimal TNF-α expression as indicated by the faint brown DAB stain, b. Myocardium from the ALC showing intense TNF-α expression as indicated by the darker shade of brown DAB stain, c. Myocardium from the ALC+SIM15 showing a moderate degree of TNF-α expression as indicated by the brown DAB stain, d. Myocardium from the SIM showing minimal TNF-α expression as indicated by the faint brown DAB stain. NT= non-treatment, ALC= alcohol only group.

### 3.2.2 Measurements of the cardiomyocyte area and diameter

The descriptive statistics for the cardiomyocyte diameter and area across the different experimental groups and for both sexes are shown in Table 3.2. In the females, the cardiomyocyte area and the diameter was the highest in the ALC but was lowest in the ALC+SIM5. A Kruskal-Wallis test revealed that the cardiomyocyte area and diameter was significantly different across the experimental groups ($P<0.000$). A Dunn's post hoc revealed that the area of cardiomyocytes in any paired groups was significantly different ($P<0.000$) (Fig. 3.5 and Fig. 3.6). The significant increase in cardiomyocyte area and diameter in the ALC compared to the NT validates the damaging effect of chronic alcohol on the cardiomyocytes. Alcohol-induced cardiomyocyte hypertrophy was significantly reduced in the ALC+SIM5 and in the ALC+SIM15. In addition, 5 mg simvastatin (ALC+SIM5) seems to be more effective against alcohol-induced cardiac hypertrophy than 15 mg simvastatin (ALC+SIM15).

In the males, the cardiomyocyte area or diameter was also highest in the ALC but was lowest in the ALC+SIM15 (Table 3.2). A Kruskal-Wallis test revealed that the cardiomyocyte area or diameter was significantly different across the experimental groups ($P<0.000$). A Dunn's post hoc revealed that the area of cardiomyocytes in any paired group was significantly different ($P<0.000$) (Fig. 3.5 and Fig. 3.6). The significant increase in cardiomyocyte area or diameter in the ALC compared to the NT also validates the damaging effect of chronic alcohol on the cardiomyocytes of adolescent mouse. Alcohol-induced cardiomyocyte hypertrophy was significantly reduced in the ALC+SIM5 and in the ALC+SIM15. In contrary to the findings in the females, 15 mg simvastatin (ALC+SIM15) seems to be more effective against alcohol-induced cardiac hypertrophy than 5 mg simvastatin (ALC+SIM5) in the males.

Table 3.2: Summary of the morphometries of the cardiomyocyte area and the diameter

| | | Cardiomyocyte area | | | Cardiomyocyte diameter | | | Collagen distribution | | | TNF-α distribution | | |
|---|---|---|---|---|---|---|---|---|---|---|---|---|---|
| | No of animals | No of cardiomyocytes assessed | Mean ± SD (µm) | Median (µm) | No. of cardiomyocytes assessed | Mean ± SD (µm) | Median (µm) | No of images assessed | Mean ± SD (µm) | Median (µm) | No of images assessed | Mean ± SD (%) | Median (%) |
| Female | | | | | | | | | | | | | |
| NT | 5 | 500 | 229.94 ± 95.27 | 226.31 | 500 | 28.66 ± 8.02 | 28.00 | 43 | 4.66 ± 2.95 | 4.57 | 20 | 8.74 ± 2.63 | 8.91 |
| SIM | 5 | 500 | 189.27 ± 79.37 | 180.17 | 500 | 24.47 ± 7.11 | 23.95 | 45 | 8.75 ±3.73 | 8.40 | 39 | 9.94 ± 6.25 | 8.69 |
| ALC | 5 | 500 | 346.21 ±105.54 | 329.83 | 500 | 35.51 ± 8.44 | 35.36 | 39 | 13.37 ±4.77 | 13.62 | 40 | 36.40 ± 4.35 | 37.03 |
| ALC+SIM 5 | 5 | 500 | 170.91 ±76.23 | 156.28 | 500 | 23.16 ± 7.07 | 22.11 | 43 | 9.70 ±7.04 | 7.83 | 41 | 9.83 ± 3.84 | 10.02 |
| ALC+SIM 15 | 5 | 500 | 179.15 ± 72.10 | 168.46 | 500 | 26.37 ± 7.38 | 25.50 | 41 | 4.32 ±2.67 | 3.81 | 41 | 24.50 ± 13.93 | 22.17 |
| Male | | | | | | | | | | | | | |
| NT | 5 | 500 | 270.75 ± 85.52 | 259.13 | 500 | 30.07 ± 7.85 | 29.73 | 43 | 8.25 ±3.66 | 8.84 | 40 | 11.58 ± 6.54 | 10.10 |
| SIM | 5 | 500 | 210.69 ± 78.77 | 193.97 | 500 | 28.00 ± 8.44 | 26.50 | 37 | 7.32 ±4.04 | 6.32 | 32 | 14.78 ± 8.03 | 13.67 |
| ALC | 5 | 500 | 289.32 ± 104.75 | 265.80 | 500 | 32.95 ± 9.96 | 31.41 | 38 | 13.96 ±4.69 | 13.52 | 40 | 39.13 ± 6.55 | 40.46 |
| ALC+SIM 5 | 5 | 500 | 223.74 ± 85.25 | 213.88 | 500 | 25.27 ± 7.06 | 24.50 | 39 | 4.78 ±3.03 | 3.57 | 40 | 31.28 ± 11.08 | 30.87 |
| ALC+SIM 15 | 5 | 500 | 184.02 ± 65.11 | 173.10 | 500 | 25.55 ± 6.89 | 24.94 | 39 | 13.70 ±5.93 | 13.84 | 40 | 24.72 ± 9.71 | 25.86 |

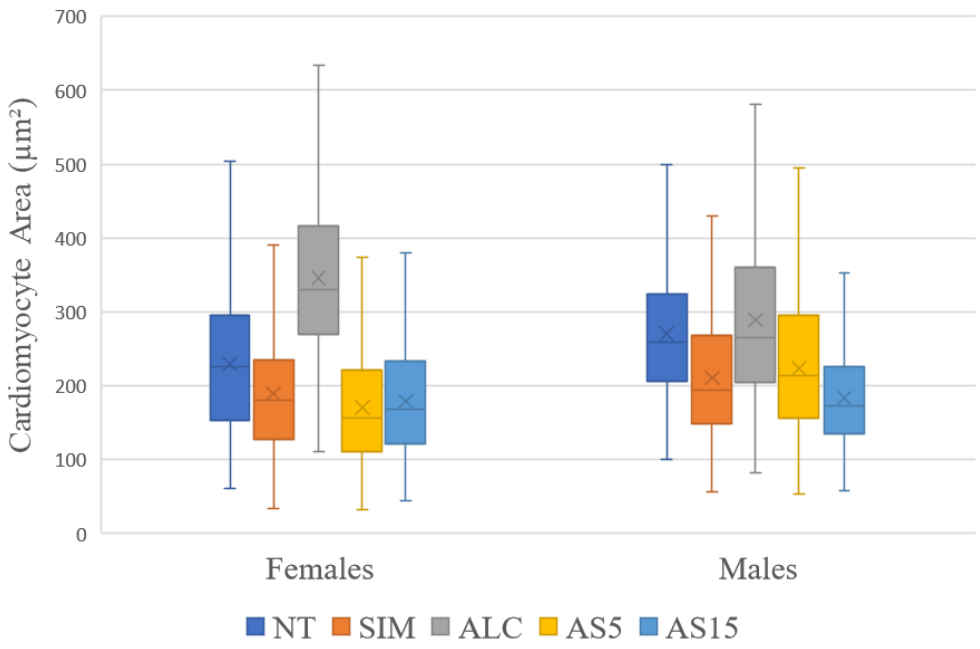



Figure 3.5: Box plots of the cardiomyocyte area across the different experimental groups and for both sexes. In both sexes, cardiomyocyte was significantly higher in the ALC than in the other groups thus confirming alcohol-induced myocardial hypertrophy. Lower dosage of simvastatin was more effective against alcohol-induced myocardial hypertrophy in females while a higher dosage of simvastatin concentration significantly reduced alcohol-induced myocardial hypertrophy in males. This seems to indicate a sex-specific differences in the effects of simvastatin against alcohol-induced myocardial hypertrophy. NT = Non-treatment; SIM = Simvastatin; ALC = Alcohol; ALC+SIM5 = 5 mg simvastatin and alcohol; ALC+SIM15 = 15 mg simvastatin and alcohol. NS = Not significant at P>0.05.

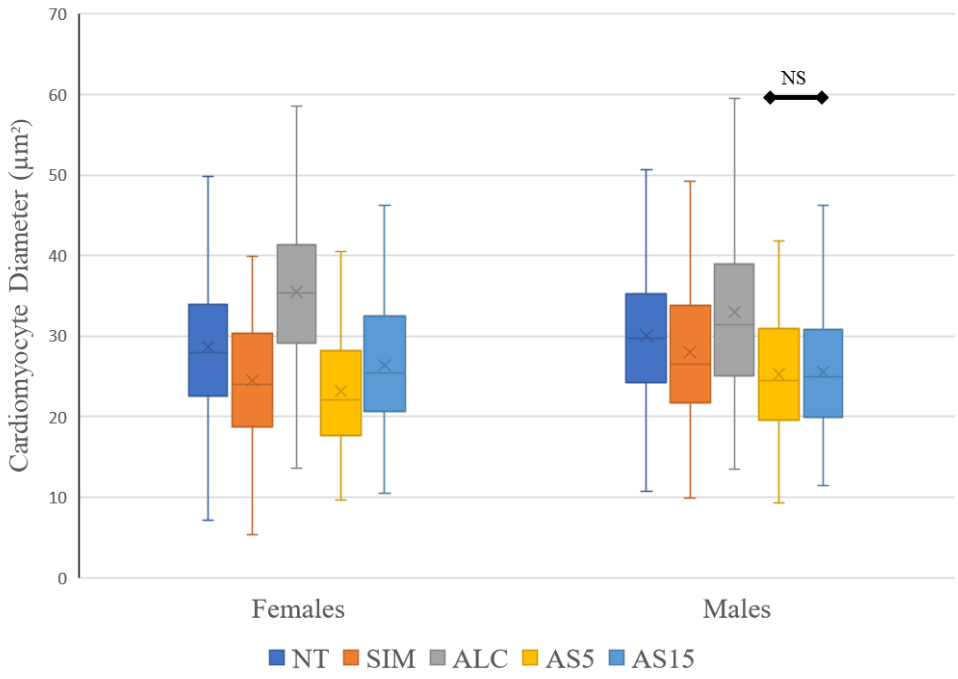



Figure 3.6: Box plots of the cardiomyocyte diameter across the different experimental groups and for both sexes. In both sexes, cardiomyocyte was significantly higher in the ALC than in the other groups thus confirming alcohol-induced myocardial hypertrophy. Lower dosage of simvastatin was more effective against alcohol-induced myocardial hypertrophy in females while both doses of simvastatin concentration significantly reduced alcohol-induced myocardial hypertrophy in males (p = 0,623). This seems to indicate a sex-specific differences in the effects of simvastatin against alcohol-induced myocardial hypertrophy. NT = Non-treatment; SIM = Simvastatin; ALC = Alcohol; ALC+SIM5 = 5 mg simvastatin and alcohol; ALC+SIM15 = 15 mg simvastatin and alcohol. NS = Not significant at P>0.05.

### 3.2.3 Measurement of collagen distribution

In the females, the collagen distribution (%) was highest in the ALC and was lowest in the NT (Table 3.2). A Kruskal-Wallis test revealed that the collagen distribution was significantly different across the experimental groups ($P$=0.000). A Dunn's post hoc revealed that collagen distribution in any paired groups was significantly different ($P$<0.000) but was similar in NT vs ALC+SIM15 ($P$=0.639) or SIM vs ALC+SIM5 ($P$=0.799) (Fig. 3.7). In addition, collagen distribution was significantly higher in the ALC than in the NT ($P$=0.000), SIM ($P$=0.002), ALC+SIM5 ($P$=0.001) or ALC+SIM15 ($P$=0.000) but it was significantly lower in the NT than in the SIM ($P$=0.000) as well as SIM was significantly lower than in the ALC+SIM15 ($P$=0.000). Similar to the cardiomyocyte hypertrophy, the significant reduction in collagen distribution in the NT than in the ALC also validates an alcohol-induced myocardial fibrosis. Similarly, both concentrations of simvastatin were effective against alcohol-induced myocardial fibrosis.

In the males, the collagen distribution (%) was also highest in the ALC but was lowest in the ALC+SIM5 (Table 3.2). A Kruskal-Wallis test revealed that the collagen distribution was significantly different across the experimental groups ($P$=0.000). A Dunn's post hoc revealed that the collagen distribution was also significantly higher in the ALC than in the NT ($P$=0.000), SIM ($P$=0.000) or ALC+SIM5 ($P$=0.000). Collagen distribution was also significantly higher in the SIM than in the ALC+SIM5 ($P$=0.013) but significantly lower than in the ALC+SIM15 ($P$=0.000). However, collagen distribution was similar in NT vs SIM ($P$=0.409) or ALC vs ALC+SIM15 ($P$=0.708) (Fig. 3.7). The significant reduction in collagen distribution in the NT than in the ALC also validates an alcohol-induced myocardial fibrosis. Surprisingly, 5 mg simvastatin was effective against alcohol-induced myocardial fibrosis to levels that are significantly lower than NT or SIM,

but 15 mg simvastatin had no benefit against alcohol-induced damage in the males unlike in the females.

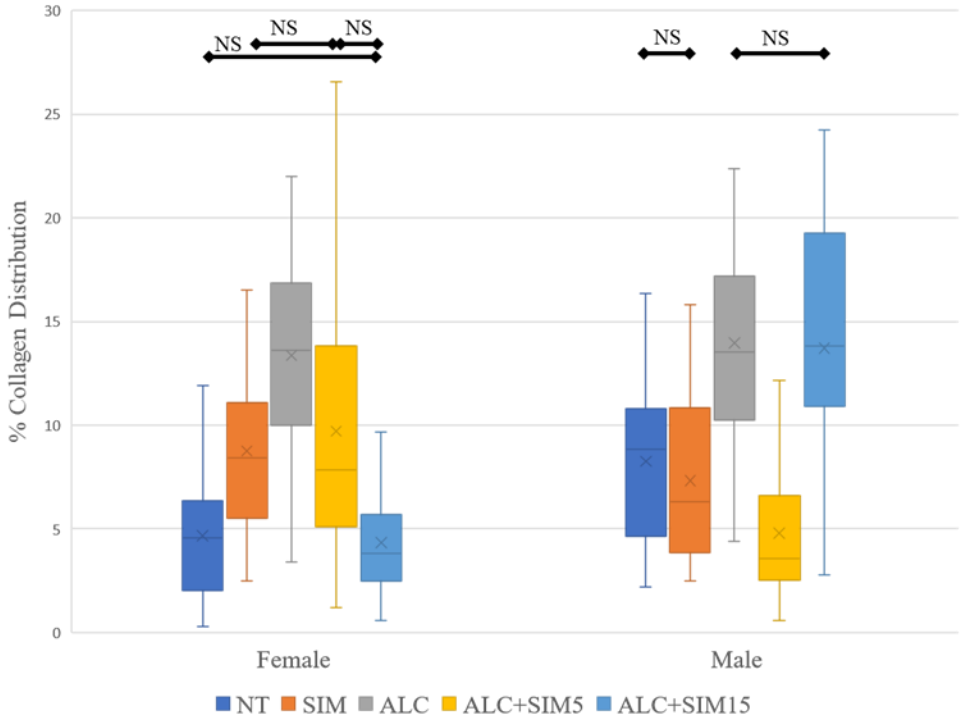



Figure 3.7: Box plots of the percentage collagen distribution across the different experimental groups and for both sexes. In both sexes, collagen distribution was significantly higher in the ALC than in the other groups thus confirming alcohol-induced myocardial fibrosis. Low and high simvastatin concentrations significantly reduced alcohol-induced myocardial fibrosis in the females but only the low simvastatin concentration was effective in the males. This seems to indicate a sex-specific differences in the effects of simvastatin against alcohol-induced myocardial fibrosis. NT = Non-treatment; SIM = Simvastatin; ALC = Alcohol; ALC+SIM5 = 5 mg simvastatin and alcohol; ALC+SIM15 = 15 mg simvastatin and alcohol. NS = Not significant at $P>0.05$.

### 3.2.4 Measurement of TNF-α distribution

In the females, the TNF-α distribution was highest in the ALC but was lowest in the NT (Table 3.2). A Kruskal-Wallis test revealed that the TNF-α distribution was significantly different across the experimental groups ($P$=0.000) while a Dunn's post hoc revealed that the TNF-α distribution in any paired groups was significantly different except for NT vs SIM ($P$=0.751), SIM vs ALC+SIM5 ($P$=0.718) or NT vs ALC+SIM5 ($P$=0.538) (Fig. 3.8). The significant reduction in TNF-α distribution in the NT than in the ALC also validates an alcohol-induced myocardial inflammation. Both concentrations of simvastatin were effective against alcohol-induced myocardial inflammation, but the low simvastatin concentration was more effective than the high simvastatin concentration against alcohol-induced myocardial inflammation.

In the males, the TNF-α distribution was highest in the ALC but was lowest in the NT like in the females (Table 3.2). A Kruskal-Wallis test revealed that the TNF-α distribution was significantly different across the experimental groups ($P$=0.000). A Dunn's post hoc revealed that the TNF-α distribution in any paired groups was significantly different except NT vs SIM ($P$=0.267) or ALC+SIM5 vs ALC+SIM15 ($P$=0.049) (Fig. 3.8). The significant reduction in TNF-α distribution in the NT than in the ALC also validates an alcohol-induced myocardial inflammation. Both concentrations of simvastatin were effective against alcohol-induced myocardial inflammation unlike in the females.

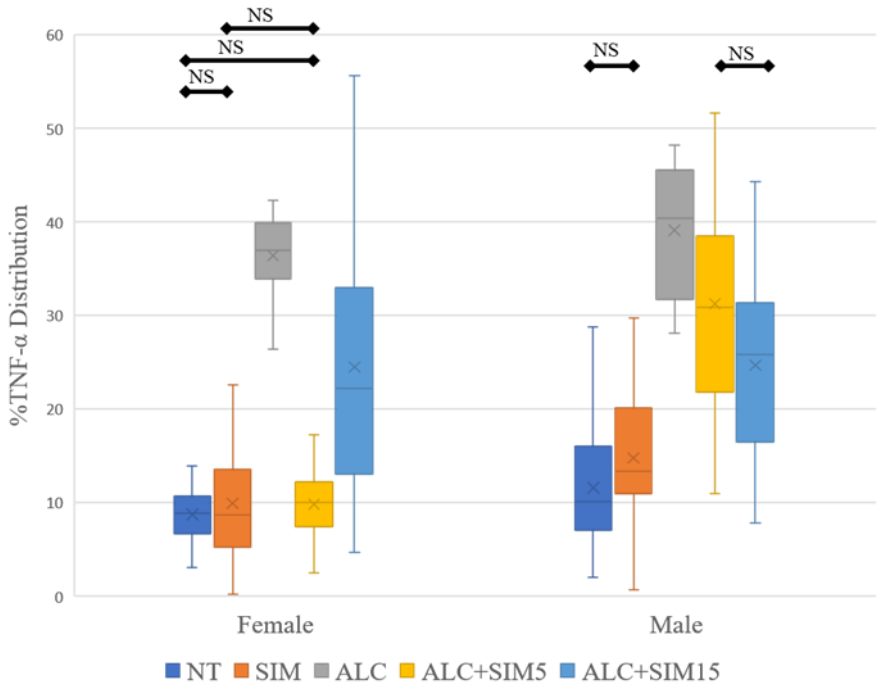



Figure 3.8: Box plots of the percentage TNF-α distribution across the different experimental groups and for both sexes. In both sexes, TNF-α distribution was significantly higher in the ALC than in the other groups thus confirming alcohol toxicity on the cardiomyocytes. TNF-α distribution was improved in the ALC+SIM5 in the females to the level of NT but not in the ALC+SIM15. However, either ALC+SIM5 or ALC+SIM15 did not significantly lower TNF-α distribution to the level of the NT in the males. This is an indication of sex-specific differences in the effect of simvastatin again alcohol effects in the cardiomyocytes. NT = Non-treatment; SIM = Simvastatin; ALC = Alcohol; ALC+SIM5 = 5 mg simvastatin and alcohol; ALC+SIM15 = 15 mg simvastatin and alcohol. NS = Not significant at P>0.05.

## 3.3 The Kidney

### 3.3.1 General morphology of the renal corpuscles and tubules

The morphology of the tubules and renal corpuscles from the NT group was normal i.e., the tubular epithelial brush border was intact, and the glomeruli were neither swollen nor retracted. The tubular epithelia from the ALC group showed loss of brush border and the glomeruli were swollen. The NT and SIM groups had no interstitial fibrosis, while most of the sections from the ALC group showed tubulointerstitial fibrosis. The NT group showed little to no TNF-α expression in the renal corpuscles and tubules while the renal corpuscles and tubules in the ALC showed intense TNF-α expression.




Figure 3.9: Representative micrograph of the cross-section of the kidney demonstrating the cortex and medulla regions. C= cortex region, M= medulla region.

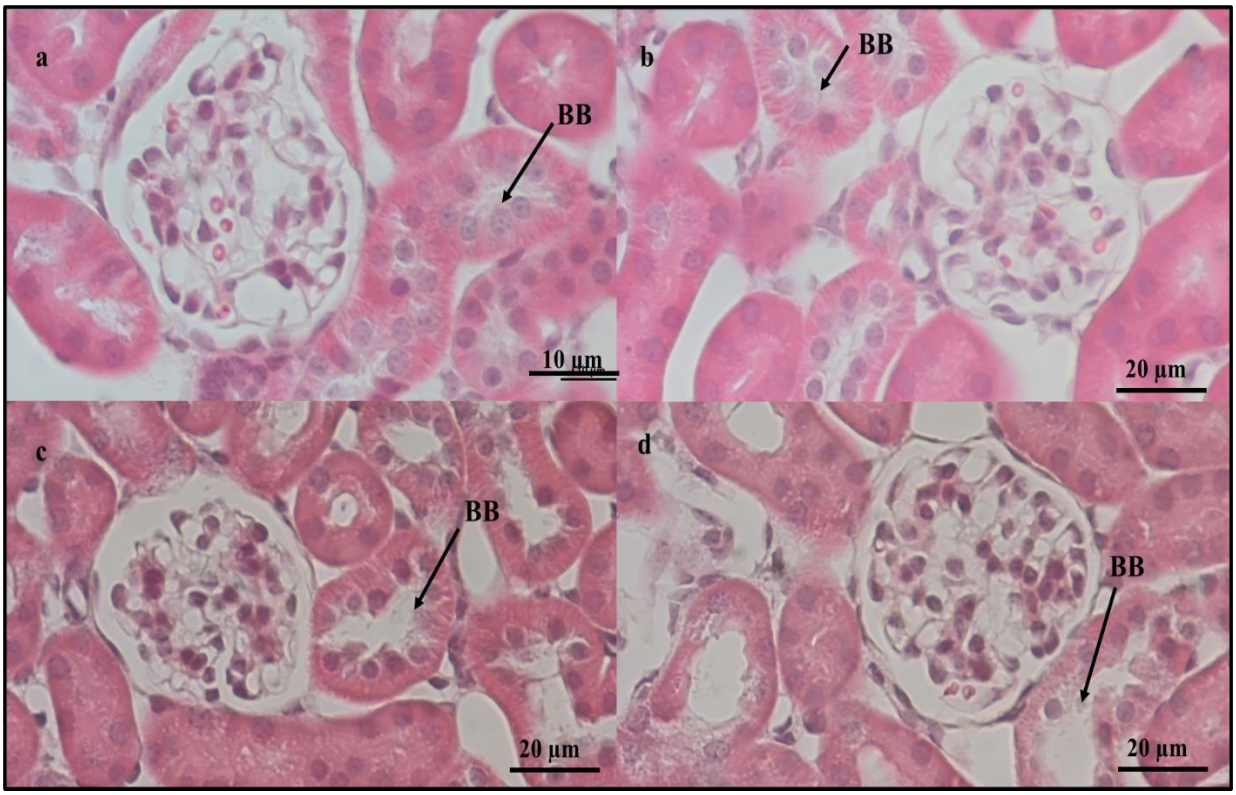



Figure 3.10: Representative micrographs of the kidney demonstrating normal renal morphology and renal tissue with pathology. a and b. Kidneys from NT showing normal morphology, c. Kidney from ALC showing a loss of brush border, d. Kidney from ALC showing a swollen glomerulus and a loss of brush border. NT= non-treatment group, ALC= alcohol only group, BB- brush border.




Figure 3.11: Representative micrograph of the kidney demonstrating how the measurements of the glomerulus and renal corpuscle was obtained, and a demonstration of tubular morphology. a. Tracing of renal corpuscle and glomerular area measurements, b. Renal tubule morphology. RC= renal corpuscle area, GL= glomerular area, RT= renal tubules.

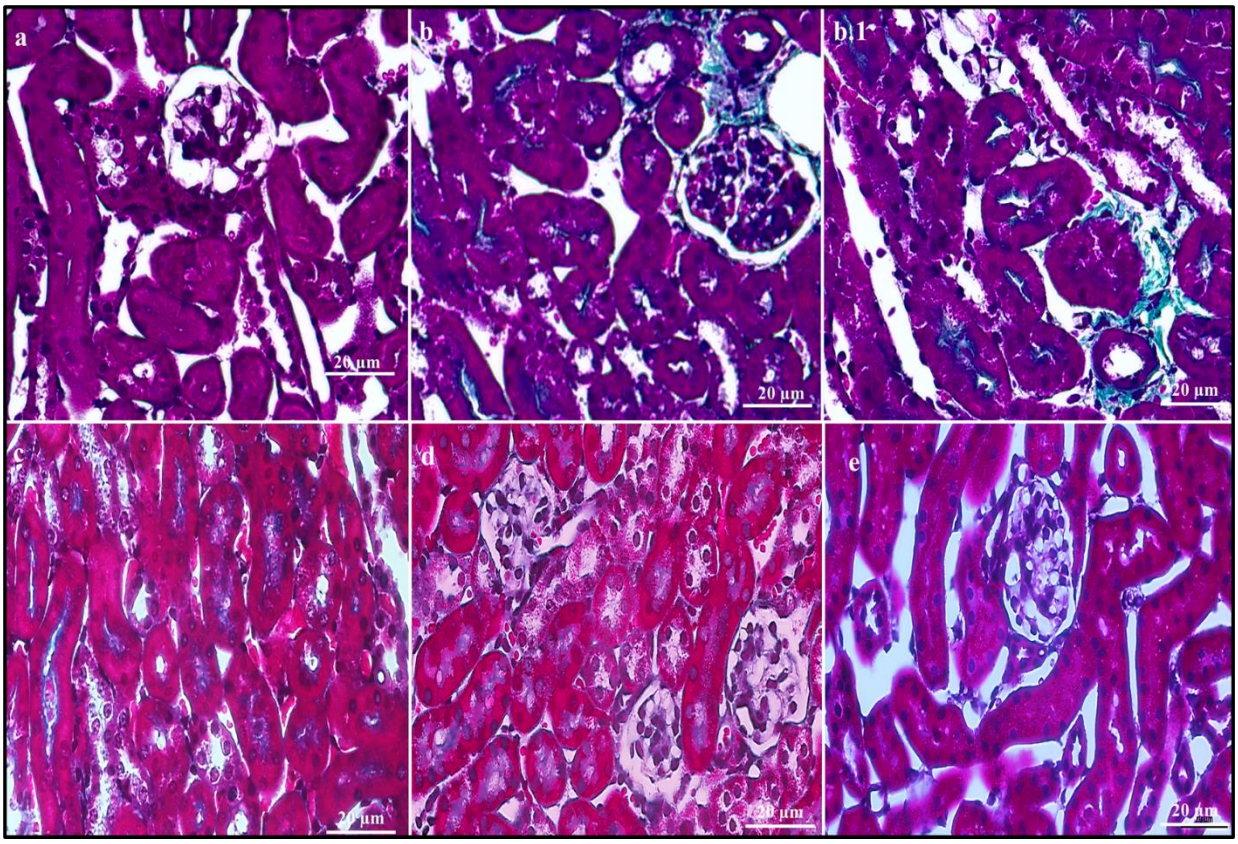



Figure 3.12: Representative micrographs of the kidney demonstrating the differences in collagen distribution in normal tissue and alcohol-treated tissue. a. Kidney from the NT showing no collagen deposition in the tubules and the interstitium, b and b.1. Kidneys from the ALC showing increased collagen deposition in the tubules and interstitium i.e., tubulointerstitial fibrosis, c. Kidney from ALC+SIM5 showing minimal collagen deposition in the tubules, d. Kidney from ALC+SIM15 showing minimal collagen deposition in the tubules and no collagen deposition in the interstitium, e. Kidney from SIM showing no collagen deposition in the tubules and the interstitium. NT= non-treatment, ALC= alcohol only group.

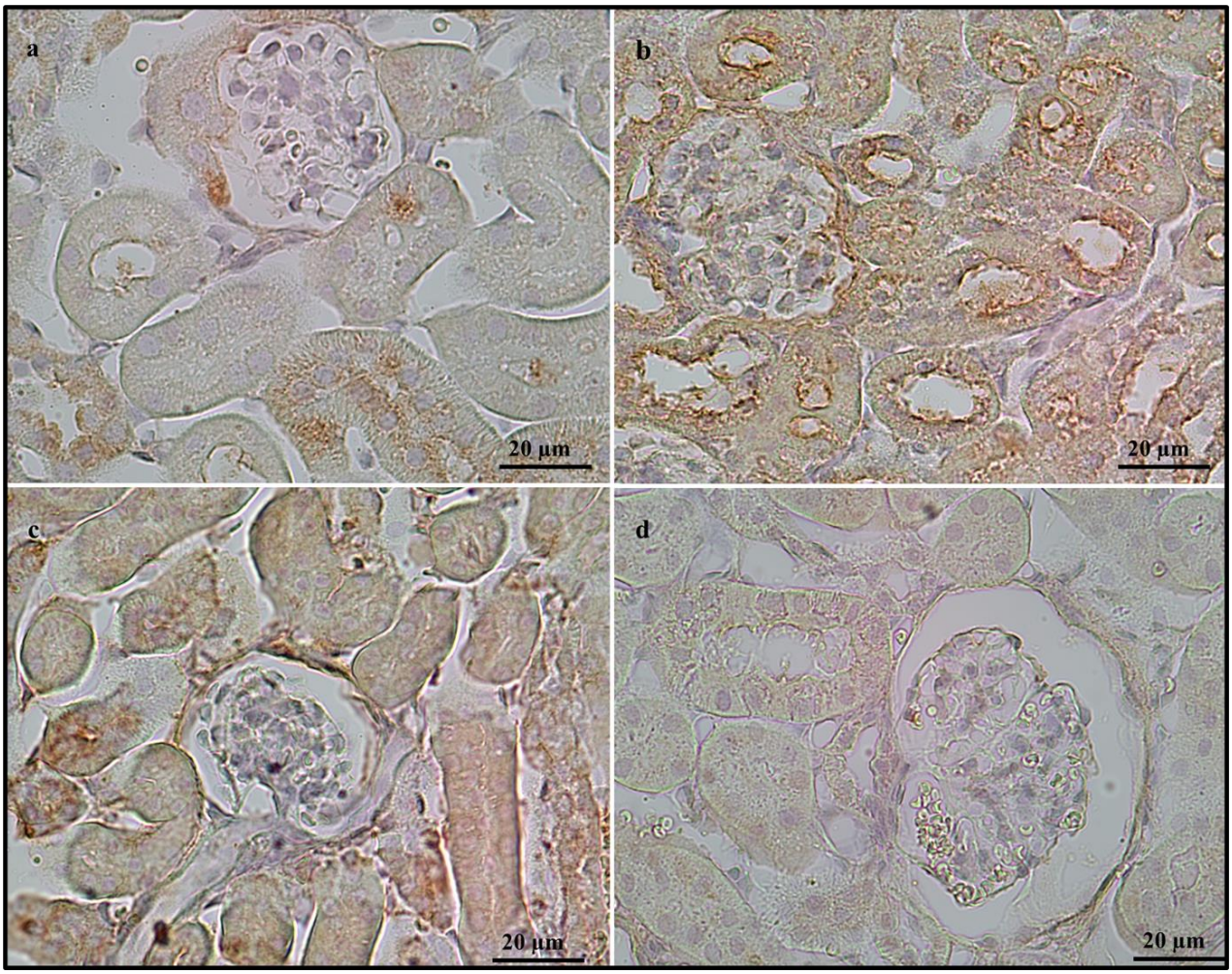



Figure 3.13: Representative micrographs of the kidney demonstrating the levels of inflammation in the renal tissues from different treatment groups. a. NT kidney showing minimal TNF-α expression in the tubules and corpuscles, b. ALC kidney showing intense TNF-α expression in the tubules and corpuscles, c. ALC+SIM5 kidney showing moderate TNF-α expression in the tubules and corpuscles, d. ALC+SIM15 kidney showing minimal TNF-α expression in the tubules and corpuscles. NT= non-treatment, ALC= alcohol only group, ALC+SIM5= alcohol and simvastatin 5 mg, ALC+SIM15= alcohol and simvastatin 15 mg.

### 3.3.2 Morphometry of the area of renal corpuscle

In the females, the area of renal corpuscle was highest in the ALC and was lowest in the ALC+SIM5 (Table 3.3). A Kruskal-Wallis test revealed that the area of renal corpuscle was significantly different across the experimental groups ($P$=0.000). A Dunn's post hoc revealed that the area of renal corpuscle was significantly higher in the ALC than in the NT ($P$=0.001) or the ALC+SIM5 ($P$=0.000). However, the area of renal corpuscle was similar in the NT vs SIM ($P$=0.155), the NT vs ALC+SIM5 ($P$=0.132), SIM vs ALC ($P$=0.073) or ALC vs ALC+SIM15 ($P$=0.140) (Fig. 3.14). The significant difference between the ALC vs NT validates the toxicity of alcohol on the size of the renal corpuscle. 5 mg simvastatin significantly reduced the effect of alcohol on the size of the renal corpuscle but not 15 mg simvastatin.

In contrary to the females, the area of renal corpuscle was highest in the ALC+SIM15 and was lowest in the ALC+SIM5 in the males (Table 3.3). A Kruskal-Wallis test revealed that the renal corpuscle area was significantly different across the experimental groups ($P$=0.000). A Dunn's post hoc revealed that the area of the renal corpuscle in any paired groups was significantly different except the SIM vs ALC+SIM5 ($P$=0.058) or ALC vs ALC+SIM15 ($P$=0.117) (Fig. 3.14). The significant difference between the ALC vs NT ($P$=0.012) also validates the toxicity of alcohol on the area of renal corpuscle. Similar to the females, 5 mg simvastatin significantly reduced the effect of alcohol on the size of the renal corpuscle but not 15 mg simvastatin.

### 3.3.3 Morphometry of the glomerular area

In the females, the glomerular area was highest in the ALC and was lowest in the ALC+SIM5 (Table 3.3). A Kruskal-Wallis test revealed that the glomerular area was significantly different across the experimental groups ($P$=0.000). A Dunn's post hoc revealed that the

glomerular area in any paired groups was significantly different except the NT vs SIM (*P*=0.557) or the NT vs ALC+SIM5 (*P*=0.188) or SIM vs ALC+SIM5 (*P*=0.057) (Fig. 3.15). In addition, the glomerular area was significantly higher in the ALC than in the NT (*P*=0.000), SIM (*P*=0.000), ALC+SIM5 (*P*=0.000) or ALC+SIM15 (*P*=0.001). The significant difference between ALC vs NT also validates the toxicity of alcohol on the glomerular area. Both concentrations of simvastatin were effective against the alcohol effect on glomerular area however, 5 mg simvastatin seems to be more effective than 15 mg simvastatin.

In the males, the glomerular area was highest in the ALC+SIM15 and was lowest in the ALC+SIM5 (Table 3.3). A Kruskal-Wallis test revealed that the glomerular area was significantly different across the experimental groups (*P*=0.000). A Dunn's post hoc revealed that the area of the glomerulus in any paired groups was significantly different except for SIM vs ALC+SIM5 (*P*=0.856) or ALC vs ALC+SIM15 (*P*=0.139) (Fig. 3.15). The significant difference between ALC vs NT also validates the toxicity of alcohol on the glomerular area. In contrary to the females, only the lower concentration of simvastatin (5 mg) was effective against the alcohol effect on the glomerular area.

### 3.3.4 Morphometry of the area of the urinary space

In the females, the area of urinary space was highest in the SIM and was lowest in the ALC (Table 3.3). A Kruskal-Wallis test revealed that the area of urinary space was significantly different across the experimental groups (*P*=0.000). A Dunn's post hoc revealed that the area of the urinary space was significantly lower in the ALC than in the NT (*P*=0.000), SIM (*P*=0.000), ALC+SIM5 (*P*=0.000) or ALC+SIM15 (*P*=0.001). However, there was no significant difference in the area of urinary space in the NT vs SIM (*P*=0.085) or the NT vs ALC+SIM5 (*P*=0.101) (Fig. 3.16). The significant difference between ALC vs NT validates the toxicity of alcohol on the area of urinary

space. Both concentrations of simvastatin were effective against the alcohol effect on the area of urinary space however, 5 mg simvastatin seems to be more effective than 15 mg simvastatin.

In the males, the area of urinary space was highest in the SIM and was lowest in the ALC+SM15 (Table 3.3). A Kruskal-Wallis test revealed that the urinary space area was significantly different across the experimental groups ($P$=0.000). A Dunn's post hoc revealed that the area of urinary space was significantly lower in the ALC than in the NT ($P$=0.000), SIM ($P$=0.000) or ALC+SIM5 ($P$=0.005) but not in the NT vs SIM ($P$=0.687) or the ALC vs ALC+SIM15 ($P$=0.449) (Fig. 3.16). The significant difference between the ALC vs NT also validates the toxicity of alcohol on the area of urinary space. In contrary to the females, only the lower concentration of simvastatin (5 mg) was effective against the alcohol effect on the area of urinary space in the males.

Table 3.3: Summary of the morphometries of the renal corpuscle, glomerular and urinary space

| | No of animals | No of images assessed | Renal corpuscle area | | Glomerular area | | Urinary Space area | |
|---|---|---|---|---|---|---|---|---|
| | | | Mean (± SD) (μm) | Median (μm) | Mean (± SD) (μm) | Median (μm) | Mean (± SD) (μm) | Median (μm) |
| Female | | | | | | | | |
| NT | 5 | 269 | 845.47 (±380.61) | 799.91 | 577.55 (±260.94) | 560.64 | 267.92 (±163.05) | 228.66 |
| SIM | 5 | 269 | 857.75 (±337.09) | 828.23 | 574.32 (±230.79) | 569.94 | 283.42 (±148.15) | 247.99 |
| ALC | 5 | 268 | 902.97 (±306.31) | 856.60 | 710.14 (±242.61) | 670.43 | 192.84 (±113.00) | 166.11 |
| ALC+SIM5 | 5 | 270 | 786.936 (±291.34) | 766.83 | 545.28 (±218.28) | 516.37 | 243.17 (±121.72) | 219.11 |
| ALC+SIM15 | 5 | 262 | 880.54 (±330.33) | 820.07 | 642.62 (±240.89) | 615.23 | 237.92 (±160.28) | 189.13. |
| Male | | | | | | | | |
| NT | 5 | 259 | 857.30 (±306.82) | 791.63 | 601.46 (±236.43) | 568.06 | 255.84 (±116.24) | 237.58 |
| SIM | 5 | 260 | 808.62 (±414.51) | 762.49 | 528.72 (±262.39) | 524.96 | 279.90 (±184.92) | 240.31 |
| ALC | 5 | 265 | 917.64 (±288.23) | 885.31 | 726.15 (±246.20) | 704.54 | 191.49 (±103.41) | 179.08 |
| ALC+SIM5 | 5 | 269 | 754.59 (±351.60) | 692.95 | 525.04 (±254.04) | 487.06 | 229.55 (±144.06) | 199.47 |
| ALC+SIM15 | 5 | 264 | 966.82 (±314.27) | 922.38 | 755.08 (±242.84) | 734.53 | 211.74 (±144.11) | 173.81 |

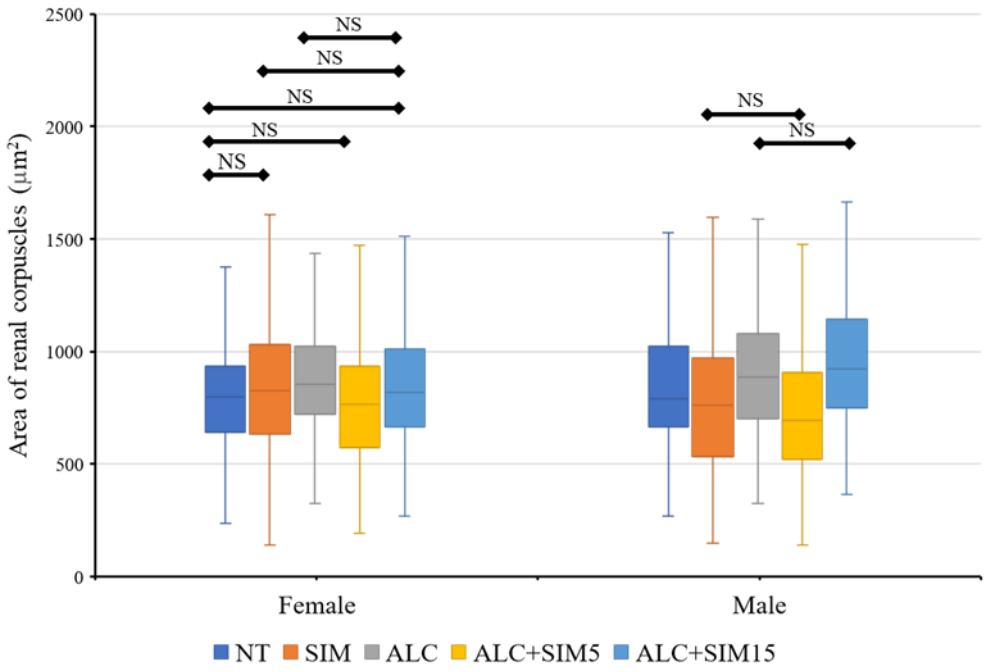



Figure 3.14: Box plots of the area of renal corpuscle across the different experimental groups and for both sexes. In both sexes, the area of renal corpuscle was significantly higher in the ALC than in the NT thus confirming alcohol-induced renal damage. Low simvastatin concentration (5 mg) significantly reduced the effect of alcohol on the area of renal corpuscle but not the high concentration of simvastatin (15 mg) in both sexes. NT = Non-treatment; SIM = Simvastatin; ALC = Alcohol; ALC+SIM5 = 5 mg simvastatin and alcohol; ALC+SIM15 = 15 mg simvastatin and alcohol. NS = Not significant at P>0.05.

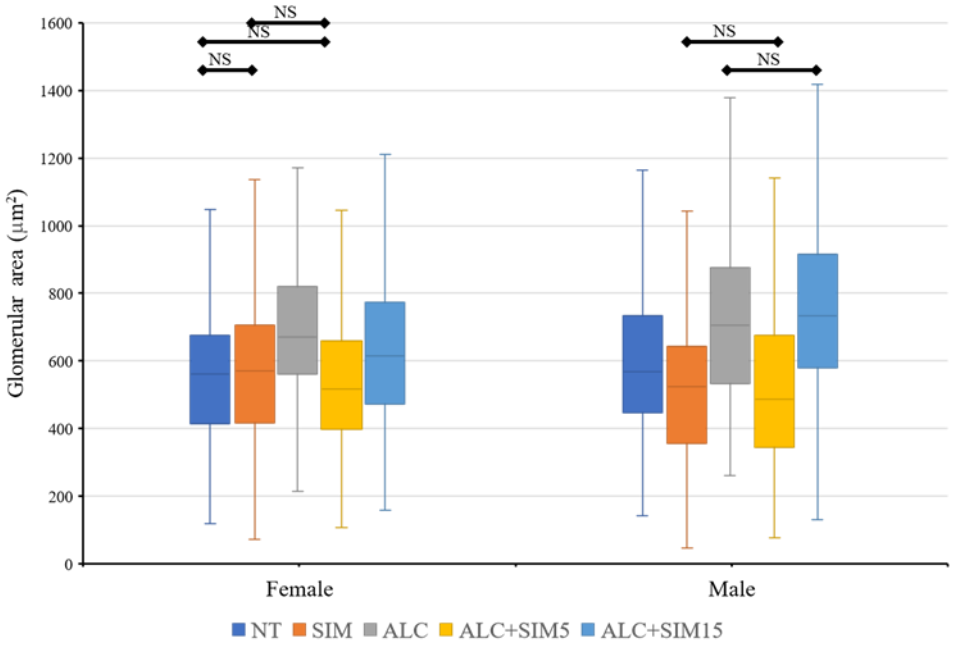



Figure 3.15: Box plots of the glomerular area across the different experimental groups and for both sexes. In both sexes, the glomerular area was significantly higher in the ALC than in the NT thus confirming alcohol-induced renal damage. In the females, both concentrations of simvastatin were effective against alcohol effect on glomerular area however only the lower concentration of simvastatin (5 mg) was effective in the males. This is an indication of a sex-specific differences in the effect of simvastatin against alcohol toxicity on the renal tissues. NT = Non-treatment; SIM = Simvastatin; ALC = Alcohol; ALC+SIM5 = 5 mg simvastatin and alcohol; ALC+SIM15 = 15 mg simvastatin and alcohol. NS = Not significant at P>0.05.

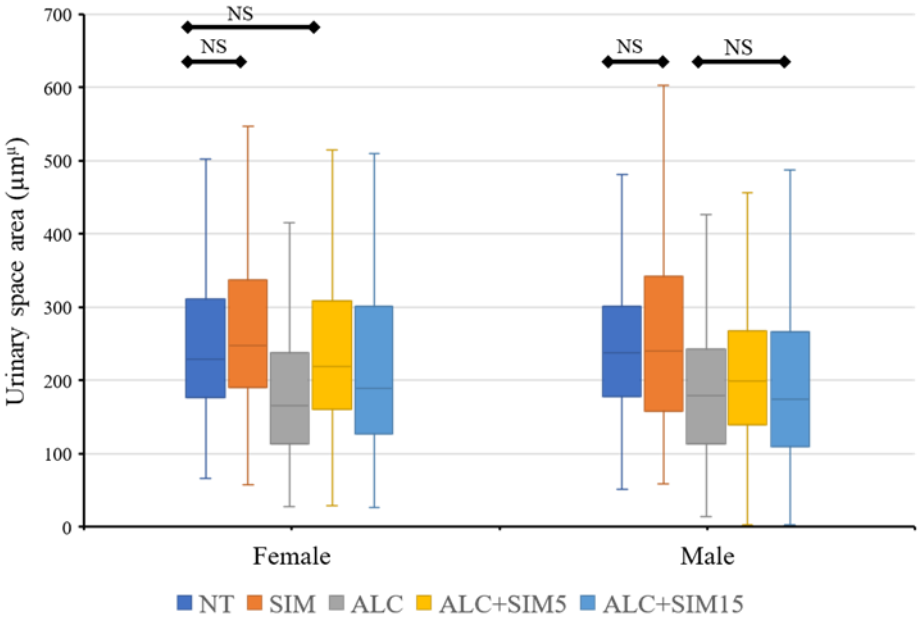



Figure 3.16: Box plots of the area of urinary space across the different experimental groups and for both sexes. In both sexes, the glomerular area was significantly lower in the ALC than in the NT thus confirming alcohol-induced renal damage. In the females, both concentrations of simvastatin were effective against alcohol effect on the area of urinary space however only the lower concentration of simvastatin (5 mg) was effective in the males. This is an indication of a sex-specific differences in the effect of simvastatin against alcohol toxicity on the renal tissues. NT = Non-treatment; SIM = Simvastatin; ALC = Alcohol; ALC+SIM5 = 5 mg simvastatin and alcohol; ALC+SIM15 = 15 mg simvastatin and alcohol. NS = Not significant at $P>0.05$.

### 3.3.5 Measurement of collagen distribution

In the females, the percentage collagen distribution in the kidney was highest in the ALC and was lowest in the NT (Table 3.4). A Kruskal-Wallis test revealed that the collagen distribution was significantly different across the experimental groups ($P$=0.000). A Dunn's post hoc revealed that the collagen distribution was significantly higher in the ALC than in the NT ($P$=0.000), SIM ($P$=0.000), ALC+SIM5 ($P$=0.000) or ALC+SIM15 ($P$=0.000) (Fig 3.17). The significant difference between ALC vs NT validates alcohol-induced fibrosis in the kidney. Both concentrations of simvastatin were significantly effective against alcohol-induced renal fibrosis, but the higher simvastatin concentration seems to be more effective.

In the males, the percentage collagen distribution in the kidney was highest in the ALC and was lowest in the NT (Table 3.4). A Kruskal-Wallis test revealed that the collagen distribution was significantly different across the experimental groups ($P$=0.000). A Dunn's post hoc revealed that the collagen distribution was significantly higher in the ALC than in the NT ($P$=0.000), SIM ($P$=0.000), ALC+SIM5 ($P$=0.000) or ALC+SIM15 ($P$=0.000) except in the SIM vs ALC+SIM15 ($P$=0.163) (Fig. 3.17). The significant difference between the ALC vs NT also validates the alcohol-induced renal fibrosis. Similar to the females, both concentrations of simvastatin were significantly effective against alcohol-induced renal fibrosis in the males.

### 3.3.6 Measurement of TNF-α distribution

The pattern of TNF-α distribution was identical in the renal tubule and in the renal corpuscle for both sexes. The TNF-α distribution in the renal tubules or in the renal corpuscle was highest in the ALC and was lowest in the NT for both sexes (Table 3.4). In the females, a Kruskal-Wallis test revealed that the TNF-α distribution was significantly different across the experimental groups ($P$=0.000) while a Dunn's post hoc revealed that the TNF-α distribution in any paired groups was significantly different except in the SIM vs ALC+SIM15 for the renal

tubule (*P*=0.453) or in the SIM vs ALC+SIM5 (*P*=0.200) for the renal corpuscle (Fig. 3.18 & 3.19). The significant difference between the ALC vs NT also validates alcohol-induced inflammation in the renal tissue. Both concentrations of simvastatin were effective in reducing alcohol-induced inflammation in the renal tissue.

In the males, a Kruskal-Wallis test also revealed that the TNF-α distribution was significantly different across the experimental groups (*P*=0.000), while a Dunn's post hoc revealed that the TNF-α distribution in any paired groups for the renal tubule or corpuscle was significantly different except in the ALC+SIM5 vs ALC+SIM15 (*P*=0.733) for the renal tubule (Fig. 3.18 & 3.19). The significant difference between the ALC vs NT also confirms alcohol-induced inflammation in the renal tissue and both concentrations of simvastatin were effective in reducing alcohol-induced inflammation in the renal tissue.

Table 3.4: Summary of the collagen and TNF-α distributions in the kidney

| | No of animals | Collagen Distribution | | | TNF-α Distribution | | | | |
|---|---|---|---|---|---|---|---|---|---|
| | | | | | | Renal tubules | | Renal corpuscles | |
| | | No of images assessed | Mean (±SD) (%) | Median (%) | No of ROIs assessed | Mean (±SD) (%) | Median (%) | Mean (±SD) (%) | Median (%) |
| Female | | | | | | | | | |
| NT | 5 | 260 | 0.51 (±0.14) | 0.48 | 225 | 1.03 (±0.15) | 1.04 | 0.70 (±0.15) | 0.68 |
| SIM | 5 | 260 | 1.48 (±1.22) | 1.14 | 215 | 1.93 (±0.84) | 1.79 | 2.39 (±1.09) | 2.13 |
| ALC | 5 | 231 | 6.52 (±2.60) | 6.35 | 260 | 11.04 (±1.54) | 11.43 | 11.13 (±2.71) | 10.61 |
| ALC+SIM5 | 5 | 259 | 3.18 (±1.73) | 2.78 | 260 | 1.69 (±0.78) | 1.74 | 2.56 (±1.60) | 2.35 |
| ALC+SIM15 | 5 | 257 | 1.35 (±1.44) | 0.76 | 259 | 1.67 (±0.20) | 1.67 | 1.41 (±0.33) | 1.43 |
| Male | | | | | | | | | |
| NT | 5 | 260 | 0.67 (±0.21) | 0.65 | 217 | 1.00 (±0.21) | 0.97 | 0.79 (±0.20) | 0.77 |
| SIM | 5 | 259 | 1.81 (±1.66) | 1.14 | 191 | 1.56 (±0.54) | 1.52 | 1.84 (±0.66) | 1.77 |
| ALC | 5 | 258 | 6.13 (±5.87) | 5.87 | 260 | 9.51 (±2.02) | 9.40 | 8.94 (±2.92) | 8.99 |
| ALC+SIM5 | 5 | 255 | 2.78 (±1.41) | 2.38 | 261 | 1.85 (±0.30) | 1.88 | 2.48 (±1.05) | 2.26 |
| ALC+SIM15 | 5 | 261 | 2.13 (±1.49) | 2.05 | 259 | 1.90 (±0.37) | 1.84 | 1.58 (±0.57) | 1.63 |

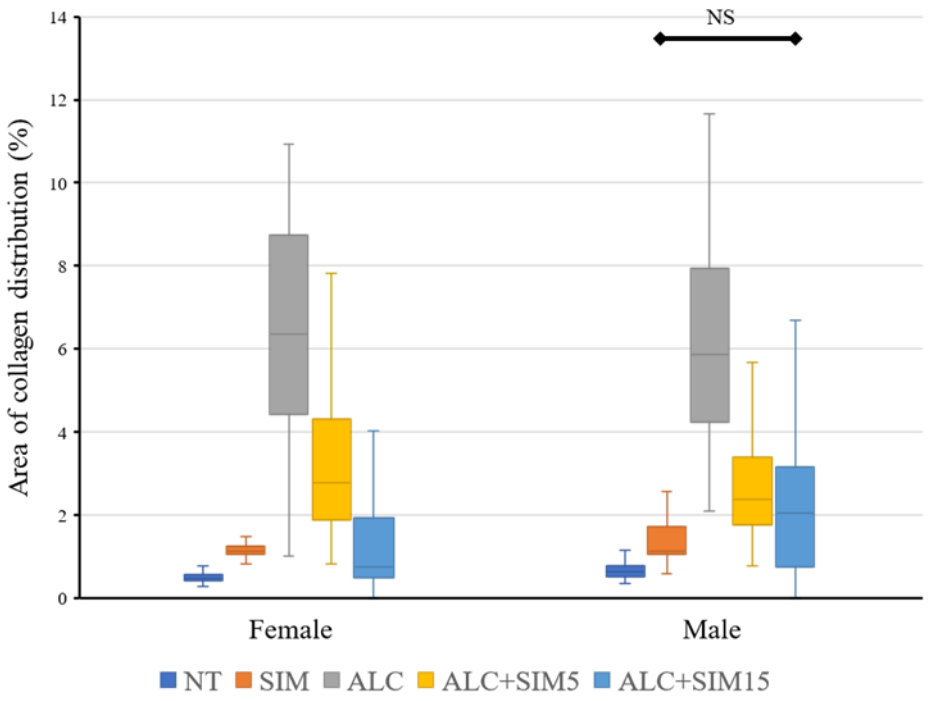



Figure 3.17: Box plots of the collagen distribution across the different experimental groups and for both sexes. In both sexes, the collagen distribution was significantly higher in the ALC than in the NT thus confirming alcohol-induced renal fibrosis. Both concentrations of simvastatin were effective against alcohol-induced renal fibrosis. NT = Non-treatment; SIM = Simvastatin; ALC = Alcohol; ALC+SIM5 = 5 mg simvastatin and alcohol; ALC+SIM15 = 15 mg simvastatin and alcohol. NS = Not significant at P>0.05.

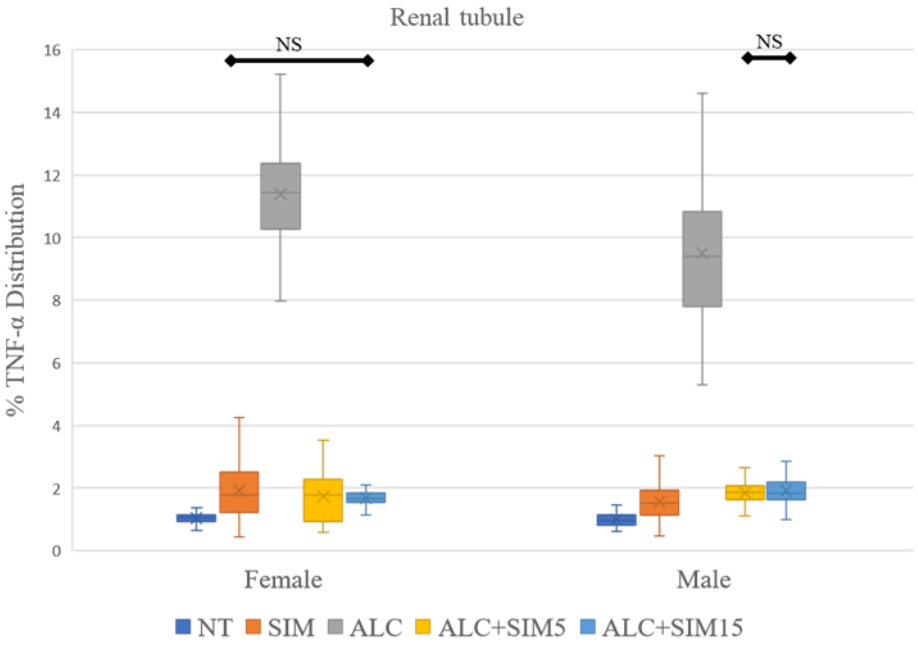



Figure 3.18: Box plots of the TNF-α distribution in the renal tubules across the different experimental groups and for both sexes. In both sexes, the TNF-α distribution was significantly higher in the ALC than in the NT thus confirming alcohol-induced renal inflammation. Both concentrations of simvastatin were effective against alcohol-induced renal inflammation in the tubules. NT = Non-treatment; SIM = Simvastatin; ALC = Alcohol; ALC+SIM5 = 5 mg simvastatin and alcohol; ALC+SIM15 = 15 mg simvastatin and alcohol. NS = Not significant at $P>0.05$.

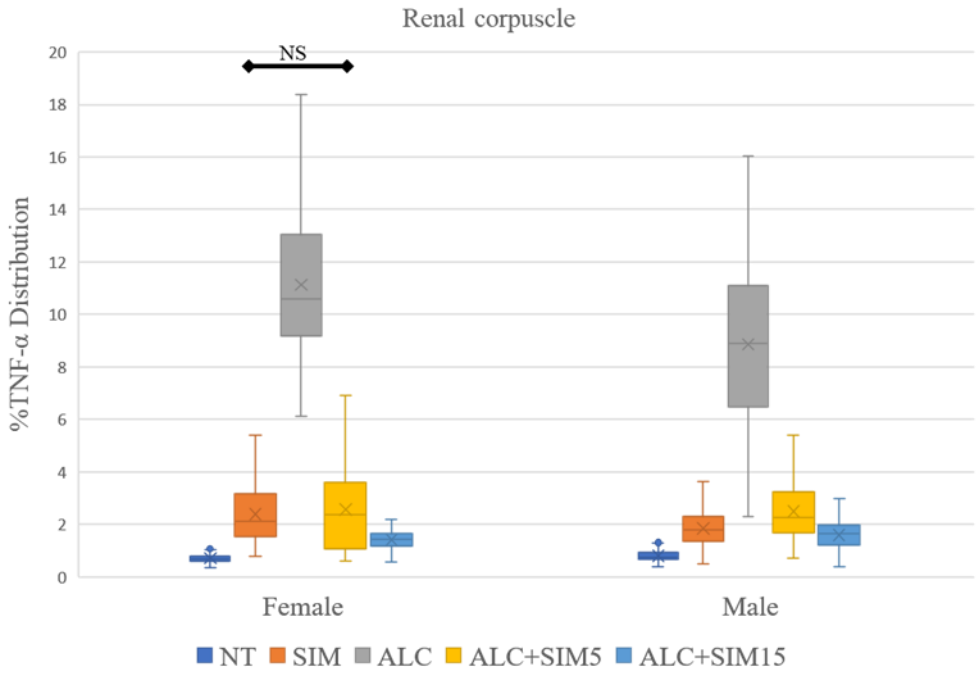



Figure 3.19: Box plots of the TNF-α distribution in the renal corpuscles across the different experimental groups and for both sexes. In both sexes, the TNF-α distribution was significantly higher in the ALC than in the NT thus confirming alcohol-induced renal inflammation. Both concentrations of simvastatin were effective against alcohol-induced renal inflammation in the corpuscles. NT = Non-treatment; SIM = Simvastatin; ALC = Alcohol; ALC+SIM5 = 5 mg simvastatin and alcohol; ALC+SIM15 = 15 mg simvastatin and alcohol. NS = Not significant at $P>0.05$.

## 3.4 The liver

### 3.4.1 General morphology of the liver

The morphology of the liver in the NT showed normal hepatic parenchyma which consists of normally arranged hepatocytes in plates radiating outward from the central vein. The hepatocytes were normally shaped with centrally placed nuclei. The plates of hepatocytes were separated by sinusoids, the lumens of the sinusoids were clear of red blood cells. There was no aggregation of Kupffer cells in the parenchyma in the NT. In the ALC, the hepatocytes in the parenchyma were normally shaped with centrally placed nuclei and there was aggregation of Kupffer cells along the length of the parenchyma. The parenchyma in the ALC+SIM5 and ALC+SIM15 had a few hepatocytes which were not normally shaped, and the radial arrangements of the parenchyma was disrupted. The hepatocytes showed ballooning degeneration also called hydropic swelling, which is characterised by a pale and distended cytoplasm. The sinusoids were filled with red blood cells. There was an aggregation of Kupffer cells along the length of the parenchyma. The livers from the ALC showed the early stages of perisinusoidal fibrosis. The parenchyma from the ALC showed intense TNF-α expression.

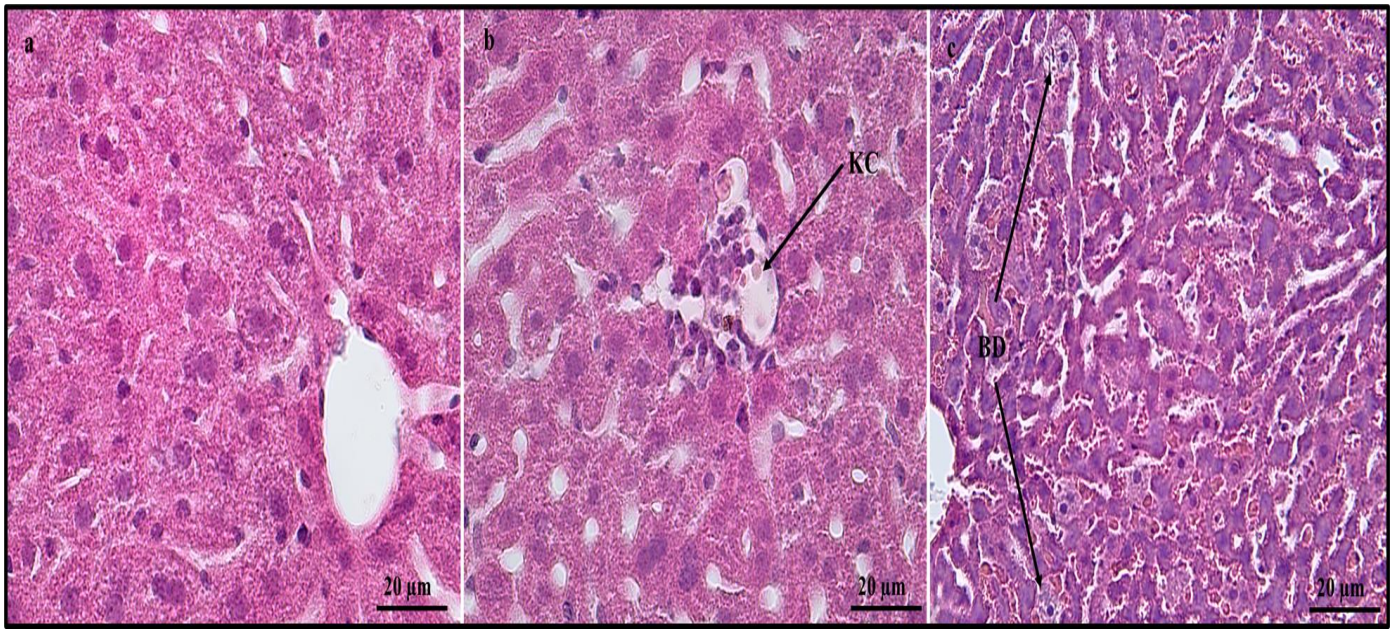



Figure 3.20: Representative micrographs of the liver demonstrating hepatic morphology from liver tissues from different treatment groups. a. Liver from NT showing normal hepatocyte and endothelial morphology, b. Liver from ALC showing normal hepatocyte morphology and an aggregation of Kupffer cells, c. ALC+SIM15 liver showing hepatocytes with ballooning degeneration and the presence of red blood cells in the sinusoids. NT= non-treatment, ALC= alcohol only group, ALC+SIM15= alcohol and simvastatin 15 mg, KC= Kupffer cells, BD= ballooning degeneration.

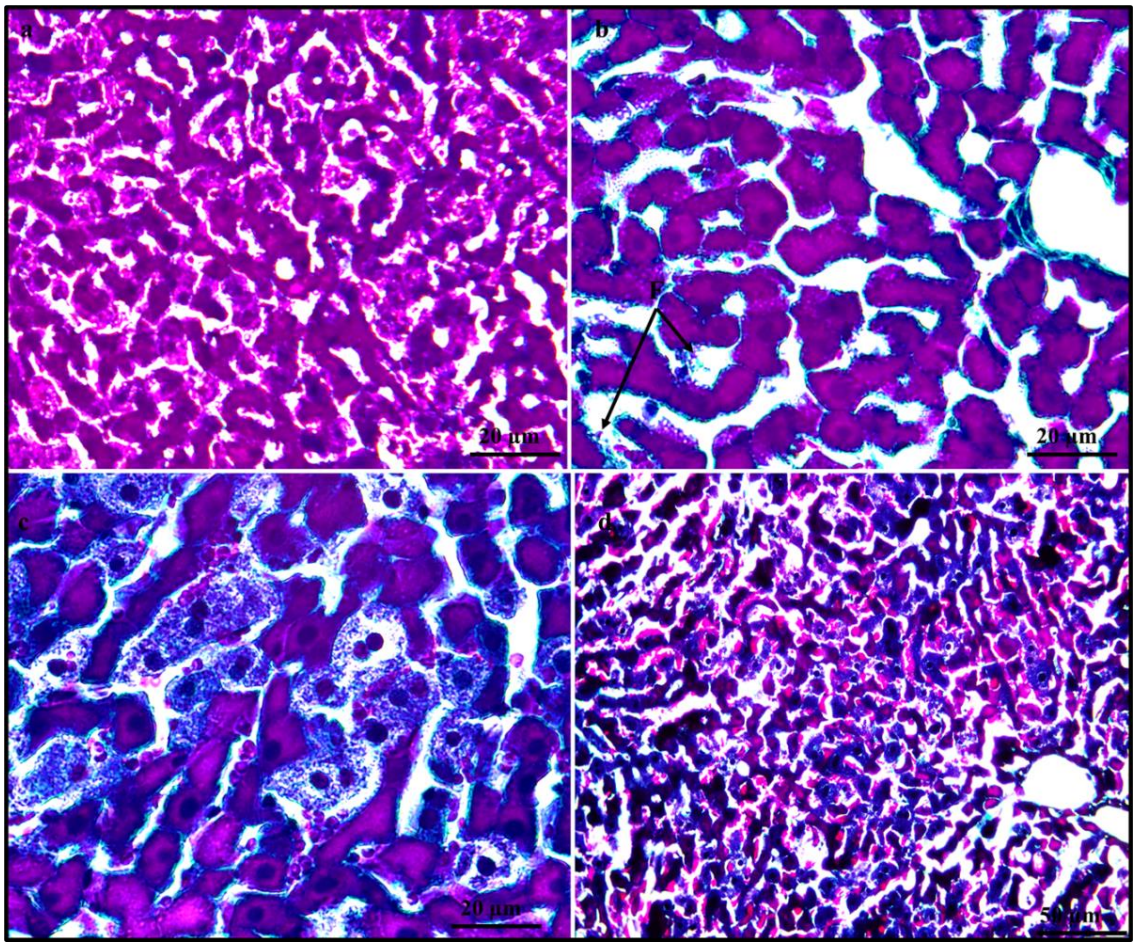



Figure 3.21: Representative micrographs of the liver demonstrating collagen distribution in hepatic tissues from different treatment and a demonstration of perisinusoidal fibrosis. a. Liver from NT showing no collagen deposition, b. Liver from ALC showing the early stages of perisinusoidal fibrosis indicated by the collagen deposition along the walls of the sinuoids, c. ALC+SIM5 liver showing extensive collagen deposition. NT= non-treatment group, ALC= alcohol only group, ALC+SIM5= alcohol and simvastatin 5 mg, F= fibrosis.

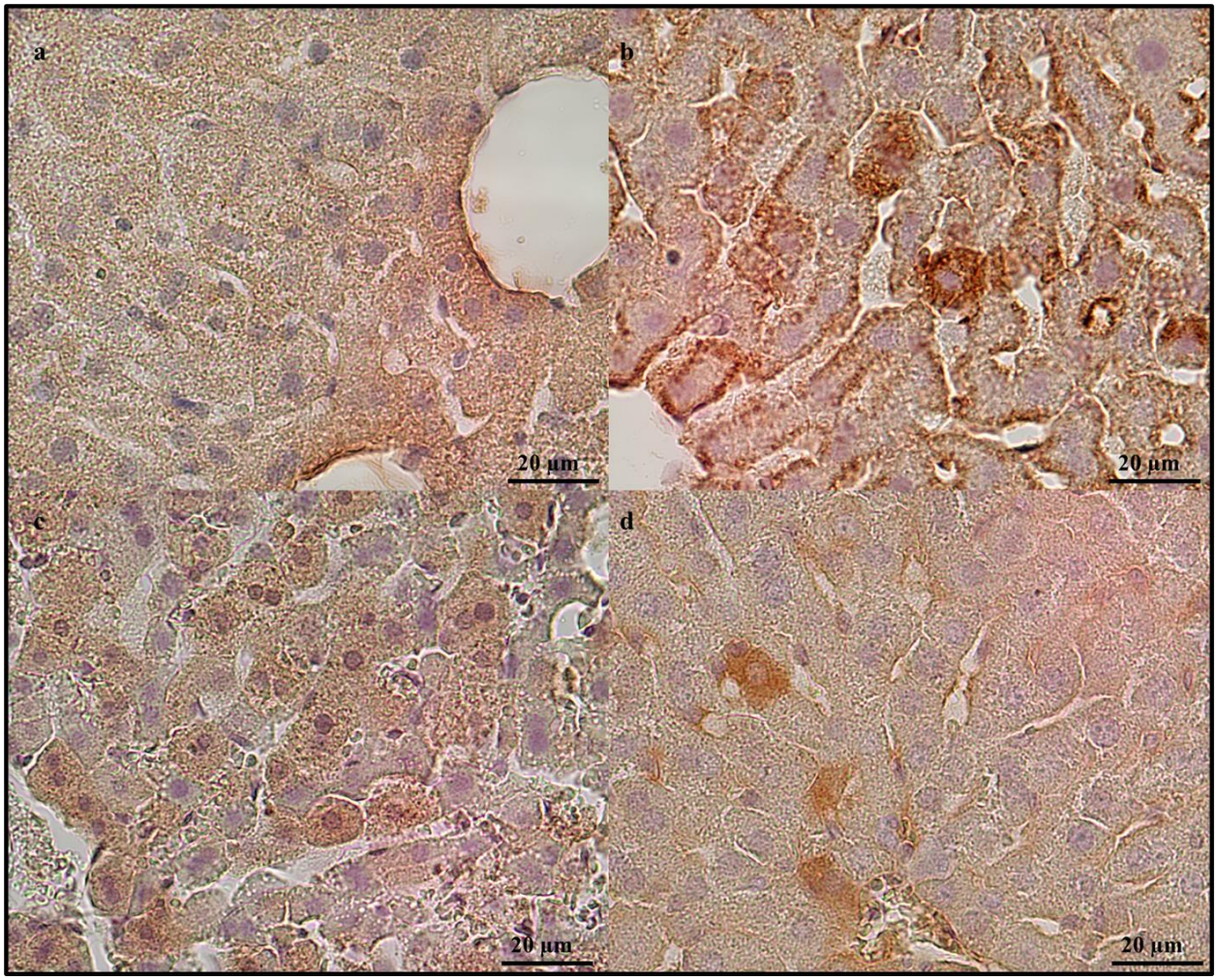



Figure 3.22: Representative micrographs of the liver demonstrating the levels of inflammation in hepatic tissues from different treatment groups. a. Liver from NT showing minimal TNF-α expression, b. Liver from ALC showing areas of intense T NF-α expression, c. Liver from ALC+SIM5 showing moderate TNF-α expression, d. Liver from ALC+SIM15 showing moderate TNF-α expression. NT= non-treatment group, ALC= alcohol only group, ALC+SIM5= alcohol and simvastatin 5 mg, ALC+SIM15= alcohol and simvastatin 15 mg.

### 3.4.2 Density of hepatocytes

In the females, the hepatocyte density was highest in the ALC and was lowest in the NT (Table 3.5). A Kruskal-Wallis test revealed that the hepatocyte cell density was significantly different across the experimental groups ($P$=0.000). A Dunn's post hoc revealed that the hepatocyte cell density in any paired groups was significantly different except in the ALC vs ALC+SIM5 ($P$=0.300), ALC vs ALC+SIM15 ($P$=0.641) or ALC+SIM5 vs ALC+SIM15 ($P$=0.568) (Fig. 3.23). From these observations, all the experimental groups that received alcohol produced a significantly higher cell densities than the NT or the SIM while the alcohol effect on the hepatocyte density was similar in the ALC, ALC+SIM5 or ALC+SIM15. This seems to show that alcohol stimulated a compensatory mechanism which may have been caused by alcohol-induced cell death of hepatocytes. Surprisingly, simvastatin did not seem to have prevented alcohol-induced cell death because the hepatocyte density in groups that were administered alcohol was significantly different from the NT (or the SIM).

In the males, the hepatocyte density was highest in the ALC and was lowest in the NT (Table 3.5). A Kruskal-Wallis test revealed that the hepatocyte density was significantly different across the experimental groups ($P$=0.000). A Dunn's post hoc revealed that the hepatocyte density in any paired groups was significantly different (Fig. 3.23). The cell density of hepatocytes was significantly higher in the ALC than in the NT ($P$=0.000), SIM ($P$=0.000) or ALC+SIM5 ($P$=0.000) but was significantly lower than in ALC+SIM15 ($P$=0.000). Like the observations in the females, all the experimental groups that received alcohol produced a significantly higher cell densities than the NT or the SIM. This seems to show that alcohol stimulated a compensatory mechanism which may have been caused by alcohol-induced cell death of hepatocytes. 15 mg simvastatin also showed a better improvement on hepatocyte density than 5 mg simvastatin.

### 3.4.3 Collagen distribution analyses

In the females, the collagen distribution in the liver was highest in the ALC+SIM5 and was lowest in the NT (Table 3.5). A Kruskal-Wallis test revealed that the collagen distribution was significantly different across the experimental groups (*P*=0.000). A Dunn's post hoc revealed that the collagen distribution was significantly higher in the ALC than in the NT (*P*=0.000) or ALC+SIM15 (*P*=0.000) but was significantly lower than in the ALC+SIM5 (*P*=0.000). Collagen distribution was however similar in the NT vs ALC+SIM15 (P=0.410) or in the SIM vs ALC (P=0.601) (Fig. 3.24). The significant difference between ALC vs NT validates the toxicity of alcohol on the hepatocytes i.e., fibrosis. Alcohol effect on collagen distribution was significantly reduced by the administration of 15 mg simvastatin but not the 5 mg simvastatin.

In the males, the collagen distribution in the liver was highest in the ALC+SIM5 and was lowest in the NT (Table 3.5). A Kruskal-Wallis test revealed that the collagen distribution was significantly different across the experimental groups (*P*=0.000). A Dunn's post hoc revealed that the collagen distribution was significantly higher in the ALC than in the NT (*P*=0.000), SIM (*P*=0.000) or ALC+SIM15 (*P*=0.000) but was significantly lower than in the ALC+SIM5 (*P*=0.000) except. On the other hand, collagen distribution was similar in the NT vs SIM (*P*=0.240) (Fig. 3.24). The significant difference between ALC vs NT also validates the toxicity of alcohol on the hepatocytes i.e., fibrosis. Similar to the observations in the females, alcohol effect on collagen distribution was improved by a higher concentration of simvastatin but not the lower concentration.

### 3.4.4 Measurement of TNF-α distribution

In the females, the TNF-α distribution in the liver was highest in the ALC+SIM5 and was lowest in the SIM (Table 3.5). A Kruskal-Wallis test revealed that the TNF-α distribution

was significantly different across the experimental groups (*P*=0.000). A Dunn's post hoc revealed that the TNF-α distribution in any paired groups was significantly different except in the NT vs ALC (*P*=0.099), NT vs ALC+SIM15 (*P*=0.600) or ALC vs ALC+SIM15 (*P*=0.218) (Fig. 3.25). The similarity in the TNF-α distribution in the NT vs ALC did not reveal alcohol toxicity. At the same time, both concentrations of simvastatin following chronic alcohol did not perform better (with respect to the expression of TNF-α) than in the ALC.

In the males, the TNF-α distribution in the liver was highest in the ALC+SIM15 and was the lowest in the SIM (Table 3.5). A Kruskal-Wallis test revealed that the TNF-α distribution was significantly different across the experimental groups (*P*=0.000). A Dunn's post hoc revealed that the TNF-α distribution in any paired groups was significantly different except in the NT vs SIM (*P*=0.224) or ALC+SIM5 vs ALC+SIM15 (*P*=0.418) (Fig. 3.25). In contrary to the females, chronic alcohol induced inflammation in the liver, an indication of alcohol toxicity in the liver but both concentrations of simvastatin did not prevent inflammation following chronic alcohol.

Table 3.5: Summary of hepatocyte morphometries, collagen and TNF-α distributions

| | | Hepatocyte cell density | | | Collagen distribution | | | TNF-α distribution | | |
|---|---|---|---|---|---|---|---|---|---|---|
| | No of animals | No of grids assessed | Mean count per grid (± SD) | Median | No of images assessed | Collagen distribution (Mean ± SD) (%) | Median | No of images assessed | TNF-α distribution (Mean ± SD) (%) | Median |
| Female | | | | | | | | | | |
| NT | 5 | 300 | 39.81 (±14.61) | 50.5 | 100 | 3.10 (±1.36) | 3.59 | 86 | 12.73 (±11.25) | 8.73 |
| SIM | 5 | 300 | 57.18 (±13.22) | 63 | 96 | 5.79 (±2.44) | 5.32 | 118 | 8.17 (±5.94) | 6.16 |
| ALC | 5 | 300 | 113.36 (±16.84) | 120 | 86 | 15.88 (±15.17) | 19.12 | 119 | 13.90 (±9.93) | 10.65 |
| ALC+SIM5 | 5 | 300 | 98.25 (±27.33) | 112 | 97 | 28.38 (±6.31) | 28.28 | 118 | 20.45 (±11.12) | 17.18 |
| ALC+SIM15 | 5 | 300 | 151.33 (±16.36) | 116.5 | 100 | 4.68 (±4.28) | 3.14 | 120 | 17.61 (±19.19) | 9.44 |
| Male | | | | | | | | | | |
| NT | 5 | 300 | 51.55 (±15.12) | 37 | 100 | 2.77 (±0.74) | 3.01 | 121 | 14.22 (±10.62) | 10.81 |
| SIM | 5 | 300 | 64.5 (±14.82) | 58 | 98 | 4.11 (±3.47) | 3.21 | 94 | 12.52 (±11.84) | 7.59 |
| ALC | 5 | 300 | 118.68 (±32.03) | 112.5 | 91 | 24.57 (±19.00) | 20.48 | 120 | 21.41 (±8.71) | 20.1 |
| ALC+SIM5 | 5 | 300 | 113.08 (±17.91) | 104 | 72 | 51.37 (±11.19) | 52.59 | 124 | 29.93 (±16.97) | 26.21 |
| ALC+SIM15 | 5 | 300 | 116.48 (±29.29) | 151 | 62 | 15.28 (±15.84) | 7.63 | 122 | 27.02 (±14.82) | 26.4 |

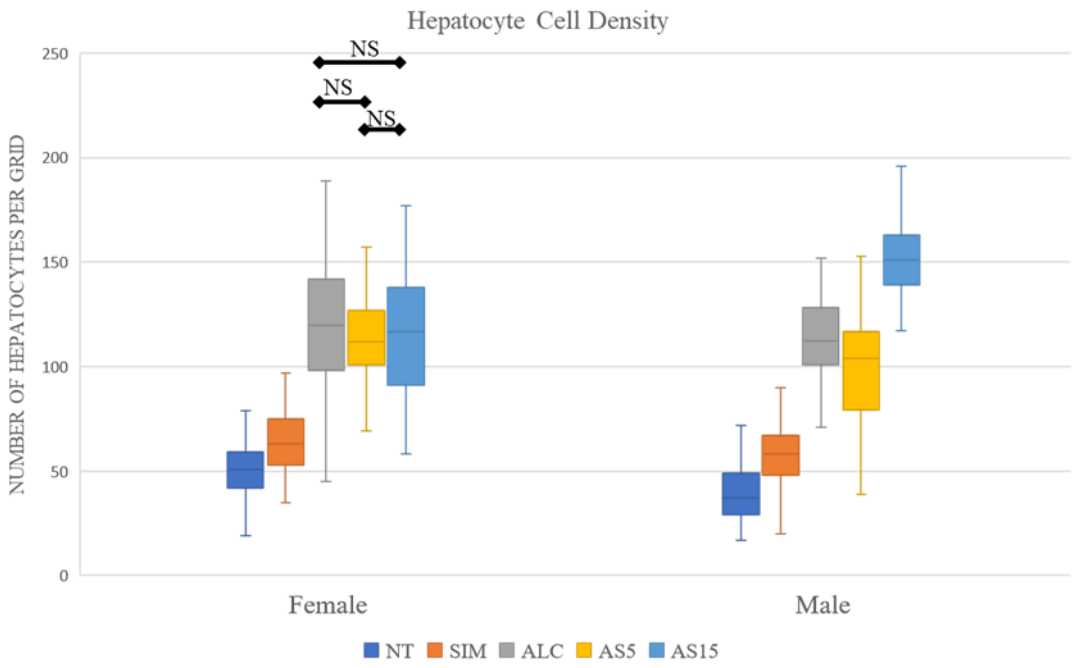



Figure 3.23: Box plots of the density of hepatocytes across the different experimental groups and for both sexes. In both sexes, hepatocyte density in the ALC was significantly higher than in the NT or SIM, an indication of a possible compensatory mechanism for an alcohol-induced hepatocyte death. Both concentrations of simvastatin were not beneficial except for 15 mg simvastatin which performed better than the 5 mg simvastatin in males. NT = Non-treatment; SIM = Simvastatin; ALC = Alcohol; ALC+SIM5 = 5 mg simvastatin and alcohol; ALC+SIM15 = 15 mg simvastatin and alcohol. NS = Not significant at P>0.05.

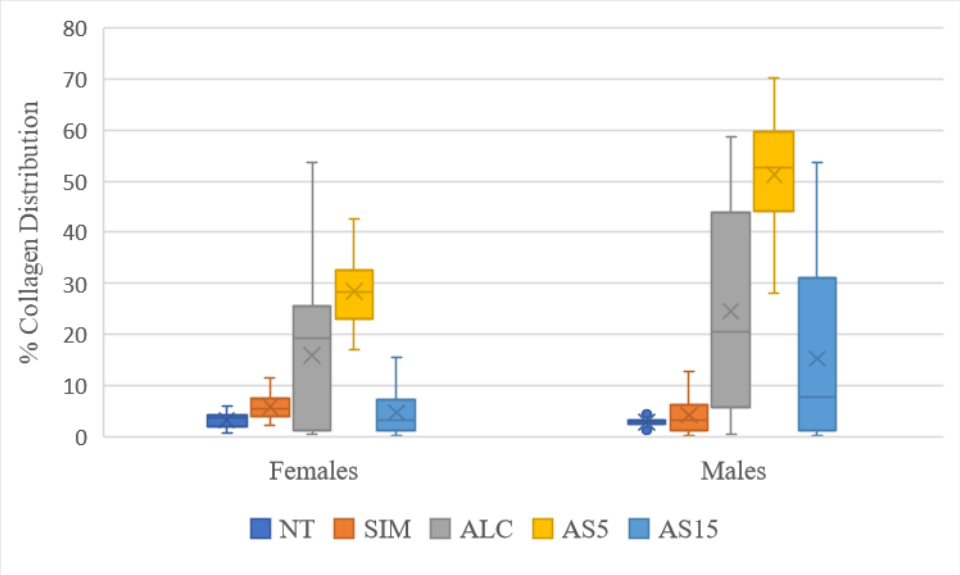



Figure 3.24: Box plots of the percentage distribution of collagen in the liver across the different experimental groups and for both sexes. In both sexes, collagen distribution in the ALC was significantly higher than in the NT or SIM, an indication of an alcohol-induced fibrosis in the liver. Only 15 mg, but not 5 mg, simvastatin prevented alcohol effect on collagen distribution. NT = Non-treatment; SIM = Simvastatin; ALC = Alcohol; ALC+SIM5 = 5 mg simvastatin and alcohol; ALC+SIM15 = 15 mg simvastatin and alcohol. NS = Not significant at P>0.05.

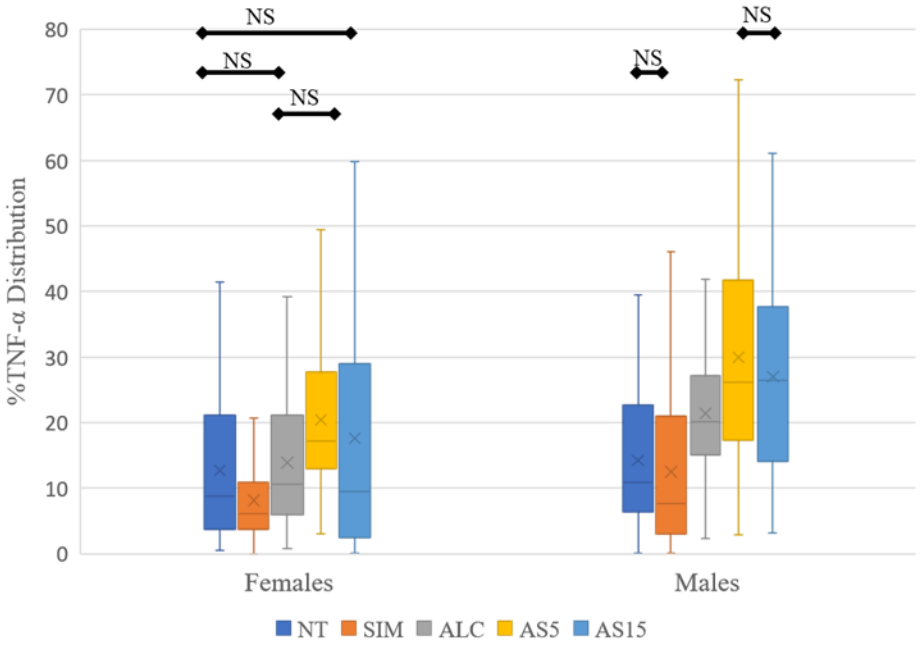



Figure 3.25: Box plots of the percentage distribution of TNF-α in the liver across the different experimental groups and for both sexes. The similarity in the TNF-α distribution in the NT vs ALC did not reveal alcohol toxicity in the females. Both concentrations of simvastatin following chronic alcohol administration were not beneficial against alcohol-induced inflammation in the liver. NT = Non-treatment; SIM = Simvastatin; ALC = Alcohol; ALC+SIM5 = 5 mg simvastatin and alcohol; ALC+SIM15 = 15 mg simvastatin and alcohol. NS = Not significant at P>0.05.

# CHAPTER 4: DISCUSSION

# Chapter 4

## 4.0 Discussion

### 4.1 The heart

Chronic alcohol consumption causes alcoholic cardiomyopathy (i.e., the disruption of the myofibrillary architecture which supports cardiac cells) (Guo & Ren, 2010) as well as cardiomyocyte hypertrophy, fibrosis, and inflammation (Wang *et al*., 2005; Guo and Ren, 2010; Lai *et al*., 2011; Law *et al*., 2012). Chronic alcohol also worsens cardiac function, weakens, and promotes the loss of cardiomyocytes (Piano, 2016). Cardiomyocyte organelles such as the mitochondria, ribosomes, plasma membrane and membrane receptors are also damaged due to the high reactivity, low molecular mass, high diffusion rate and the high permeability of alcohol (Fernandez-Sola, 2020). Alcohol permeability is also implicated in the disruption of the signalling processes, activation of apoptosis and the loss of heart contraction (Obad *et al*., 2018; Fernandez-Sola, 2020). Even, an acute alcohol exposure has been demonstrated to elicit haemodynamic changes (cardiac stress) leading to the enlargement of cardiomyocytes (Ai *et al*., 2020; Guo & Ren, 2010; Obad *et al*., 2018). However, it must be noted that myocardial hypertrophy may occur at the early stages of an alcohol damage as a compensatory mechanism for the sarcoplasmic reticular dysfunction (arising from alcohol) which is responsible for the thickening of ventricular wall (Law *et al*., 2012; Coelho-Filho *et al*., 2013; Piano, 2016; Fernández-Solà, 2020). In a situation where the compensatory phase fails, ventricular failure is eminent (Law *et al*., 2012) as well as an increase in circulatory cytokines and growth factors (Obad *et al*., 2018).

Likewise, alcohol hinders the repair mechanism of the cardiomyocytes by suppressing regeneration while promoting cardiac lesions through its ability to trigger apoptosis and necrosis of cardiomyocytes (Fernandez-Sola, 2020). A hindered repair mechanism promotes

myocardial fibrosis (Fernandez-Sola, 2020) and then disrupts myocardial remodelling which is an essential contributor to the repair of ventricular wall damage (Wang *et al*., 2005; Fernandez-Sola, 2018). The failure of remodelling after a ventricular wall damage leads to ventricular dysfunction (Wang *et al*., 2005) characterised by a dilated left ventricle, a thin left ventricular wall, a disrupted myofibrillary architecture and a contractile dysfunction (Guo and Ren, 2010, Law *et al*., 2012; Ai *et al*., 2020). Ventricular dysfunction in alcoholics is also caused by the disruption of calcium ion homeostasis and its regulation by inhibiting endothelial nitric oxide synthase (eNOS) (Alleyne & Dopico, 2021; Fernández-Solà, 2020; Kawano, 2010).

Alcohol induces inflammation and promotes the secretion of cytokines such as TNF-α (Obad *et al*., 2018). The upregulation of TNF-α signals inflammation and cell abnormality (e.g., apoptosis) thus it plays a key role in myocardial homeostasis (Obad *et al*., 2018). TNF-α is mainly released by the immune cells (e.g., macrophages and T-lymphocytes) however it is also secreted by the cardiomyocytes (Calabrese *et al*., 2004) which is why the heart is also called a TNF-α producing organ, especially in heart failure where there is a surge in secretion (Irwin *et al*., 1999; Obad *et al*., 2018). Low levels of TNF-α were reported to prevent minor cardiac injuries but inflammation is exacerbated at high concentrations (Calabrese *et al*., 2004). Thus TNF-α regulates autocrine and paracrine activities of the endothelial cells at low concentrations which makes it a crucial monitor of inflammation (Calabrese *et al*., 2004). With respect to chronic alcohol, an elevated expression of TNF-α indicates an alcohol-related cardiomyocyte damage as is the case in the present study (Obad *et al*., 2018; Schumacher & Naga Prasad, 2018). It is thus not surprising that a 28–day chronic alcohol induced myocardial hypertrophy, fibrosis and inflammation which confirms the damaging effects of alcohol on the adolescent cardiac tissue in the present study.

Generally, simvastatin is a commonly used drug for treating different cardiovascular diseases especially hypercholesterolaemia (Thabit *et al*., 2014; Liu *et al*., 2016; Morse *et al*., 2018; Murphy *et al*., 2020), coronary heart disease (Atef *et al*., 2019; Murphy *et al*., 2020), cardiac cell death (MacDougall *et al*., 2017), myocardial inflammation and fibrosis (Cahyawati, 2019; Lee *et al*., 2019; Skrzypiec-Spring *et al*., 2021; Sun *et al*., 2015; Xiao *et al*., 2016) due to the inter-relationships between these diseases. Simvastatin also has the capabilities to inhibit the TGF-β1 pathway which is responsible for interstitial fibrosis and cardiomyocyte hypertrophy (Xiao *et al*., 2016). In addition, it has been shown that simvastatin is able to prevent cardiac dysfunction and remodelling through its unique ability to stimulate some important pathways such as Krüppel-like Factor 2 (Klf2) in endothelial cells. It directly regulates the activities of the TGF-β1 target genes in these cells, and this provides a non-cholesterol evidence of simvastatin effects against cardiac failures (Li *et al*., 2018). Simvastatin also reduces cardiac hypertrophy due to its ability to upregulates peroxisome proliferator-activated receptors (Qin *et al*., 2010) and inhibits autophagy (Su *et al*., 2018). It is obvious that simvastatin has the capabilities to protect and prevent damages to the cardiomyocytes (Su *et al*., 2012; Qin *et al*., 2010; Al-Rasheed *et al*., 2015; Ahmed *et al*., 2016; Xiao *et al*., 2016; Su *et al*., 2018; Li *et al*., 2021).

In addition, simvastatin is also effective against several induced-toxins such as cyclophosphamide induced toxicity via the modulation of inflammasome/caspase1/interleukin 1β (Refaie *et al*., 2022), lipopolysaccharide-induced myocardial injury by up-regulating survivin that inhibits caspase-3 activation (Nežić *et al*., 2020) and Ischemia-reperfusion-induced myocardial damage by reducing oxidative stress (Rohilla *et al*., 2015). In the light of the ability of simvastatin to protect cardiac tissues from being damaged by toxins, it became necessary to explore its effectiveness against alcohol-induced cardiomyocyte damage. It is also not surprising that simvastatin (at 5 mg or 15 mg) significantly reduced alcohol-induced

cardiomyocyte hypertrophy, cardiac fibrosis, and inflammation. Likewise, several studies have shown that higher concentrations of simvastatin are also beneficial (e.g., Qin *et al*. (2010) at 25 mg/kg/day and Xiao *et al*. (2016) at a range of 10 – 40 mg/kg/day). Although the molecular pathway was not explored in the present study, but it is assumed that the simvastatin's ability to modulate, several and well-researched, intracellular activities may have come to play in the process of preventing alcohol damage.

4.2 The kidney

Chronic alcohol damages the renal tissues in diverse ways. It promotes the accumulation of inflammatory cells to infiltrate the interstitial tissue. Even though this is essential for triggering a repair process, a prolonged accumulation of inflammatory cells and pro-inflammatory cytokines e.g., TGF-β hinders the repair process which then progresses to renal disease (Black *et al*., 2019). Structural renal damages such as tubular epithelial cell atrophy, renal interstitial oedema and tubular interstitial fibrosis hinder renal function (Das and Vasudevan, 2008; Wu *et al*., 2021). Renal tubular cell injury and apoptosis also disrupt selective reabsorption of molecules from the fluid in the tubules (Edelstein *et al*., 1997; Epstein, 1997) and water conservation in the body is also lost as the secretion of antidiuretic hormone (ADH) is hindered by chronic alcohol due to the renal tubules becoming impermeable to water leading to electrolyte imbalance (Epstein, 1997; Singh *et al*., 2013). Chronic alcohol thickens the glomerular basement membrane, increases the proliferation of mesangial cells, and causes the swelling of the glomeruli thereby reducing contributing to the loss of water (i.e., renal dysfunction) (Das & Vasudevan, 2008; Rikalo and Romanenko, 2018).

Alcohol is also implicated in promoting extracellular matrix build-up (i.e., fibrosis) between the renal tubules and the surrounding capillaries. At the early stages of renal injury, myofibroblasts are stimulated by the inflammatory cytokines to produce collagen in order to

initiate a repair process (Eddy, 2014; Latchoumycandane *et al*., 2015), however, when the injury is prolonged as in the case of chronic alcohol, a sustained accumulation of collagen damages the endothelium of capillaries and increases the distance between the capillaries and tubules thus delaying or reducing the oxygen supply and nutrients to the renal tubular cells and the surrounding cells, invariably leading to a renal dysfunction (Wu *et al*., 2021). This is also true about the observations in the present study where chronic alcohol produced a significant accumulation of collagen in the renal tissue.

Likewise, the basal concentration of TNF-α [produced by the renal cells (Mehaffey and Majid, 2017; Fard *et al*., 2021)] is considerably low or undetectable under normal conditions but sporadically increases at the onset of renal inflammation to trigger a recovery pathway (Mehaffey and Majid, 2017). TNF-α at low levels promotes tissue repair and induces the regeneration of renal cells in order to promote recovery from injury (Mehaffey and Majid, 2017). Also, TNF-α also regulates renal function and controls haemodynamics through its ability to control constriction of renal vessels thereby regulating the rate of glomerular filtration (Mehaffey and Majid, 2017). However, this system is destabilized by chronic alcohol through its ability to induce a prolonged inflammatory stress leading to structural damage and renal dysfunction (Fard *et al*., 2021). This also aligns with the observations in the present study that found that chronic alcohol significantly increased the expression of TNF-α in the renal tissue and thus an indication of alcohol-induced renal inflammation.

In the present study, chronic alcohol damaged the microvilli brush border lining the cells of the renal tubules which are essential for renal function i.e., reabsorption. The brush-border consists of the microvilli on the apical surface of the epithelial cells, and they provide a large surface area which is required for the reabsorption of electrolytes and nutrients needed by the body (Basile *et al*., 2012; Ho and Morgan, 2022). Alcohol causes a significant damage to the brush-border along the length of the renal tubules by disrupting and breaking down the

cytoskeleton of the brush-border (filamentous-actin of the apical microvilli) which leads to a significant loss of the brush border and a reduced surface area for the reabsorption of nutrients in the renal tubules and therefore a loss of nutrients via the filtrate because there is little to no reabsorption occurring along the length of the renal tubules (Basile *et al*., 2012; Ho and Morgan, 2022). This is also true about the observations in the present study where chronic alcohol significantly altered the morphology of the renal tubules by causing loss of brush-border cells. In addition, the glomeruli were considerably enlarged in the mice that were administered chronic alcohol. The possible explanation for the glomerular hypertrophy observed in the present study, although not evaluated, is that structural damages by alcohol may have induced renal hypertension causing the enlargement of glomeruli (Zamami *et al*., 2021). It is also possible that alcohol may have caused the loss of glomeruli thereby putting pressure on the remaining glomeruli causing them to hypertrophy– a compensatory mechanism (Jacobson, 1991; Zamami *et al*., 2021). Usually, glomerular hypertrophy is associated with hyperfiltration with a corresponding increase in the size of urinary space (Henehar *et al*., 2001). However, this was not the case in the present study because an increased alcohol-induced glomerular hypertrophy resulted in a reduction in the size of urinary space which seems to suggest an alcohol-specific renal damage compared to a diabetic kidney as reported in other studies (Henehar *et al*., 2001). In all, alcohol-induced renal damage (both morphologically and morphometrically) observed in this study is consistent with other reports in the literature (Brzóska *et al*., 2003; Hassan *et al*., 2015; De Sousa *et al*., 2018; Rikalo and Romanenko, 2018; Dawodu *et al*., 2019).

With the rising prevalence of alcohol use amongst adolescents, it will not be far-fetched to find that the prevalence of chronic kidney diseases caused by alcohol (or other substance abuse) will also be on a rise even though there is no data available on the prevalence of alcohol-related kidney diseases specifically in this age group (Steele *et al*., 2012). But it is a fact that

acute or chronic alcohol can hinder renal function and this may be worsened in the presence of other metabolic diseases (Epstein, 1997). This thus calls for an urgent intervention especially where the cost of health care is a significant burden on the health system.

Simvastatin seems to be a promising intervention for treating renal diseases as it is widely used in the treatment of cardiovascular diseases due to its ability to reduce inflammation, cell death and fibrosis in the heart (Thabit *et al*., 2014; Sun *et al*., 2015; Liu *et al*., 2016; Xiao *et al*., 2016; MacDougall, *et al*., 2017; Morse *et al*., 2018; Murphy *et al*., 2020; Atef *et al*., 2019; Cahyawati, 2019; Lee *et al*., 2019; Skrzypiec-Spring *et al*., 2021). Generally, statins e.g., simvastatin inhibits the upregulation of Angiotensin-dependent oxidative stress (Zhou & Liao 2009; Zhang *et al*., 2014). More so, simvastatin inhibits the differentiation of fibroblasts into myofibroblasts thus reducing the activity of myofibroblasts and subsequently reducing collagen deposition (Cahyawati *et al*., 2019). Simvastatin is also effective for lowering blood cholesterol in subjects with chronic kidney disease (Baigent *et al*., 2011) while in another study, Christensen *et al*. (2006) reported that 10 or 25 mg simvastatin, but not 1 mg, was effective against the development of glomerular hypertrophy and glomerulonephritis. Information on the effect of simvastatin, specifically, against alcohol-related kidney disease is lacking in the literature. However, Mohammadi *et al*. (2015) found that simvastatin was effective against lead-induced renal damage. In the same study, the sizes of the glomeruli and urinary space were improved in mice that were treated with 20 mg simvastatin, more effective than the lower concentrations (5 or 10 mg). It is therefore not surprising that simvastatin significantly reduced glomerular hypertrophy, renal fibrosis, and inflammation in the present study. These observations are also consistent with the findings of the simvastatin effects on alcohol-induced myocardial damage. It is also obvious that both concentrations (5 and 10 mg) of simvastatin were generally effective against the onset of alcohol-induced renal damage and to almost similar degrees in both sexes.

4.3 The liver

Chronic alcohol consumption is detrimental to the heart (Wang *et al*., 2005; Guo and Ren, 2010; Lai *et al*., 2012; Law *et al*., 2012), the kidney (Edelstein *et al*., 1997; Epstein, 1997; Das and Vasudevan, 2008; Rikalo and Romanenko, 2018; Wu *et al*., 2021) and the liver (Apte *et al*., 2004; Robin *et al*., 2005; Baumgardner *et al*., 2007; Chavez *et al*., 2011; Duly *et al*., 2015; Ambade *et al*., 2016; Atef *et al*., 2019; Sengupta *et al*., 2021) evident by several studies that have reported the effects of alcohol on these organs. In the liver, alcohol increases collagen deposition and inflammation (Atef *et al*., 2019; Sengupta *et al*., 2021) and the metabolic functions of the liver are significantly impaired by chronic alcohol. It must be emphasized that the liver metabolizes majority of alcohol consumed and ensures that is removed from the body (Hassan *et al*., 2015; Obad *et al*., 2018; Hu *et al*., 2020). Likewise, other metabolic functions (e.g., lipid regulation) of the liver are also hindered (Cohen and Nagy 2011; Jeon and Carr 2020; Sengupta *et al*., 2021) causing the build-up of triglycerides and fatty acids i.e., steatosis in the tissue. This problem is often accompanied by inflammation and death of hepatocytes (Cohen and Nagy, 2011; Duly *et al*., 2015; de Lucca *et al*., 2019; Jeon and Carr, 2020; Celli & Zhang, 2014; Sengupta *et al*., 2021).

However, it is surprising that alcohol increased hepatocyte density in all the experimental groups that were administered alcohol despite histological evidence that revealed steatosis and the accumulation of Kupffer cells in the alcohol–treated mice in the present study. Steatosis is considered the earliest and commonest feature of alcohol liver disease caused predominantly by fat droplets arising from the accumulation of triglycerides and fatty acids due to hepatic dysfunction (Romulo and Xuchen 2014). In light of the histology of the alcohol-treated liver, it is obvious that the chronic alcohol induced alcohol liver disease although this

observation was not substantiated by a corresponding decrease in hepatocyte density. It is thus assumed that alcohol may have caused a significant cell death in the alcohol-treated groups (although not explored in the present study) and this occurrence may have triggered a compensatory mechanism which then resulted into an increase in hepatocyte density as seen in the ALC, ALC+SIM5 and ALC+SIM15 in both sexes compared to the NT or SIM. Compensatory mechanism is a cellular process which has been reported in the central nervous system (Kwiecien 2010), in a diabetic model (Lamont *et al*., 2014), and in studies on the liver (Webber *et al*., 1994). It is also important to note that alcoholic steatosis is often reversed immediately when alcohol consumption is stopped (Celli & Zhang, 2014; Donohue *et al*., 2017). The possible explanation for this is that the fatty hepatocytes were not damaged in the first place, or it could also be that the subject (human or experimental animal) is able to trigger a compensatory mechanism to counteract a hepatic damage as demonstrated in a study by Yang *et al*. (2004). Similarly, when the liver is exposed to a toxin such as alcohol, hepatocytes including those with damaged DNA may go through multiple cycles of proliferation in order to restore hepatocyte population to a functional level (Apte *et al*., 2004; Ambade *et al*., 2016). Other factors evaluated in the present study confirmed alcohol-induced hepatic damage evident by significant increases in fibrosis and inflammation in the alcohol than in the non-treated except in the TNF-α distribution in the females.

Statins has been shown to be effective in treating or managing cardiovascular and renal diseases (Christensen *et al*., 2006; Matzopoulos *et al*., 2014; Mohammadi *et al*., 2015; Obad *et al*., 2018). Likewise, statins have been shown to be effective in reducing portal hypertension, improving vascular remodelling, preventing hepatic dysfunction, preventing the development of hepatic carcinoma, improving hepatic steatosis, improving the survival of hepatocytes, and preventing inflammation (La Mura *et al*., 2013; Atef *et al*., 2019; Gu *et al*., 2019).

In the present study, simvastatin had a beneficial effect against alcohol-induced fibrosis in the liver in both sexes. It must be noted that simvastatin has the ability to decrease the activity of myofibroblasts resulting in a decrease in the expression of collagen type I and alpha-Smooth Muscle Actin (α-SMA) (Wang et al., 2013). Interestingly, simvastatin did not prevent the onset of inflammation by chronic alcohol in the present study. This is consistent with a study by La Mura *et al*. (2013) that showed that 25 mg/kg/day simvastatin did not lower the expression of TNF-α against lipopolysaccharide (LPS)-induced liver injury, thus not beneficial in preventing or improving inflammation. This is an important observation in that the effect of simvastatin seems to be specific i.e., it may be dependent on the type of pathology caused by chronic alcohol. Unfortunately, there are no reports in the literature to directly compare the findings of this study. However, simvastatin was reported to significantly lower alcohol-induced triglycerides and aspartate aminotransferase levels in Wistar rats that were co-administered 25% v/v alcohol and 65 mg/100 g simvastatin for a period of 8 weeks. The same study suggested that a moderate alcohol and simvastatin is considered safe in experimental animals and simvastatin is effective against alcohol-induced hepatic damage (Kolovou *et al*., 2003). Transforming growth factor-β1 (TGF-β1) suppresses alcohol effects on the hepatocytes by regulating their growth and differentiation as well as promoting apoptosis, simvastatin was reported to downregulate the hepatic TGF-β1 signalling pathway thus allowing increased proliferation of hepatocytes (Fang *et al*., 2017).

In non-alcohol related studies, simvastatin was reported to improve portal hypertension owing to its ability to specifically increase the production of nitric oxide in cirrhotic liver (Abraldes *et al*., 2007). Likewise, 1 mg/kg simvastatin significantly reversed cisplatin-induced hepatotoxicity by preventing liver peroxidization, fibrosis and inflammation (Iseri *et al*., 2007) and 0.2 mg/kg simvastatin was also effective in protecting against hepatic damage arising from obstructive jaundice through its ability to reduce the expression of chemokines and the

recruitment of immune cells (Dold *et al*., 2009). Tripathi *et al*., (2018) also demonstrated that 25 mg/kg simvastatin prevented carbon tetrachloride (CCl4)-induced liver failure and the progression of cirrhosis. With the evidence on simvastatin effects against liver damage or hepatoxicity, the present study could not ascertain the reasons for the specific beneficial effects of simvastatin. Thus, there is need for further studies to better understand simvastatin effects and the progression of liver pathologies.

# CHAPTER 5: CONCLUSION AND RECOMMENDATIONS

# CHAPTER 5

# 5.0 CONCLUSION AND RECOMMENDATIONS

## 5.1 Conclusion and recommendations

This study further demonstrates the degree of alcohol-induced cardiac, renal, and hepatic damage and demonstrated the effects of simvastatin against alcohol-induced damage in the heart, kidney, and liver on adolescent mice. This study demonstrates the effectiveness of simvastatin in preventing the onset of alcohol-related myocardial, renal, and hepatic damage. Although the mechanism of action was not explored in the present study, it is assumed that the ability of simvastatin to modulate intracellular activities may have played a vital role in preventing alcohol damage. Further studies on its molecular pathway needs to be explored. In addition, the reason for the specific effect of simvastatin needs to be explored further. Information from this novel study is also crucial to the treatment and management of alcohol-related myocardial, renal, and hepatic diseases. It is also important that the use of an FDA–approved and an easily accessible drug such as simvastatin will help in lowering the prevalence of alcohol-related myocardial, renal, and hepatic diseases especially in adolescents. This is expected to reduce the burden on the health systems.

## REFERENCES


Ai, L., Perez, E., Asimes, A., Kampaengsri, T., Heroux, M., Zlobin, A., Hiske, M. A., Chung, C. S., Pak, T. R., & Kirk, J. A. (2020). Binge alcohol exposure in adolescence impairs normal heart growth. *Journal of the American Heart Association*, *9*(9). https://doi.org/10.1161/JAHA.119.015611

Alleyne, J., & Dopico, A. M. (2021). Alcohol Use Disorders and Their Harmful Effects on the Contractility of Skeletal, Cardiac and Smooth Muscles. *Advances in Drug and Alcohol Research*, *1*. https://doi.org/10.3389/adar.2021.10011

Ambade, A., Satishchandran, A., Gyongyosi, B., Lowe, P., & Szabo, G. (2016). Adult mouse model of early hepatocellular carcinoma promoted by alcoholic liver disease. *World Journal of Gastroenterology*, *22*(16), 4091–4108. https://doi.org/10.3748/wjg.v22.i16.4091

Apte, U. M., McRee, R., & Ramaiah, S. K. (2004). Hepatocyte Proliferation is the Possible Mechanism for the Transient Decrease in Liver Injury During Steatosis Stage of Alcoholic Liver Disease. *Toxicologic Pathology*, *32*(5), 567–576. https://doi.org/10.1080/01926230490508812

Atef, M. M., Hafez, Y. M., Alshenawy, H. A., & Emam, M. N. (2019). Ameliorative effects of autophagy inducer, simvastatin on alcohol-induced liver disease in a rat model. *Journal of Cellular Biochemistry*, *120*(5), 7679–7688. https://doi.org/10.1002/jcb.28042

Balzano, T., Arenas, Y. M., Dadsetan, S., Forteza, J., Gil-Perotin, S., Cubas-Nuñez, L., Casanova, B., Gracià, F., Varela-Andrés, N., Montoliu, C., Llansola, M., & Felipo, V. (2020). Sustained hyperammonemia induces TNF-A in Purkinje neurons by activating the TNFR1-NF-κB pathway. *Journal of Neuroinflammation*, *17*(1). https://doi.org/10.1186/s12974-020-01746-z

Basile, D. P., Anderson, M. D., & Sutton, T. A. (2012). Pathophysiology of acute kidney injury. *Comprehensive Physiology*, *2*(2), 1303–1353. https://doi.org/10.1002/cphy.c110041

Baudouy, D., Michiels, J. F., Vukolic, A., Wagner, K. D., & Wagner, N. (2017). Echocardiographic and histological examination of cardiac morphology in the mouse. *Journal of Visualized Experiments*, *2017*(128). https://doi.org/10.3791/55843

Baumgardner, J. N., Shankar, K., Korourian, S., Badger, T. M., J Ronis, M. J., & J Ronis, M. J. (2007). First published May 17. *Am J Physiol Gastrointest Liver Physiol*, *293*, 355–364. https://doi.org/10.1152/ajpgi.00038.2007.-To

Bertscher, A., London, L., & Röhrs, S. (2020). *A human rights analysis of South Africa's Control of Marketing of Alcoholic Beverages Bill 1 A HUM AN RIGHTS AN ALYSIS OF SOUTH AFRI C A' S CONTRO L OF M ARKETING OF ALCO HOLIC BEVERAG ES BI LL U M A N Á L I S E D O S D I R E I T O S H U M A N O S D O P R O J E T O D E L E I D E C O N T R O L E D E M A R K E T I N G D E B E B I D A S A L C O Ó L I C A S D A Á F R I C A D O S U L*.

Bielawski, D.M., & Abel, E.L. (1997). Acute treatment of paternal alcohol exposure produces malformations in offspring. *Alcohol, 14*(4), 397-401.

Black, L.M., Lever, J.M., & Agarwal, A. (2019). Renal Inflammation and Fibrosis: A Double-edged Sword. Journal of Histochemistry & Cytochemistry, 67(9), 663-681. https://doi.org/10.1369/0022155419852932

Brzóska, M. M., Moniuszko-Jakoniuk, J., Piłat-Marcinkiewicz, B., & Sawicki, B. (2003). Liver and kidney function and histology in rats exposed to cadmium and ethanol. *Alcohol and Alcoholism*, *38*(1), 2–10. https://doi.org/10.1093/alcalc/agg006

Cahyawati, P. N. (2019). Effect of simvastatin on histopathology of the heart after 5/6 subtotal nephrectomy. *International Journal of Applied Pharmaceutics*, *11*(Special Issue 5), 131–133. https://doi.org/10.22159/ijap.2019.v11s5.T0105

Calabrese, F., Carturan, E., Chimenti, C., Pieroni, M., Agostini, C., Angelini, A., Crosato, M., Valente, M., Boffa, G. M., Frustaci, A., & Thiene, G. (2004). Overexpression of tumor necrosis factor (TNF) α and TNFα receptor I in human viral myocariditis: Clinicopathologic correlations. *Modern Pathology*, *17*(9), 1108–1118. https://doi.org/10.1038/modpathol.3800158

Cardoso De Sousa, M., Vegian, M. R. D. C., Biserra, M. A., Costa, B. C. A., Camargo, S. E. A., Rode, S. D. M., Ramos, C. J., Dias De Oliveira, L., & Vasconcellos, L. M. R. de. (2018). Influence of Chronic Alcohol Use on Osteoblastic Differentiation of Bone Marrow Cells, Bone Properties, and Hepatic and Renal Morphology of Rats. *Scientific World Journal*, *2018*. https://doi.org/10.1155/2018/2494918

Celli, R., & Zhang, X. (2014). Pathology of alcoholic liver disease. In *Journal of Clinical and Transitional Hepatology* (Vol. 2, pp. 103–109). https://doi.org/10.14218/jcth.2014.00010

Chauke, T.M., Van der Heever, H., & Hoque, M.E. (2015). Alcohol amongst learners in rural high school in South Africa. *African Journal of Primary Health Care and Family Medicine*, *7*(1), 1-6. http://dx.doi.org/10.4102/phcfm.v7i1.755

Chavez, P. R. G., Lian, F., Chung, J., Liu, C., Paiva, S. A. R., Seitz, H. K., & Wang, X. D. (2011). Long-term ethanol consumption promotes hepatic tumorigenesis but impairs normal hepatocyte proliferation in rats. *Journal of Nutrition*, *141*(6), 1049–1055. https://doi.org/10.3945/jn.110.136531

Chen, Y., Yu, Q. & Xu, C., 2017. A convenient method for quantifying collagen fibers on atherosclerotic lesions by ImageJ software. International Journal of Clinical and Experimental Medicine, 10(10), pp. 14904-14910.

Christensen, M., Su, A. W., Snyder, R. W., Greco, A., Lipschutz, J. H., & Madaio, M. P. (2006). Simvastatin protection against acute immune-mediated glomerulonephritis in mice. *Kidney International*, *69*(3), 457–463. https://doi.org/10.1038/sj.ki.5000086

Coelho-Filho, O. R., Shah, R. v., Mitchell, R., Neilan, T. G., Moreno, H., Simonson, B., Kwong, R., Rosenzweig, A., Das, S., & Jerosch-Herold, M. (2013). Quantification of cardiomyocyte hypertrophy by cardiac magnetic resonance: Implications for early cardiac remodeling. *Circulation*, *128*(11), 1225–1233. https://doi.org/10.1161/CIRCULATIONAHA.112.000438

Cohen, J. I., & Nagy, L. E. (2011). Pathogenesis of alcoholic liver disease: Interactions between parenchymal and non-parenchymal cells. *Journal of Digestive Diseases*, *12*(1), 3–9. https://doi.org/10.1111/j.1751-2980.2010.00468.x

Das, S. K., & Vasudevan, D. M. (2008). Alcohol induced effects on kidney. In *Indian Journal of Clinical Biochemistry* (Vol. 23, Issue 1, pp. 4–9). https://doi.org/10.1007/s12291-008-0003-9

Dawodu, O. G., Ebuehi, O. A. T., Odesanmi, O. S., & Olalekan, M. O. (2019). Determination of Biochemical and Histological Parameters of Alcohol Administration in Wistar Rats. *Annual Research & Review in Biology*, 1–8. https://doi.org/10.9734/arrb/2019/v32i630102

de Almeida, J. M., Cabrera Pazmino, V. F., Noronha Novaes, V. C., Mogami Bomfim, S. R., Hitomi Nagata, M. J., Pinto Oliveira, F. L., Matheus, H. R., & Ervolino, E. (2020). Chronic consumption of alcohol increases alveolar bone loss. *PLoS ONE*, *15*(8 August). https://doi.org/10.1371/journal.pone.0232731

de Lucca, M.S., Pereira, E.T., Righi, T., de Carvalho, C.A., Nogueira, C.I., da Cunha, D.N.Q., Natali, A.J., & Lima, L.M. (2018). Liver Histology after Chronic Use of Alcohol and Exercise Training in Rats. *Journal of Pharmacy and Pharmacology*, *6*(1). https://doi.org/10.17265/2328-2150/2018.01.006

Donohue, T. M., Kharbanda, K. K., & Osna, N. A. (2017). Alcoholic Liver Disease: Pathogenesis and Current Management. *Alcohol Research: Current Review*, *38*(2), 147–161.

Dold, S., Laschke, M. W., Lavasani, S., Menger, M. D., Jeppsson, B., Thorlacius, H. (2009). Simvastatin protects against cholestasis-induced liver injury. *British Journal of Pharmacology*, *156*(3), 466-474.

Duly, A. M. P., Alani, B., Huang, E. Y. W., Yee, C., Haber, P. S., McLennan, S. v., & Seth, D. (2015). Effect of multiple binge alcohol on diet-induced liver injury in a mouse model of obesity. *Nutrition and Diabetes*, *5*. https://doi.org/10.1038/nutd.2015.4

Eddy, A. A. (2014). Overview of the cellular and molecular basis of kidney fibrosis. In *Kidney International Supplements* (Vol. 4, Issue 1, pp. 2–8). Nature Publishing Group. https://doi.org/10.1038/kisup.2014.2

Edelstein, C. L., Ling, H., & Schrier, R. W. (1997). The nature of renal cell injury. *Kidney International*, *51*(5), 1341–1351. https://doi.org/10.1038/ki.1997.183

Epstein, M. (1997). Alcohol's Impact on Kidney Function [1997]. *Alcohol, Health and Research World*, *21*(1), 84–91.

Fard, A. A., Samadi, M., Shirpoor, A., & Rasmi, Y. (2022). Ethanol Consumption Promotes TNF-α Signaling Pathway in Rat Kidney: Rescue Effect of Curcumin. *Journal of Chemical Health Risks*, *12*(2), 271–280. https://doi.org/10.22034/jchr.2021.1913474.1211

Fernandes, C. E., Marcondes, S. F., Galindo, G. M., & Franco-Belussi, L. (2019). Kidney anatomy, histology and histometric traits associated to renosomatic index in gymnotus inaequilabiatus (Gymnotiformes: Gymnotidae). *Neotropical Ichthyology*, *17*(4). https://doi.org/10.1590/1982-0224-20190107

Fernández-Solà, J. (2020). The effects of ethanol on the heart: Alcoholic cardiomyopathy. In *Nutrients* (Vol. 12, Issue 2). MDPI AG. https://doi.org/10.3390/nu12020572

Gao, K., Wang, G., Wang, Y., Han, D., Bi, J., Yuan, Y., Yao, T., Wan, Z., Li, H., & Mei, X. (2015). Neuroprotective Effect of Simvastatin via Inducing the Autophagy on Spinal Cord Injury in the Rat Model. *BioMed Research International*, *2015*. https://doi.org/10.1155/2015/260161

Gandhi, C. R., (2012). Oxidative stress and hepatic stellate cells: A paradoxical relationship. *Trends in cell and molecular biology*, *7*, 1-10.

Gu, Y., Yang, X., Liang, H., & Li, D. (2019). Comprehensive evaluation of effects and safety of statin on the progression of liver cirrhosis: A systematic review and meta-analysis. *BMC Gastroenterology*, *19*(1). https://doi.org/10.1186/s12876-019-1147-1

Guo, R., & Ren, J. (2010). Alcohol dehydrogenase accentuates ethanol-induced myocardial dysfunction and mitochondrial damage in mice: Role of mitochondrial death pathway. *PLoS ONE*, *5*(1). https://doi.org/10.1371/journal.pone.0008757

Harash, G., Richardson, K. C., Alshamy, Z., Hünigen, H., Hafez, H. M., Plendl, J., & Masri, S. al. (2019). Heart ventricular histology and microvasculature together with aortic histology and elastic

lamellar structure: A comparison of a novel dual-purpose to a broiler chicken line. *PLoS ONE*, *14*(3). https://doi.org/10.1371/journal.pone.0214158

Hassan, S. M., Saeed, A. K., & Jabbar Hussein, A. (2015). Ethanol-Induced Hepatic and Renal Histopathological Changes in BALB/c mice Photoprotective measurement of Almond oil on UVB irradiated mouse's skin View project Ultraviolet Type B-Radiation-Induced Hyperplasia and Seborrheic Keratosis is Reduced by Application of Commercial Sunscreens View Project Ethanol-Induced Hepatic and Renal Histopathological Changes in BALB/c mice. In *Journal of Natural Sciences Research www.iiste.org ISSN* (Vol. 5, Issue 10). https://www.researchgate.net/publication/279192913

Haycock, P.C., & Ramsay, M. (2009). Exposure of mouse embryos to ethanol during preimplantation development: Effect on DNA methylation in the H19 imprinting control region. Biology of reproduction, 81(4), 18-27. Doi: 10.1095/biolreprod.108.074682.

Henegar, J.R., Bigler, S.A., Henegar, L.K., Tyagi, S.C., & Hall, J.E. (2001). Functional and structural changes in the kidney in the early stages of obesity. Journal of the American Society of Nephrology, 12(6), 1211-1217. Doi: 10.1681/ASN.V1261211.

Ho, K. M., & Morgan, D. J. R. (2022). The Proximal Tubule as the Pathogenic and Therapeutic Target in Acute Kidney Injury. In *Nephron* (Vol. 146, Issue 5, pp. 494–502). S. Karger AG. https://doi.org/10.1159/000522341

Hu, C. Q., Bo, Q. L., Chu, L. L., Hu, Y. di, Fu, L., Wang, G. X., Lu, Y., Liu, X. J., Wang, H., & Xu, D. X. (2020). Vitamin D Deficiency Aggravates Hepatic Oxidative Stress and Inflammation during Chronic Alcohol-Induced Liver Injury in Mice. *Oxidative Medicine and Cellular Longevity*, *2020*. https://doi.org/10.1155/2020/5715893

Hu, P. J., Wu, M. Y., Lin, T. C., Chen, T. T., Wu, Y. C., Su, S. L., Lu, K. C., Chen, J. S., Sung, F. C., Lee, C. te, Yang, Y., Hwang, S. J., Wang, M. C., Hsu, Y. H., Chiou, H. Y., Wong, C. S., & Lin, Y. F. (2018). Effect of Statins on Renal Function in Chronic Kidney Disease Patients. *Scientific Reports*, *8*(1). https://doi.org/10.1038/s41598-018-34632-z

Irwin, M. W., Mak, S., Mann, D. L., Qu, R., Penninger, J. M., Yan, A., Dawood, F., Wen, W.-H., Shou, Z., & Liu, P. (1999). *Tissue Expression and Immunolocalization of Tumor Necrosis Factor-in Postinfarction Dysfunctional Myocardium*. http://www.circulationaha.org

Iseri, S., Ercan, F., Gedik, N., Yuksel, M., & Alican, I. (2007). Simvastatin attenuates cisplatin-induced kidney and liver damage in rats. *Toxicology, 230*, 256-264.

Jeon, S., & Carr, R. (2020). Alcohol effects on hepatic lipid metabolism. In *Journal of Lipid Research* (Vol. 61, Issue 4, pp. 470–479). American Society for Biochemistry and Molecular Biology Inc. https://doi.org/10.1194/jlr.R119000547

Kawano, Y. (2010). Physio-pathological effects of alcohol on the cardiovascular system: Its role in hypertension and cardiovascular disease. In *Hypertension Research* (Vol. 33, Issue 3, pp. 181–191). https://doi.org/10.1038/hr.2009.226

Kolovou, G. D., Salpea, K. D., Anagnostopoulou, K. K., & Mikhailidis, D. P. (2006). Alcohol use, vascular disease, and lipid-lowering drugs. In *Journal of Pharmacology and Experimental Therapeutics* (Vol. 318, Issue 1, pp. 1–7). American Society for Pharmacology and Experimental Therapy. https://doi.org/10.1124/jpet.106.102269

Kolovou, G. L., Mikhailidis, D. P., Daskalova, D. C., & Kafaltis, N. (2003). The effect of co-administration of simvastatin and alcohol in rats. *In Vivo*, *17*(6), 523-527.

Kwiecien, J. M. (2010). Cellular compensatory mechanisms in the CNS of dysmyelinated rats. *Comparative medicine*, *60*(3), 205-217.

la Mura, V., Pasarín, M., Meireles, C. Z., Miquel, R., Rodríguez-Vilarrupla, A., Hide, D., Gracia-Sancho, J., García-Pagán, J. C., Bosch, J., & Abraldes, J. G. (2013). Effects of simvastatin administration on rodents with lipopolysaccharide-induced liver microvascular dysfunction. *Hepatology*, *57*(3), 1172–1181. https://doi.org/10.1002/hep.26127

Lai, Y.-J., Hung, C.-L., Hong, R.-C., Tseng, Y.-M., Lin, C.-I., Ko, Y.-S., Tsai, C.-H., & Yeh, H.-I. (2011). *Slow conduction and gap junction remodeling in murine ventricle after chronic alcohol ingestion*. http://www.jbiomedsci.com/content/18/1/72

Latchoumycandane, C., Hanouneh, M., Nagy, L. E., & McIntyre, T. M. (2015). Inflammatory PAF receptor signaling initiates hedgehog signaling and kidney fibrogenesis during ethanol consumption. *PLoS ONE*, *10*(12). https://doi.org/10.1371/journal.pone.0145691

Latiff, S., & Olateju, O. I. (2022). Quantification and comparison of tenocyte distribution and collagen content in the commonly used autografts for anterior cruciate ligament reconstruction. *Anatomy & Cell Biology*, *55*(3), 304-310. https://doi:10.5115/acb.22.005.

Law, B. A., Levick, S. P., & Carver, W. E. (2012). Alterations in cardiac structure and function in a murine model of chronic alcohol consumption. *Microscopy and Microanalysis*, *18*(3), 453–461. https://doi.org/10.1017/S1431927612000372

Leal, S., Ricardo Jorge, D. O., Joana, B., Maria, S. S., & Isabel, S. S. (2017). Heavy Alcohol Consumption Effects on Blood Pressure and on Kidney Structure Persist after Long-Term Withdrawal. *Kidney and Blood Pressure Research*, *42*(4), 664–675. https://doi.org/10.1159/000482022

Lee, M. M. Y., Sattar, N., McMurray, J. J. V., & Packard, C. J. (2019). Statins in the Prevention and Treatment of Heart Failure: A Review of the Evidence. In *Current Atherosclerosis Reports* (Vol. 21, Issue 10). Current Medicine Group LLC 1. https://doi.org/10.1007/s11883-019-0800-z

Lespine, L-F., & Tirelli, E. (2017). Wheel-running exercise during adolescence does substantially affect cocaine conditioned place preference in male C57BL/6J mice. *Frontiers in Neuroscience*, *11*. Doi: 10.3389/conf.fnins.2017.94.0069.

Letsela, L., Weiner, R., Gafos, M., & Fritz, K. (2019). Alcohol Availability, Marketing, and Sexual Health Risk Amongst Urban and Rural Youth in South Africa. *AIDS and Behavior*, *23*(1), 175–189. https://doi.org/10.1007/s10461-018-2250-y

Li, X., Nie, Y., Lian, H., & Hu, S. (2018). Histopathologic features of alcoholic cardiomyopathy compared with idiopathic dilated cardiomyopathy. *Medicine (United States)*, *97*(39). https://doi.org/10.1097/MD.0000000000012259

Liu, D., Liu, Y., Yi, Z., & Dong, H. (2016). Simvastatin protects cardiomyocytes from doxorubicin cardiotoxicity by suppressing endoplasmic reticulum stress and activating Akt signaling. In *Int J Clin Exp Med* (Vol. 9, Issue 2). www.ijcem.com/

MacDougall, D. A., Pugh, S. D., Bassi, H. S., Lotteau, S., Porter, K. E., & Calaghan, S. (2017). Simvastatin promotes cardiac myocyte relaxation in association with phosphorylation of troponin I. *Frontiers in Pharmacology*, *8*(APR). https://doi.org/10.3389/fphar.2017.00203

Maldonado-Devincci, A.M., Badanich, K.A., & Kirstein, C.L. (2010). Alcohol during adolescence selectively alters immediate long-term behaviour and neurochemistry. *Alcohol*, *44*(1), 57-66. Doi: 10.1016/j.alcohol.2009.09.035.

Marshall, E. J. (2014). Adolescent alcohol use: Risks and consequences. *Alcohol and Alcoholism*, *49*(2), 160–164. https://doi.org/10.1093/alcalc/agt180.

Maserumule, O.M., Skaal, L., & Sithole, S.L. (2019). Alcohol use among high school learners in rural areas of Limpopo province. *South African Journal of Psychiatry, 25*(0), 1-6. https://doi.org/10.4102/sajpsychiatry.v25i0.1183

Matsuo, K., Murakami, T., Kawaguchi, D., Hiroshima, Y., Koda, K., Yamazaki, K., Ishida, Y., & Tanaka, K. (2016). Histologic features after surgery associating liver partition and portal vein ligation for staged hepatectomy versus those after hepatectomy with portal vein embolization. *Surgery*, *189*, 1289-1298.

Matzopoulos, R. G., Truen, S., Bowman, B., & Corrigall, J. (2014). The cost of harmful alcohol use in South Africa. *South African Medical Journal*, *104*(2), 127–132. https://doi.org/10.7196/SAMJ.7644

McKay, A., Leung, B. P., McInnes, I. B., Thomson, N. C., & Liew, F. Y. (2004). A novel anti-inflammatory role of simvastatin in a murine model of allergic asthma. *Journal of Immunology, 172*, 2903-2908.

Mehaffey, E., & Majid, D. S. A. (2017). Tumor necrosis factor-, kidney function, and hypertension. *REVIEW Inflammation and Inflammatory Mediators in Kidney Disease American Journal of Physiology and Renal Physiology*, *313*, 1005–1008. https://doi.org/10.1152/ajprenal.00535.2016.-Hypertension

Mohammadi, S., Zamani, E., Mohadeth, Z., Mogtahedi, F., Chopan, H., Moghimi, F., Mohammadi, M., Karimi, M., Abtahi, H., Tavakkoli, K., Mohammadzadeh, F., Biglari, H., Delshad, A., Ghayour-Mobarhan, M., Ferns, G. A. A., & Mohammadzadeh, A. (2015). Effects of different doses of simvastatin on lead-induced kidney damage in Balb/c male mice. *Pharmaceutical Sciences*, *20*(4), 157–162. https://doi.org/10.5681/PS.2015.005

Morojele, N.K., & Ramsoomar, L. (2016). Addressing alcohol use in South Africa. *South African Medical Journal*, *106*(6), 551-553. DOI:10.7196/SAMJ.2016.v106i6.10944

Morse, L. R., Coker, J., & Battaglino, R. A. (2018). *STATINS AND BONE HEALTH: A MINI REVIEW*.

Murphy, C., Deplazes, E., Cranfield, C. G., & Garcia, A. (2020). The role of structure and biophysical properties in the pleiotropic effects of statins. In *International Journal of Molecular Sciences* (Vol. 21, Issue 22, pp. 1–29). MDPI AG. https://doi.org/10.3390/ijms21228745

Nežić, L., Škrbić, R., Amidžić, L., Gajanin, R., Milovanović, Z., Nepovimova, E., Kuča, K., & Jaćević, V. (2020). Protective effects of simvastatin on endotoxin-induced acute kidney injury through activation of tubular epithelial cells' survival and hindering cytochrome c-mediated apoptosis. *International Journal of Molecular Sciences*, *21*(19), 1–18. https://doi.org/10.3390/ijms21197236

Obad, A., Peeran, A., Little, J. I., Haddad, G. E., & Tarzami, S. T. (2018). Alcohol-mediated organ damages: Heart and brain. In *Frontiers in Pharmacology* (Vol. 9, Issue FEB). Frontiers Media S.A. https://doi.org/10.3389/fphar.2018.00081

Olsson, C. A., Romaniuk, H., Salinger, J., Staiger, P. K., Bonomo, Y., Hulbert, C., & Patton, G. C. (2016). *Drinking patterns of adolescents who develop alcohol use disorders: results from the Victorian Adolescent Health Cohort Study*. https://doi.org/10.1136/bmjopen-2015

Ortiz, A. (2000). Apoptotic regulatory proteins in renal injury. *Nephrology Forum*, *58*(1), 467-485. https://doi.org/10.1046/j.1523-1755.2000.00188.x

Piano, M. R. (2016). Alcohol's Effects on the Cardiovascular System. *Alcohol Research: Current Reviews*, *38*(2), 219–238. https://www.niaaa.nih.gov/

Qin, Y. W., Ye, P., He, J. Q., Sheng, L., Wang, L. Y., & Du, J. (2010). Simvastatin inhibited cardiac hypertrophy and fibrosis in apolipoprotein E-deficient mice fed a Western-style diet by increasing PPAR α and γ expression and reducing TC, MMP-9, and Cat S levels. *Acta Pharmacologica Sinica*, *31*(10), 1350–1358. https://doi.org/10.1038/aps.2010.109

Ramsoomar, L., Morojele, N. K., & Norris, S. A. (2013). Alcohol use in early and late adolescence among the birth to twenty cohort in Soweto, South Africa. *Global Health Action*, *6*, 19274. https://doi.org/10.3402/gha.v6i0.19274

Refaie, M. M. M., El-Hussieny, M., Bayoumi, A. M. A., Shehata, S., Welson, N. N., & Abdelzaher, W. Y. (2022). Simvastatin cardioprotection in cyclophosphamide-induced toxicity via the modulation of inflammasome/caspase1/interleukin1β pathway. *Human and Experimental Toxicology*, *41*. https://doi.org/10.1177/09603271221111440

Rikalo, N. A., & Romanenko, I. V. (2018). Morphological Changes in Kidney Tissues of Rats. *Journal of Education, Health and Sport*, *8*(2), 272–279.

Robin, M. A., Demeilliers, C., Sutton, A., Paradis, V., Maisonneuve, C., Dubois, S., Poirel, O., Lettéron, P., Pessayre, D., & Fromenty, B. (2005). Alcohol increases tumor necrosis factor α and decreases nuclear factor-κB to activate hepatic apoptosis in genetically obese mice. *Hepatology*, *42*(6), 1280–1290. https://doi.org/10.1002/hep.20949

Rohilla, A., Ahmad, A., Khan, M.U., & Khanam, R. (2015). A comparative study on the cardioprotective potential of artovastatin and simvastatin in hyperhomocysteinemic rat hearts. *European Journal of Pharmacology, 764*(5), 48-54. https://doi.org/10.1016/j.ejphar.2015.06.045

Schumacher, S. M., & Naga Prasad, S. V. (2018). Tumor Necrosis Factor-α in Heart Failure: An Updated Review. In *Current Cardiology Reports* (Vol. 20, Issue 11). Current Medicine Group LLC 1. https://doi.org/10.1007/s11886-018-1067-7

Sengupta, M., Abuirqeba, S., Kameric, A., Cecile-Valfort, A., Chatterjee, A., Griffett, K., Burris, T. P., & Flaveny, C. A. (2021). A two-hit model of alcoholic liver disease that exhibits rapid, severe fibrosis. *PLoS ONE*, *16*(3 March). https://doi.org/10.1371/journal.pone.0249316

Singh, V. P., Singh, N., & Jaggi, A. S. (2013). A review on renal toxicity profile of common abusive drugs. In *Korean Journal of Physiology and Pharmacology* (Vol. 17, Issue 4, pp. 347–357). https://doi.org/10.4196/kjpp.2013.17.4.347

Skrzypiec-Spring, M., Sapa-Wojciechowska, A., Haczkiewicz-Leśniak, K., Piasecki, T., Kwiatkowska, J., Podhorska-Okołów, M., & Szeląg, A. (2021). Hmg-coa reductase inhibitor, simvastatin is effective in decreasing degree of myocarditis by inhibiting metalloproteinases activation. *Biomolecules*, *11*(10). https://doi.org/10.3390/biom11101415

Steele, M.R., Belostotsky, V. & Lau, K.K. (2012). The dangers of substance in adolescent with chronic kidney disease: a review of the literature. *Canadian Association of Nephrology Nurses and Technologists*, *22*(1), 15-22.

Su, F., Shi, M., Zhang, J., Zheng, Q., Zhang, D., Zhang, W., Wang, H., & Li, X. (2018). Simvastatin protects heart from pressure overload injury by inhibiting excessive autophagy. *International Journal of Medical Sciences, 15(3)*, 1508-1516.

Sun, F., Duan, W., Zhang, Y., Zhang, L., Qile, M., Liu, Z., Qiu, F., Zhao, D., Lu, Y., & Chu, W. (2015). Simvastatin alleviates cardiac fibrosis induced by infarction via up-regulation of TGF-β receptor

III expression. *British Journal of Pharmacology*, *172*(15), 3779–3792. https://doi.org/10.1111/bph.13166

Swart, L. A., Seedat, M., & Nel, J. (2015). Alcohol consumption in adolescent homicide victims in the city of Johannesburg, South Africa. *Addiction*, *110*(4), 595–601. https://doi.org/10.1111/add.12825

Thabit, A., Alhifany, A., Alsheikh, R., Namnqani, S., Al-Mohammadi, A., Elmorsy, S., Qari, M., & Ardawi, M. (2014). Effect of simvastatin and atorvastatin on serum vitamin D and bone mineral density in hypercholesterolemic patients: A cross-sectional study. *Journal of Osteoporosis*, *2014*. https://doi.org/10.1155/2014/468397

Tripathi, D. M., Vilaseca, M., Lafoz, E., Garcia-Calderó, H., Viegas Haute, G., Fernández-Iglesias, A., Rodrigues de Oliveira, J., García-Pagán, J. C., Bosch, J., & Gracia-Sancho, J. (2018). Simvastatin Prevents Progression of Acute on Chronic Liver Failure in Rats with Cirrhosis and Portal Hypertension. *Gastroenterology*, *155*(5), 1564–1577. https://doi.org/10.1053/j.gastro.2018.07.022

Wang, L., Zhou, Z., Saari, J. T., & Kang, Y. J. (2005). Alcohol-Induced Myocardial Fibrosis in Metallothionein-Null Mice Prevention by Zinc Supplementation. *American Journal of Pathology*, *167*(2), 337–344.

Wang, W., Zhao, C., Zhou, J., Zhen, Z., Wang, Y., & Shen, C. (2013). Simvastatin Ameliorates Liver Fibrosis via Mediating Nitric Oxide Synthase in Rats with Non-Alcoholic Steatohepatitis-Related Liver Fibrosis. *PLoS ONE*, *8*(10). https://doi.org/10.1371/journal.pone.0076538

Webber, E. M., Wu, J. C., Wang, L., Merlino, G., & Fausto, N. (1994). Overexpression of Transforming Growth Factor-α causes liver enlargement and increased hepatocyte proliferation in transgenic mice. *American Journal of Pathology*, *145*(2), 398-408.

Wu, Y., Song, P., Yuan, X., & Li, D. (2021). Exploring the Effect of Dapagliflozin on Alcoholic Kidney Injury and Renal Interstitial Fibrosis in Rats Based on TIMP-1/MMP-24 Pathway. *Evidence-Based Complementary and Alternative Medicine*, *2021*. https://doi.org/10.1155/2021/6538189

Xiao, X., Chang, G., Liu, J., Sun, G., Liu, L., Qin, S., & Zhang, D. (2016). Simvastatin ameliorates ventricular remodeling via the TGF-β1 signaling pathway in rats following myocardial infarction. *Molecular Medicine Reports*, *13*(6), 5093–5101. https://doi.org/10.3892/mmr.2016.5178

Yang, S., Koteish, A., Lin, H., Huang, J., Roskams, T., Dawson, V., & Diehl, A.M. (2004). Oval cells compensate for damage and replicative senescence of mature hepatocytes in mice with fatty liver disease. *Hepatology*, *40*(2), 403-411. Doi: 10.1002/hep.20082

Zamami, R., Kohagur, K., Kinjyo, K., Nakamura, T., Kinjo, T., Yamazato, M., Ishida, A., & Ohya, Y. (2021). The association between glomerular diameter and secondary focal segmental glomerulosclerosis in chronic kidney disease. *Kidney and Blood Pressure Research*, *46*, 433-440. https://doi.org/10.1159/000515528

Zhang, J., Patel, M.B., Griffiths, R., Mao, A., Song, Y., Karlovich, N.S., Sparks, M.A.., Jin, H., Wu, M., Lin, E.E., & Crowley, S.D. (2014). Tumor necrosis factor-alpha produced in the kidney contributes to angiotensin II-dependent hypertension. *Hypertension*, *64*, pp. 1275-1281.

Zhou, Q., & Liao, J. K. (2009). Statins and Cardiovascular Diseases: From Cholesterol Lowering to Pleiotropy. *Current Pharmaceutical Design*, *15*(5), 467–478.

## APPENDICES

Ethical clearance certificate

ANIMALS RESEARCH ETHICS COMMITTEE (AREC)

UNIVERSITY OF THE WITWATERSRAND JOHANNESBURG

STRICTLY CONFIDENTIAL

CLEARANCE CERTIFICATE NUMBER: 2019/11/63/C

**APPLICANT: Dr O Olateju**
**School: School of Anatomical Sciences; Department: N/A;**
**Location: CAS**

**PROJECT TITLE: Does simvastatin have neuroprotective effects against Alcohol-induced brain damage in C57BL/6J**

**Category: C; Species and Numbers involved:** *150X 3 Weeks old (9-15g) male Mus musculus C57BL/6J and 150X 3 Weeks old (9-15g) female Mus musculus C57BL/6J*

Approval is hereby given for the use of animals for the research project named above and described in the application reviewed by a quorate meeting of the AREC held on 1 Oct 2019. This approval remains valid until 20 Jan 2022.

All material changes to the approved research must be reported to the AREC before they are implemented. Failure to do so will invalidate this clearance certificate.

An annual progress report must be provided to the AREC.

The use of these animals is subject to AREC guidelines on the use and care of laboratory animals, is limited to the procedures described in the application and is subject to additional conditions listed below:

I, the Chair of the AREC (or my designated representative) am satisfied that the proposed research is ethical as judged by local law, international standards and University policy.

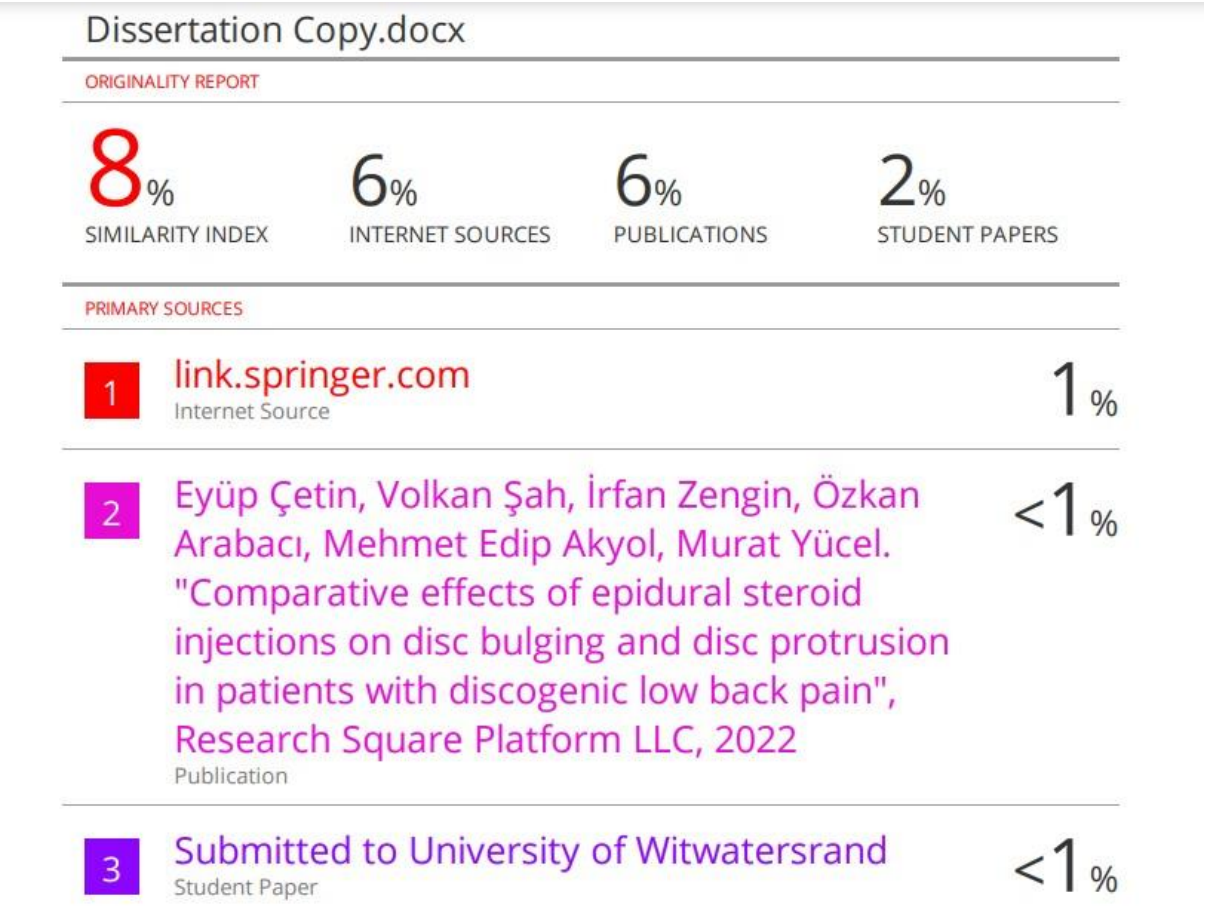
Signed: _____ Date: 28th FEBRUARY 2020
(Chairperson of the AREC)

I am satisfied that the persons listed in this application are competent to perform the procedures described in the application, in the context of Section 23 (1) (c) of the veterinary and Para-veterinary Professions Act (19 of 1982).

Signed: _____ Date: 28 February 2020
(Registered Veterinarian)

CC: Student supervisor: N/A N/A
Director Central Animals Service: Dr Kim Jardine

Turnitin report



Dissertation Copy.docx

ORIGINALITY REPORT

| 8% | 6% | 6% | 2% |
|---|---|---|---|
| SIMILARITY INDEX | INTERNET SOURCES | PUBLICATIONS | STUDENT PAPERS |

PRIMARY SOURCES

| | | |
|---|---|---|
| 1 | link.springer.com<br>Internet Source | 1% |
| 2 | Eyüp Çetin, Volkan Şah, İrfan Zengin, Özkan Arabacı, Mehmet Edip Akyol, Murat Yücel. "Comparative effects of epidural steroid injections on disc bulging and disc protrusion in patients with discogenic low back pain", Research Square Platform LLC, 2022<br>Publication | <1% |
| 3 | Submitted to University of Witwatersrand<br>Student Paper | <1% |

Buffer and fixative recipes for primary and secondary antibodies

**10mM Sodium Citrate buffer pH 6**

| | |
|---|---|
| Tri Sodium citrate (dehydrate) | 2.9g |
| Distilled water | 1000ml |

Mix to dissolve sodium citrate and adjust pH to 6 with 1M HCl

Add 0,05% Tween 20 if required

**1M Phosphate buffer pH7.4**

| | |
|---|---|
| NaCl | 16g |
| $Na_2HPO_4$ | 3.5g |
| KCl | 0.4g |
| $KH_2PO_4$ | 0.4g |
| Distilled water | 2000ml → 2L |

**DAB working solution**

In a clean bijou bottle measure out

1mg DAB (0.001g) To this add

2ml Tris HCl and mix well.

In a separate tube add:

29ul cold distilled water

1µl hydrogen peroxide (100%)

Add 20µl of sol (b) to DAB sol (a)